



REDE NORDESTE DE BIOTECNOLOGIA - RENORBIO
UNIVERSIDADE FEDERAL DO ESPÍRITO SANTO – UFES
PROGRAMA DE PÓS-GRADUAÇÃO EM BIOTECNOLOGIA

AFRÂNIO CÔGO DESTEFANI

**OTIMIZAÇÃO DO PROCESSO DE DESCELULARIZAÇÃO RENAL PARA
OBTENÇÃO DE ARCABOUÇO ACELULAR**

Vitória – ES

2018

AFRÂNIO CÔGO DESTEFANI

**OTIMIZAÇÃO DO PROCESSO DE DESCELULARIZAÇÃO RENAL PARA
OBTENÇÃO DE ARCABOUÇO ACELULAR**

Tese de Doutorado apresentada ao Programa de Pós-Graduação em Biotecnologia (RENORBIO) - Ponto focal Universidade Federal do Espírito Santo como parte dos requisitos para obtenção do grau de Doutor em Biotecnologia, sob Orientação do Prof. Dr. Breno Valentim Nogueira.

Vitória – ES

2018

Dados Internacionais de Catalogação-na-publicação (CIP)
(Biblioteca Central da Universidade Federal do Espírito Santo, ES, Brasil)

D476o Destefani, Afrânio Côgo, 1982-
Otimização do processo de descelularização renal para obtenção
de arcabouço acelular. / Afrânio Côgo Destefani. - 2018.
113 f. : il.

Orientador: Breno Valentim Nogueira.
Tese (Doutorado em Biotecnologia) - Universidade Federal
do Espírito Santo, Centro de Ciências da Saúde.

1. Doença Renal Crônica. 2. Descelularização. 3. Recelularização.
4. Bioengenharia de Tecidos. 5. Matriz extracelular. I. Nogueira,
Breno Valentim. II. Universidade Federal do Espírito Santo.
Centro de Ciências da Saúde. III. Título.

CDU: 61

AFRÂNIO CÔGO DESTEFANI

**OTIMIZAÇÃO DO PROCESSO DE DESCELULARIZAÇÃO RENAL PARA
OBTENÇÃO DE ARCABOUÇO ACELULAR**

Tese de Doutorado apresentada ao Programa de Pós-Graduação em Biotecnologia (RENORBIO) - Ponto focal Universidade Federal do Espírito Santo, como parte dos requisitos para obtenção do grau de Doutor em Biotecnologia.

Aprovada em: ___ / ___ / ___

BANCA EXAMINADORA

Prof. Dr. Breno Valentim Nogueira
Universidade Federal do Espírito Santo
Orientador

Prof. Dr. Marco Cesar Cunegundes Guimarães
Universidade Federal do Espírito Santo
Examinador Interno

Prof. Dr. Alexandre Martins Costa Santos
Universidade Federal do Espírito Santo
Examinador Interno

Prof. Dr. Raul Cavalcante Maranhão
Universidade de São Paulo/INCOR
Examinador Externo

Profa. Dra. Camille de Moura Balarini
Universidade Federal da Paraíba
Examinador Externo

Prof. Dr. Fausto Edmundo Lima Pereira
Universidade de Vila Velha
Examinador Externo

À Deus.

AGRADECIMENTOS

À Deus, pela certeza de não estar sozinho.

À minha eterna namorada Aluanny por tornar os meus dias mais felizes.

Aos professores Breno Valentim Nogueira e Marco Cesar Cunegundes Guimarães, exemplos de pesquisadores, pela orientação, confiança e apoio no desenvolvimento deste trabalho. Minha formação como pesquisador foi de excelência pelos mestres que tive.

À equipe atual e anterior do laboratório de Ultraestrutura Celular Carlos Alberto Redins (LUCCAR) por todo o aprendizado, tenho certeza que a convivência com vocês tornou os meus dias mais agradáveis.

À Fundação de Amparo à Pesquisa e Inovação do Espírito Santo (FAPES) (EDITAL FAPES Nº 006/2014-UNIVERSAL: processo 0606/2015; EDITAL FAPES/CNPq Nº 012/2014-DCR: processo 0832/2015; EDITAL FAPES/CAPES PROFIX 009/2014-63/2017 processo 79522882/17), à Coordenação de Aperfeiçoamento de Pessoal de Nível Superior (CAPES) e ao Conselho Nacional de Desenvolvimento Científico e Tecnológico (CNPQ) pelo financiamento da pesquisa.

Ao apoio institucional da Universidade Federal do Espírito Santo (UFES), do Departamento de Morfologia e ao Laboratório Multiusuário de Análises Biomoleculares (LABIOM).

Ao Programa de Pós-Graduação em Biotecnologia (PGBiotec) e à Rede Nordeste de Biotecnologia (RENORBIO).

RESUMO

A Doença Renal Crônica (DRC) é caracterizada pela deterioração progressiva da função renal, que pode comprometer diferentes tecidos e órgãos. O principal tratamento indicado para pacientes com DRC é o transplante renal. No entanto, a falta de órgãos disponíveis, bem como a alta taxa de rejeição de órgãos, sustenta a necessidade de novas terapias. Assim, a implementação da bioengenharia tecidual para a regeneração de órgãos surgiu como uma alternativa ao transplante tradicional de órgãos. Atualmente, demasiado tempo tem sido expandido na descellularização renal total por perfusão com detergentes. Nestes casos há perda de componentes essenciais da matriz extracelular (MEC) e desarranjos na arquitetura do arcabouço obtido o quê substancialmente pode influenciar no repovoamento celular subsequente. Neste trabalho a descellularização total de rins de ratos foi obtida em um tempo reduzido (6 horas) com a utilização de solução de detergente iônico (SDS, 1%) através da artéria renal sob pressão (100 mmHg) e fluxo (1,0 mL/min) controlados. Ao final desta etapa, os arcabouços renais apresentavam características físicas translúcidas e condutos vasculares preservados. A análise histoquímica e a microscopia eletrônica revelaram glomérulos com a membrana basal preservada, além de rede tubular e vascular sem resíduo de restos celulares e DNA. A análise proteômica identificou a preservação de proteínas majoritárias relacionadas aos compostos da MEC. Assim, o uso de baixa concentração de SDS por 6 horas promoveu uma descellularização bem-sucedida, além de preservar a MEC com mínimo resíduo de SDS (<0,01%). Além disso desenvolvemos um índice de retração como cálculo de correção devido a retração elástica do rim após o processamento. A microscopia eletrônica, a quantificação espectrofotométrica e as análises de espectrometria de massas foram realizadas para comparar os resultados. Demonstramos que a análise histológica, técnica fácil e de baixo custo, apresentou excelentes resultados quando o índice de retração foi aplicado, permitindo a comparação das amostras antes e após o processo com dados confiáveis. De posse desses dados demonstramos que é possível a redução no tempo de descellularização com a preservação de componentes importantes da MEC.

Palavras-chave: Doença Renal Crônica, Descellularização, Bioengenharia Tecidual.

ABSTRACT

Chronic Kidney Disease (CKD) is characterized by progressive deterioration of renal function, which can compromise various tissues and organs. The main therapy indicated for patients with CKD is renal transplantation. However, the absence of available organs, as well as an organ rejection rate, is required for new therapies. Thus, the implementation of bioengineering for organ regeneration has emerged as an alternative to traditional organ transplantation. Currently, overtime has been expended on total renal decellularization by perfusion with detergents. In these cases, there is a loss of essential components of the extracellular matrix (ECM) and derangements in the scaffold architecture obtained which can substantially influence subsequent cell repopulation. In this work, the total discoloration of rat kidneys was measured in reduced time with the use of detergent solution (SDS, 1%) by renal technique under pressure (100 mmHg) and flow (1.0 mL/min). At the end of this stage, the scaffolds were incorporated as translucent physical characteristics and preserved vascular conduits. An electron microscopic and histochemical analysis revealed glomeruli with a preserved basement membrane, as well as a tubular and vascular network with no cell and DNA residues. Proteomic analysis identified the preservation of majority proteins related to ECM compounds. Thus, the use of low concentration of SDS for 6 hours promoted a successful thawing, in addition to preserving a MEC with the minimum residue of SDS (<0,01%). Also, we developed a retraction index as a correction calculation due to elastic retraction of the kidney after processing. Electron microscopy, spectrophotometric quantification, and mass spectrometry analyzes were performed to compare the results. We demonstrated that the histological analysis, easy technique, and low cost, presented excellent results when the correction index was applied, allowing the comparison of samples before and after the process with reliable data. With these data, we demonstrate that it is possible to reduce the time of decellularization with the preservation of essential components of the ECM.

Keywords: Chronic Kidney Disease, Decellularization, Tissue Bioengineering.

SUMÁRIO

ESTRUTURA DA TESE.....	9
1. INTRODUÇÃO	10
2. OBJETIVOS	13
3. REVISÃO DE LITERATURA	14
3.1. Arcabouço e engenharia tecidual.....	14
3.2. Arcabouços de matriz extracelular.....	17
3.3. Descelularização tecidual.....	18
4. CAPÍTULO 1	21
5. CAPÍTULO 2	50
6. CAPÍTULO 3	70
7. CONCLUSÕES	98
8. REFERÊNCIAS	99
9. ANEXOS	106
9.1. Anexo 1: Protocolo CEUA nº 033/2014 de 03/10/14.	106
9.2. Anexo 2: Protocolo CEUA nº 042/2016 de 07/10/16.	107
9.3. Anexo 3: Produções Correlatas	108
9.3.1. Patente referente à Sensor Óptico aplicado à Descelularização de Órgãos.....	108
9.3.2. Patente referente ao Processo de Indução de Células-tronco pela utilização de peptídeos. .	110
9.3.3. Co-autoria no artigo “ <i>Chronic administration of antioxidant resin from <i>Virola oleifera</i> attenuates atherogenesis in LDLr^{-/-} mice</i> ”	112

ESTRUTURA DA TESE

Para melhor compreensão dos resultados deste trabalho, optamos por estruturar este documento da seguinte maneira: Introdução, Objetivos e em seguida os 3 Capítulos já formatados como artigo.

Relação de artigos:

Artigo I - Advances in the Knowledge about Kidney Decellularization and Repopulation;

(Status: Publicado / Frontiers in Bioengineering and Biotechnology)

Artigo II - Time optimization in rat kidney decellularization process: ECM characterization by mass spectrometry;

(Status: Submetido)

Artigo III - The decellularization process causes significant changes in the 3D structure of the scaffold requiring corrections in the histomorphometric analysis;

(Status: Submetido)

1. INTRODUÇÃO

Atualmente existem milhões de pessoas com doença renal crônica (DRC) que evoluem subsequentemente para a falência renal as quais necessitam de transplante para sobreviverem. Somente nos Estados Unidos existem cerca de 26 milhões de americanos nestas condições e o número de novos casos de falência renal ultrapassam 90.000 anualmente (CORESH et al., 2007). No Brasil o cenário não é diferente. Existem atualmente cerca de 90 mil pacientes em diálise no Brasil. Nos últimos 10 anos, esse número cresceu 115% e deve aumentar em uma proporção de 500 casos por milhão de habitantes a cada ano. O gasto com o programa de diálise e transplante renal situa-se ao redor de 1,4 bilhões de reais ao ano (LAI et al., 2013; USRDS, 2015, 2016).

A DRC caracteriza-se por uma perda progressiva da função renal devido majoritariamente ao aumento dos níveis de resíduos tóxicos circulante no sangue os quais levam o indivíduo a diversas complicações como o aumento da pressão arterial, anemia, fragilidade óssea, carência nutricional e danos no sistema nervoso. Sabe-se que a DRC pode ser causada por diabetes, aumento da pressão sanguínea e outras desordens menos recorrentes. Os atuais tratamentos para a falência renal consistem na diálise e no transplante. No que se refere à diálise esta não promove a cura da falência renal e as despesas envolvidas para a manutenção das seções são onerosas além de que os pacientes necessitam realizar o tratamento dialítico por toda a vida e/ou até estarem aptos a receber um novo órgão transplantado. Com relação ao transplante renal este advém de órgãos doados por pacientes vivos ou cadáveres e requer tecido e tipo sanguíneos compatíveis com o receptor a fim de se reduzir o risco de rejeição imunológica (TAKAHASHI et al., 2007). Além do mais o tratamento requer a espera, às vezes demasiada, pelos pacientes de um tecido/órgão compatível e a administração de medicamentos anti-rejeição os quais são caros e podem causar maior susceptibilidade a doenças.

Mundialmente, a escassez de órgãos para transplantes tem estimulado cada vez mais o interesse urgente pela obtenção de tecnologias que envolvam a regeneração tecidual em pacientes acometidos de diferentes doenças. Preferivelmente ao processo de geração de novo órgão (JORAKU et al., 2009; LITTLE, 2006; YOKOO; MATSUMOTO; YOKOTE, 2011) estudos têm demonstrado com sucesso o repovoamento de arcabouços renais acelulares com células de vários outros tecidos (ATALA, 2006; BHRANY et al., 2006; GUYETTE et al.,

2015; MATSUNUMA et al., 2006; NARITA et al., 2008; OTT, 2015; TAKAHASHI et al., 2007). Sabe-se que para DRC, há pouca chance de que a grande maioria da população mundial tenha acesso a terapia de substituição renal com diálise ou transplante (BONANDRINI et al., 2014).

Estudos recentes têm demonstrado a obtenção de órgãos bioartificiais funcionais através da descclularização e recelularização (repovoamento) de um órgão cadavérico (BAPTISTA et al., 2009; BONANDRINI et al., 2014; BURGKART et al., 2014; CARALT et al., 2015; CHAE et al., 2014; GUAN et al., 2015a; KHAN et al., 2014; NAKAYAMA et al., 2011; PARK; WOO, 2012a, 2012b; PELOSO et al., 2013; SONG et al., 2013a; SUN; ALTALHI; NUNES, 2015; UZARSKI et al., 2015b; WILLENBERG et al., 2015; YU et al., 2014; ZVAROVA et al., 2016). Apesar de os estudos terem sido conduzidos em murinos alega-se que o conceito dos experimentos pode ser aplicado para órgãos humanos. Através da mimetização do procedimento de descclularização de um rim retirado de um camundongo e subsequente recelularização da matriz extracelular com células do próprio animal, um rim bioartificial funcional pode ser obtido. Assim a engenharia de tecidos ajudaria a resolver esta lacuna pela regeneração do rim danificado usando arcabouços repovoados com células renais precursoras (BONANDRINI et al., 2014).

Os processos de descclularização empregados podem despender dezenas de horas à dias para gerarem um arcabouço acelular (DESTEFANI; SIRTOLI; NOGUEIRA, 2017). Entretanto há perda de componentes essenciais da MEC e modificações importantes na microarquitetura do arcabouço produzido. Dependendo da combinação de detergentes este tempo pode ser reduzido. Nestes casos há restos celulares que podem gerar respostas imunogênicas. Além do mais muitas vezes despreza-se o controle da pressão das substâncias perfundidas e o fluxo das mesmas.

Neste trabalho propomos uma melhoria no processo de descclularização com a redução do tempo de perfusão do SDS (6h) e conseqüentemente a preservação de componentes da MEC, redução de resíduos celulares e resíduos de DNA o que possibilitará o repovoamento com células. Além disso a solução de SDS foi perfundida sob controle de fluxo (1,0 mL/min) e pressão (100 mmHg) em contraste com estudos que não utilizaram/informaram essas condições, p.e., (SONG et al., 2013b) utilizou 1% SDS por 12hs, com 30 mmHg, sem

informar o fluxo de perfusão; (BONANDRINI et al., 2014): 1% SDS por 17 hs, $62\pm 16 - 107\pm 23$ mmHg, 0,4 mL/min e (CARALT et al., 2015): 0,1% SDS 24 hs – 48 hs, sem informar a pressão e o fluxo de perfusão. Também analisamos a possível modificação estrutural do arcabouço renal após o processo de descclularização; e propomos a utilização de um índice de retração para corrigir análises semi-quantitativas do arcabouço renal em análises histológicas.

2. OBJETIVOS

2.1 OBJETIVO GERAL

- Otimizar o processo de descelularização renal em modelo experimental.

2.2 OBJETIVOS ESPECÍFICOS

- Avaliar o processo de descelularização com a utilização de SDS à 1% por 6 horas sob controle de fluxo (1,0 mL/min) e pressão (100 mmHg);
- Caracterizar a matriz extracelular renal comparativamente por diferentes técnicas;
- Desenvolver um índice de retração para corrigir análises semi-quantitativas do arcabouço renal em análises histológicas;
- Quantificar o DNA residual no arcabouço renal;
- Quantificar o SDS residual no perfusato.

3. REVISÃO DE LITERATURA

3.1. Arcabouço e engenharia tecidual

Os biomateriais têm sido utilizados para proporcionar às células um local de ancoragem e de reparo renal desejado; suporte à contenção de células e polarização; medição de respostas destrutivas do hospedeiro; e até mesmo promover a diferenciação celular e a estruturação do tecido (BASU et al., 2011; LANZA et al., 2002; SWETHA et al., 2011). O objetivo geral é fornecer um ambiente bioativo protegido que promova a viabilidade celular e eventual montagem de estruturas funcionais do tecido. Os biomateriais podem ser sintéticos ou naturais. Um exemplo simples do uso de biomateriais é a da entrega de células epiteliais parietais CD24+ de camundongos no parênquima renal usando coágulo coletado de uma hemorragia autóloga da veia da cauda. O coágulo, um biomaterial simples, serviu para manter as células localizadas propositalmente (SWETHA et al., 2011). Em contraste, outro estudo implantou uma variedade de construções utilizando biomateriais em um rim *in vivo* para testar a resposta imunológica e determinar o material mais adequado para uma construção de material celular implantável. Os biomateriais testados incluíram combinações de gelatina, ácido hialurônico, policaprolactona (PCL) e poliácido láctico-co-glicólico (PLGA). O hidrogel de gelatina foi o material mais promissor a ser utilizado na construção de acordo com parâmetros histopatológicos, tais como, inflamação, fibrose, necrose e mineralização, e medidas de biocompatibilidade, incluindo degradação, neovascularização e formação de tecidos novos. O implante primário promoveu a união de células em novas estruturas renais (BASU et al., 2011). Em uma aplicação alternativa de biomateriais, uma camada de colágeno I foi utilizada para ancorar as células epiteliais renais em estágio de desenvolvimento precoce em membranas de policarbonato na construção de um pequeno implante renal que produziu fluido semelhante a urina, vide Figura 1 (LANZA et al., 2002). Esses exemplos de biomateriais utilizados na engenharia de tecido renal são relativamente simples na sua estrutura, porém, dada a complexidade arquitetônica do tecido renal, um arcabouço de tecido pode ser mais eficaz na orientação da formação de tecido renal.

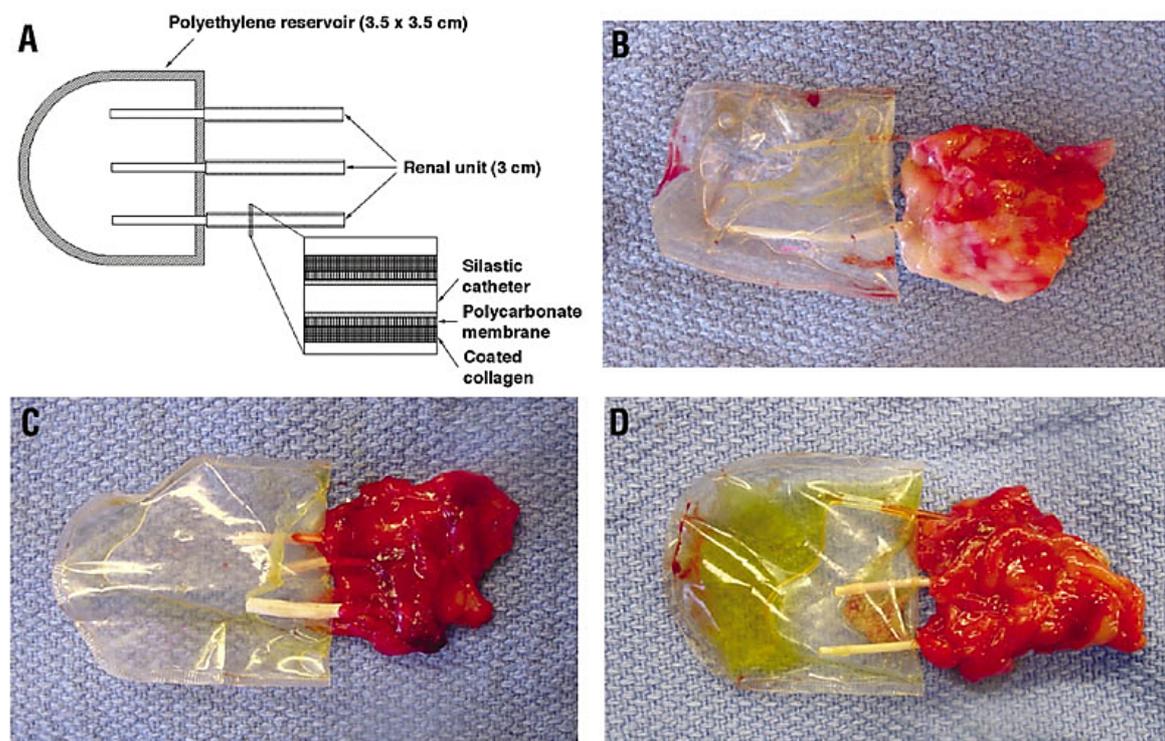


Figura 1. Unidades renais modificadas por tecidos.

(A) Ilustração da unidade renal e unidades recuperadas três meses após a implantação. (B) Controle sem cortes. (C) Cultura com células de controle alogênico. (D) Semeadura com células clonadas, mostrando o acúmulo de urina. *Adaptado com permissão de Lanza, R. P. et al. Generation of histocompatible tissues using nuclear transplantation. Nat. Biotechnol. 20, 689–696 (2002) (LANZA et al., 2002).*

O arcabouço tecidual tem sido descrito como promissor quando são avaliadas as quatro funções ou características seguintes: arquitetura, estabilidade mecânica, compatibilidade celular e de tecido e bioatividade (CHAN; LEONG, 2008). A arquitetura apropriada do tecido é a estrutura que possui espaço e forma para disposição de células funcionais, vascularização e transferência de nutrientes e metabólitos adequadamente. Mecanicamente, a estrutura precisa suportar os estresses esperados no local de implantação, mantendo a estabilidade arquitetônica. Além disso, propriedades mecânicas como a rigidez do tecido podem afetar as tendências de diferenciação; é desejável combinar o tecido do arcabouço com o do alvo (receptor). A compatibilidade é a capacidade do arcabouço de se integrar no tecido receptor e permitir a fixação celular, o crescimento e a diferenciação sem causar resposta adversa ao tecido. A bioatividade é a regulação ativa do comportamento celular.

Esta pode ser uma característica intrínseca do arcabouço ou obtida através de modificação. Por exemplo, ligantes podem ser incorporados em um arcabouço para promover a proliferação e a diferenciação celular (GOH; HOLMES, 2017; GRIFFIN et al., 2016).

Estruturas porosas intrincadas foram criadas a partir de polímeros usando técnicas à base de gás que incluem moldagem em espuma, em emulsão de CO₂-água e uso de CO₂ de alta pressão durante a reticulação. Demonstrou-se que estes permitem infiltração celular, invasão vascular e tráfego de nutrientes e resíduos (DEHGHANI; ANNABI, 2011). Outra técnica de fabricação para a produção de arcabouços artificiais é o *eletrospinning*. Ela usa carga elétrica para conduzir uma solução de polímero em fibras em nanoescala que podem estar em camadas para formar uma malha. Essas malhas foram produzidas a partir de polímeros sintéticos e de proteínas da ECM, como laminina ou policaprolactona (PCL) e colágeno, e também foram incorporadas a peptídeos bioativos, vide figura 2 (CHIU et al., 2016; HARTMAN et al., 2010; KANG et al., 2016; LEE et al., 2008; NEAL et al., 2009). Apesar desses avanços, os arcabouços artificiais ainda não podem imitar as estruturas heterogêneas e elaboradas contidas na MEC natural e, portanto, não é provável que reproduzam o microambiente *in vivo* necessário para o comportamento celular adequado ao tecido (HUBBELL, 2003). Felizmente, há vários métodos para isolar matrizes extracelulares intactas de tecidos visando a utilização como arcabouços acelulares.

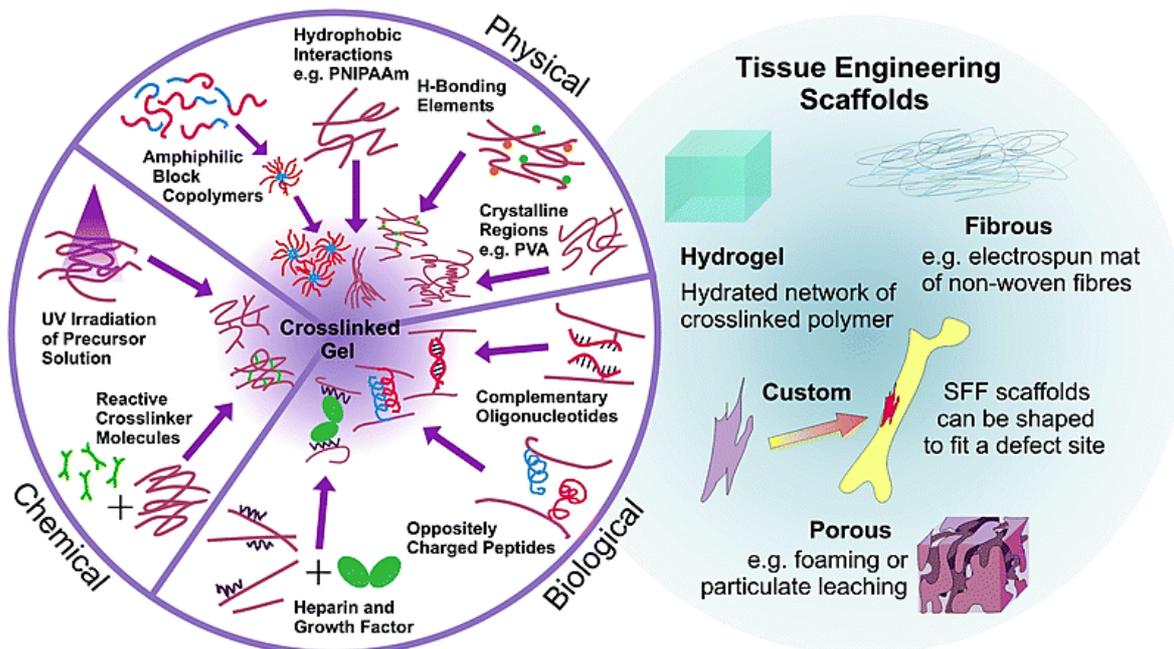


Figura 2. Arcabouços de polímeros sintéticos para engenharia de tecidos.

(Esquerda) Reticulação dentro de hidrogéis. As ligações permanentes e covalentes entre as cadeias poliméricas podem ser criadas por irradiação UV ou por meio de grupos reativos, com ou sem iniciadores, criando géis "químicos". Os *crosslinks* físicos são ligações reversíveis com base em uma variedade de interações não covalentes, e esta abordagem pode ser estendida através do uso de agentes biológicos, como peptídeos. (Direito) Além dos hidrogéis, os arcabouços obtidos por engenharia tecidual podem apresentar morfologias fibrosas, porosas ou derivadas. *Adaptado com permissão de PLACE, E. S. et al. Synthetic polymer scaffolds for tissue engineering. Chemical Society Reviews, v. 38, n. 4, p. 1139, 24 mar. 2009. (PLACE et al., 2009).*

3.2. Arcabouços de matriz extracelular

As matrizes extracelulares naturais, dadas as suas estruturas teciduais específicas, apresentam-se como arcabouços de tecido pronto. Elas podem ser isoladas dos tecidos utilizando um processo de remoção celular denominado descelularização (GILBERT; SELLARO; BADYLAK, 2006). Esse processo geralmente diminui a bioatividade e a integridade estrutural por causa da biocompatibilidade. Foi demonstrado, em relação ao crescimento celular e à diferenciação direta das células-tronco, que a cultura com MEC integral intacta é superior às misturas heterogêneas de proteínas da MEC, que por sua vez são superiores aos componentes individuais da matriz (CORTIELLA et al., 2010; PHILP et al., 2005). A MEC implantada demonstrou promover a angiogênese, o recrutamento de células progenitoras circulantes e a remodelação construtiva do tecido (BADYLAK, 2002).

Os arcabouços de MEC não correspondentes ao doador, tanto de origem humana como de origem xenogênica, têm sido implantados clinicamente por promoverem reparo tecidual. Os constituintes da MEC são geralmente conservados entre espécies e é possível preparar xenoenxertos que são imunologicamente tolerados e que não desencadeiam processo de rejeição por implante mediado por células (ALLMAN et al., 2001; HUBBELL, 2003; HUDSON et al., 2004; SUN et al., 2006). A possibilidade de implantar enxertos de MEC não humanos aumenta significativamente a variedade de materiais disponíveis para arcabouços. Os arcabouços derivados de tecidos humanos e de porcos têm sido implantados clinicamente. Estes incluem osso, pele, bexiga, nervo, válvula cardíaca e intestino delgado (BROOKS et al., 2012; BROWN et al., 2010; BUINEWICZ; ROSEN, 2004; CHEUNG; DUAN; BUTCHER, 2015; CHUNG et al., 2016; EL-KASSABY et al., 2003; IOP; GEROSA, 2015; ISAACS; SAFA, 2017; PU, 2005; WANG et al., 2007; XUE et al., 2016). Uma tendência recente é a descelularização de órgãos para o propósito de regeneração de órgãos inteiros; esses arcabouços estão sendo criados a partir de rim, coração, pulmão, baço, fígado e pâncreas (BAPTISTA et al., 2011; CARALT et al., 2015; CHOI et al., 2015; CONRAD et al., 2010; CORTIELLA et al., 2010; DE KOCK et al., 2011; DESTEFANI; SIRTOLI; NOGUEIRA, 2017; GAO et al., 2015; GUAN et al., 2015a, 2015b; KHAN et al., 2014; OTT et al., 2008, 2010; PETERSEN et al., 2010; POORNEJAD et al., 2016; SHUPE et al., 2010; UYGUN et al., 2010; UZARSKI et al., 2015a; WAINWRIGHT et al., 2010; WANG et al., 2015; WILLENBERG et al., 2015).

3.3. Descelularização tecidual

A remoção de células de um tecido, ou descelularização, permite a obtenção de uma MEC residual. Esta matriz pode então ser usada como um arcabouço para repovoamento celular. O processo de descelularização pode envolver métodos físicos como deformação, pressurização, agitação, sonicação ou ciclos de congelamento-descongelamento; métodos químicos como ácido, base, álcool ou exposição à detergentes, tratamentos de quelação ou uso de estresse osmótico; ou métodos enzimáticos para degradar o material celular ou inibir proteases endógenas de degradação da ECM (CRAPO; GILBERT; BADYLAK, 2011; GILBERT; SELLARO; BADYLAK, 2006). Cada passo em um protocolo de

descelularização pode produzir um resultado exclusivo dependente do tecido, localização, espécie e idade (BADYLAK, 2002). O objetivo geral é a criação de um arcabouço que evoque a resposta celular máxima com imunogenicidade mínima (HUDSON et al., 2004). Isto é alcançado com a remoção de detritos celulares, incluindo DNA e outros antígenos celulares, e pela preservação de proteínas e estruturas de MEC (CRAPO; GILBERT; BADYLAK, 2011). O principal desafio é que cada etapa no processo de remoção de células pode ter um efeito nocivo sobre a MEC nativa, como a desnaturação de proteínas de adesão celular, de modo que o procedimento deve ser cuidadosamente equilibrado entre remoção de células e a destruição ou remoção de proteínas nativas da MEC.

O método mais usual para a descelularização tecidual é o tratamento com detergentes biológicos (CRAPO; GILBERT; BADYLAK, 2011; GILBERT; SELLARO; BADYLAK, 2006). Os detergentes desestabilizam as interações lipídicas e proteicas e são utilizados para quebrar as membranas celulares e carrear o material celular. As propriedades detergentes são derivadas da natureza anfifílica. A carga do grupo da cabeça do detergente define-o como não iônico, catiônico, aniônico ou zwitteriônico. A capacidade detergentes, ou a eficácia do detergente, depende da concentração crítica de micelas (CCM). A CCM é a concentração na qual uma micela se formará. Abaixo da CCM, as moléculas de detergente incorporarão uma membrana celular, mas a auto associação ao detergente, incluindo os complexos lipídico-detergente e proteína-detergente, não se formará a menos que a CCM seja excedido. Os detergentes com CCM baixos formam micelas mais estáveis com a incorporação lenta de moléculas. A CCM varia com a temperatura, o pH, a força dos contra-íons e a presença de proteínas, lipídios e outros agentes tensoativos (SEDDON; CURNOW; BOOTH, 2004). Os detergentes iônicos podem modificar a estrutura proteica e impedir os agregados proteicos em maior extensão do que os detergentes não iônicos ou zwitteriônicos. Eles são, portanto, mais eficazes na remoção de detritos celulares, mas também podem causar maiores danos às proteínas da membrana basal. Fatores como o grupamento químico da cabeça, a concentração e a duração da exposição ao detergente afetam o resultado de uma descelularização (GILBERT; SELLARO; BADYLAK, 2006). Os protocolos baseados em detergentes têm sido particularmente efetivos na descelularização de órgãos inteiros (BAPTISTA et al., 2011; CRAPO; GILBERT; BADYLAK, 2011; DESTEFANI; SIRTOLI; NOGUEIRA, 2017). As soluções são tipicamente perfundidas através da vasculatura, o que

promove uma difusão eficiente para todas as áreas do órgão (PLENICEANU; HARARI-STEINBERG; DEKEL, 2010). O estabelecimento de um protocolo efetivo de descelularização utilizando detergentes para a produção de arcabouços de órgãos inteiros seria um passo significativo para a possibilidade do desenvolvimento *in vitro* de rim funcional.

4. CAPÍTULO 1

Artigo I

ADVANCES IN THE KNOWLEDGE ABOUT KIDNEY DECELLULARIZATION AND REPOPULATION



Advances in the Knowledge about Kidney Decellularization and Repopulation

Afrânio Côgo Destefani^{1,2,3†}, Gabriela Modenesi Sirtoli^{1,2†} and Breno Valentim Nogueira^{1,2,3*}

¹Tissue Engineering Core—LUCCAR, Morphology, Federal University of Espírito Santo (UFES), Vitória, Brazil, ²Health Sciences Center, Federal University of Espírito Santo (UFES), Vitória, Brazil, ³Health Sciences Center, Postgraduate Program in Biotechnology/RENORBIO, Vitória, Brazil

OPEN ACCESS

Edited by:

Paul De Vos,
University Medical Center
Groningen, Netherlands

Reviewed by:

Martin (Marco) Harmsen,
University Medical Center
Groningen, Netherlands
Emilio Isaac Alarcon,
University of Ottawa, Canada

*Correspondence:

Breno Valentim Nogueira
brenovalentim@gmail.com

[†]These authors have contributed
equally to this work.

Specialty section:

This article was submitted
to Biomaterials,
a section of the journal
Frontiers in Bioengineering and
Biotechnology

Received: 18 January 2017

Accepted: 03 May 2017

Published: 01 June 2017

Citation:

Destefani AC, Sirtoli GM and
Nogueira BV (2017) Advances in the
Knowledge about Kidney
Decellularization and Repopulation.
Front. Bioeng. Biotechnol. 5:34.
doi: 10.3389/fbioe.2017.00034

End-stage renal disease (ESRD) is characterized by the progressive deterioration of renal function that may compromise different tissues and organs. The major treatment indicated for patients with ESRD is kidney transplantation. However, the shortage of available organs, as well as the high rate of organ rejection, supports the need for new therapies. Thus, the implementation of tissue bioengineering to organ regeneration has emerged as an alternative to traditional organ transplantation. Decellularization of organs with chemical, physical, and/or biological agents generates natural scaffolds, which can serve as basis for tissue reconstruction. The recellularization of these scaffolds with different cell sources, such as stem cells or adult differentiated cells, can provide an organ with functionality and no immune response after *in vivo* transplantation on the host. Several studies have focused on improving these techniques, but until now, there is no optimal decellularization method for the kidney available yet. Herein, an overview of the current literature for kidney decellularization and whole-organ recellularization is presented, addressing the pros and cons of the actual techniques already developed, the methods adopted to evaluate the efficacy of the procedures, and the challenges to be overcome in order to achieve an optimal protocol.

Keywords: kidney transplantation, bioengineering, decellularization, regenerative medicine, stem cell

INTRODUCTION

Chronic kidney disease (CKD) and its complications are of paramount importance in the context of public health (Lai et al., 2013), reaching approximately 8–16% of the adult population worldwide (Jha et al., 2013; United States Renal Data System, 2015). Its overall prevalence progresses at an alarming rate and is correlated with the dramatic increase in obesity in the last 30 years, leading to Type II diabetes, metabolic syndrome, and renal failure—also known as end-stage renal disease (ESRD) (Nguyen and El-Serag, 2010; Yokote et al., 2012). In the USA, it is estimated that one in every ten Americans, approximately 23 million people aged 20 years or older, has some form of CKD [Centers for Disease Control and Prevention (CDC), 2014], and this number is expected to rise given that the elderly population is also growing (Murray et al., 2013).

Although the incidence of CKD is rising, the available therapeutic options remain limited (Levey and Coresh, 2012). Current therapeutic options for renal replacement are limited to peritoneal dialysis, hemodialysis, or kidney transplantation (KT). Renal transplantation is the ideal treatment for patients with ESRD: it improves long-term survival (Wolfe et al., 1999), leads to a better quality of

life (Dew et al., 1997; Anil Kumar and Mattoo, 2015), and is effective in terms of cost compared with long-term dialysis (Hutton, 1999). The success of renal transplantation depends on the donor type, age, sex, race, and primary cause of ESRD. In general, the 1-year graft survival and patient survival advantage experienced by living donor transplant recipients persist at 5 and 10 years post-transplant (USRDS, 2016). According to the United States Renal Data System, in 2013, the rate of 5-year graft survival was 73% for recipients of deceased donor transplants, while it was 85% for living donor transplant recipients (United States Renal Data System, 2015). However, KT is often associated with chronic dysfunction linked to immune rejection (National Kidney and Urologic Diseases Information Clearinghouse, 2012). In addition, the significant increase in the use of living kidney donors and cadavers is not compatible with the availability of organs; in the last years, there were more than 100,000 patients in the USA waiting for a transplant with an average of more than 3.6 years (Matas et al., 2015; United States Renal Data System, 2015).

ALTERNATIVE MANAGEMENT OF KIDNEY DISEASE

For patients with ESRD, KT is closely associated with an increase in life expectancy, improving the quality of life, and is a cost-effective therapy (Wolfe et al., 1999; Johnson et al., 2000; Ojo et al., 2001; Merion et al., 2005; Tonelli et al., 2011; Rana et al., 2015). To emphasize further this growing disparity between the supply and demand for organs, the total number of KTs performed annually in the United States has remained static over the last decade (Valapour et al., 2014). Furthermore, there are an increasing number of elderly donors and recipients for KT (Wolfe et al., 2010; Abecassis et al., 2012). US initiatives, for example, have resulted in an increase in non-conventional sources of donors, such as expanded criteria donors (ECD) (Port et al., 2002; Stratta et al., 2006; Pascual et al., 2008; Klein et al., 2010), donors after cardiac death donation (DCD) (Howard et al., 2005; Abt et al., 2006; Farney et al., 2011), standard criteria donors (SCD) with warm ischemia times or prolonged cold (CIT) (Roodnat et al., 2003; Kayler et al., 2011; Kim et al., 2013; Debout et al., 2015; Xia et al., 2015), acute kidney injury (AKI) donors (Anil Kumar et al., 2006; Kayler et al., 2009; Farney et al., 2013; Hall et al., 2015; Heilman et al., 2015; Xia et al., 2015), double-kidney transplantation (DKT) and donors at the extremes of age (Johnson et al., 1996; Cruzado et al., 2007; De Serres et al., 2010; Fernández-Lorente et al., 2012). Recently, it was demonstrated that desensitization of the patient and subsequent transplantation with a kidney from an incompatible live donor increase the patient survival rate compared with those who remain on the waiting list for transplantation (Orandi et al., 2016). However, all of these alternatives have the drawback of requiring donors.

Several studies have shown that regenerative therapy using mature adult or stem cells may have success. They have demonstrated that postnatal mammalian kidneys may be partially repaired after resection, and this regeneration is mainly due to the proliferation of mature surviving cells or stem cells present in the kidney, such as glomerular parietal epithelial cells (a type of renal

progenitor cell) (Vogetseder et al., 2008; Swetha et al., 2011; Wen et al., 2012; Franquesa et al., 2013). After stress, these cells migrate to the damaged area and proliferate and then differentiate into new somatic cells (Hanna et al., 2010; Yamanaka and Blau, 2010; Wen et al., 2012). These results suggest that regenerative solutions offer great potential for the treatment of ESRD. However, achieving a clinically significant regeneration level has proven to be extremely difficult due to the complexity of this organ (Yu et al., 2014).

Another alternative to the shortage of organs would be xenotransplantation using animal organs (Yokoo and Kawamura, 2009; Wang et al., 2014), through a strategy that combines organ decellularization and the insertion of patient's cells to avoid the risk of adverse immunological reactions (Barakat et al., 2012). The use of pig kidneys for tissue engineering is an attractive approach, mainly because the size of porcine organs is similar to that of humans, and pig scaffolds may allow better adhesion, survival, and maintenance of human cells than scaffolds obtained from dogs or monkeys (Nakayama et al., 2010; Song and Ott, 2011; Faulk et al., 2014a,b; Habka et al., 2015; Moini et al., 2015; Rana et al., 2017; Lih et al., 2016; McKee and Wingert, 2016). The idea of building a functional kidney using specific stem cells from the patient supports a tangible alternative. In the last 2 years, there has been substantial progress toward this goal (Uzarski et al., 2014). In theory, this approach could increase the range of options for KT, enabling the improvement of more patients and potentially minimizing or eliminating the need for long-term immunosuppressive therapy and reducing the waiting time for treatment.

TISSUE ENGINEERING

The increasing number of patients facing end-stage diseases, the shortage of organ donors, and challenges that surround allogenic transplants drive the evolution of tissue engineering and regenerative medicine (Caldas et al., 2011). Tissue engineering is a promising alternative to organ transplantation, with a huge potential in tissue regeneration and repair processes, providing solutions to the conditions in which native tissue is compromised (Lu et al., 2011; He and Callanan, 2013; Teodori et al., 2014). Recent advances in the use of stem cells and regenerative medicine have offered new hope for the treatment of kidney disease, especially ESRD (Krause and Cantley, 2005; Ross et al., 2009; Li et al., 2010).

To reconstruct a new tissue, a triad of components is needed: cells, biomaterials to be used as supports or scaffolds, and growth factors (Ahn et al., 2007; Narayanan et al., 2009; Ng et al., 2011). Biomaterials play a central role because most mammalian cell types are dependent on anchorage (Hollister, 2005; O'Brien, 2011; Cheng et al., 2013; Guan et al., 2015a), and one of the crucial challenges of this area is the selection of the ideal scaffold for cell attachment to ensure its functional integrity. Using a decellularized organ composed of extracellular matrix (ECM), regenerative medicine proposes new horizons (Gilbert et al., 2006; Crapo et al., 2011).

Biological scaffolds consisting of ECM are commonly used for various reconstructive surgical applications, and their use in regenerative medicine for tissue and organ replacement has

increased in the last decade. ECM common sources include the dermis, pericardium, small intestine, sub-mucosa, and bladder (Badylak, 2002; Badylak et al., 2009; Rose et al., 2009; Orlando et al., 2011a; Yagi et al., 2013). It is possible to obtain ECM scaffolds from different animals, which can later be recolonized with human cells and then used for transplantation in humans (Cooper et al., 2002).

The ECM is a three-dimensional network that forms a milieu surrounding cells that reciprocally influences cellular function to modulate diverse fundamental aspects of cell biology (Hynes, 2009) such as support for organs and tissues, for cell layers in the form of basement membranes, and for individual cells as substrates for cell motility (Hynes, 2009). Two main classes of extracellular macromolecules make up the matrix (Lai et al., 2013) polysaccharide chains of the class called glycosaminoglycans (GAGs)—a gel-like polysaccharide ground substance, which are usually found covalently linked to protein in the form of proteoglycans, and (United States Renal Data System, 2015) fibrous proteins, including collagen, elastin, and several other molecules (laminins, fibronectins, tenascins) (Brown et al., 2006), which have both structural and adhesive functions (Alberts et al., 2002). GAGs are highly negatively charged and they bind positively charged ions and trap water molecules to form hydrated gels, thereby providing mechanical support to the ECM (Cooper, 2000). In addition, this structure allows nutrition, innervation, cell signaling, and tissue regeneration (Bosman and Stamenkovic, 2003; Naranjo et al., 2009; Ramage, 2011; Keane et al., 2012; Reticker-Flynn et al., 2012). In the kidney cortex, the ECM is present in different anatomical areas, with different functions depending on their molecular components. The ECM present in the interstitial medulla is physiologically more prominent than cortical interstitial ECM and quantitatively greater from the exterior to the interior of the medulla/papilla. The hilar region—renal pelvis (e.g., sub-urothelial basement membrane) and renal capsule also comprise the ECM. Renal interstitial ECM normally consists of collagen type I, III, V, VI, VII, and XV; sulfated- and non-sulfated GAGs; and polysaccharides (Genovese et al., 2014). Specifically, regarding the composition of the ECM of the glomerular basement membrane, the major compounds are laminin, type IV collagen, heparan sulfate proteoglycan (including agrin), and nidogen (Suh and Miner, 2013).

It is possible that scaffolds composed of ECM that integrate the basic structure of the organ that may be used to promote kidney regeneration. In the last decade, numerous studies have demonstrated that constructed ECM scaffolds can support the growth and differentiation of multiple cell types (Reing et al., 2010; Lu et al., 2011; Moroni and Mirabella, 2014). For success clinically, the ECM must be decellularized (Freytes et al., 2008; Choi et al., 2012). It has been shown that decellularized scaffolds may maintain the tri-dimensional composition and biological activity of the ECM; this enables it to be a useful material for cell adhesion, differentiation, and proliferation (Barkan et al., 2010; Vorotnikova et al., 2010; Tien and Nelson, 2014). The advantage of using acellular scaffolds of organs is the possibility not only of using the ECM as a structural scaffold but also allowing the spread of signals that can be exchanged with the cells that adhere to induce migration and differentiation (Gilbert et al.,

2007; Gong et al., 2008). The ECM also plays an important role in the maintenance of an adequate network of vessels and growth factors, which allows the appropriate structure of the organ when rebuilt (Ross et al., 2012). These characteristics are indispensable in complex tissues with different cellular components.

Because of the high complexity of the anatomical structure and composition of kidney, renal ECM scaffold has been proposed as a promisor strategy for the reconstruction of a viable kidney. However, obtaining a viable kidney ECM is extremely difficult because of its complex composition, including amino acids, collagens, glycoproteins, GAGs, and microstructures required for filtration (Badylak, 2004; Gagliardini et al., 2010; Mecham, 2001). The appropriate process for the decellularization of tissues/organs must preserve the essential components of the ECM (Song and Ott, 2011). By contrast, synthetic organic scaffolds are inappropriate in terms of complexity. Regarding highly artificial efficient membranes and cell-based bioreactors, there have been successful attempts concerning the miniaturization of the existing bioartificial kidney using various silicon and related thin-film material substrates commonly used in the construction of microelectromechanical systems (MEMS), as well as novel silicon nanopore membranes (SNMs) (Fissell et al., 2006; Fissell and Roy, 2009). The final developmental step based on prior success of the renal tubule cell assist device (RAD) in acute disorders and wearable bioartificial kidney (WEBAK) in preclinical models is the current approach to design, fabricate, and test in preclinical models a functional fully implantable bioartificial kidney (IBAK) (Roy et al., 2011). However, there are still substantial technical challenges regarding the safety and operation of the device, as well as its effectiveness, which need to be overcome (Kooman et al., 2015).

The implantation of renal ECM scaffolds has shown benefit in the promotion of angiogenesis, recruitment of circulating progenitor cells, minimization of immunogenic reactions, and reduction of disease transmission risks (Vavken et al., 2009). Thus, decellularization of an entire organ arises as a novel approach to the generation of a natural 3D architecture.

METHODS AND PROCESSES APPLIED FOR ORGAN DECELLULARIZATION

Decellularization is a process that may involve a blend of chemical, physical, and enzymatic treatments (Bolland et al., 2007; Badylak et al., 2009; Lu et al., 2011; He and Callanan, 2013). More specifically, it may employ detergents, salts, enzymes, and/or physical agents for the removal of tissue and organ cells. There are many existing methods for different applications (Gilbert et al., 2006; Badylak et al., 2011; Gilbert, 2012; Ofenbauer et al., 2015). In general, the process removes the cells present in the tissue, preserving partly the proteins of the ECM, such as collagen, with significantly reduced immunogenic potential (Mirmalek-Sani et al., 2013; Caralt et al., 2015). Thus, the ECM can be repopulated with cells extracted from the patient, creating a new organ with minimal probability of being rejected (Hammerman, 2002; Badylak and Gilbert, 2008).

Currently, the most efficient and robust method for decellularization is the use of chemical infusion. The chemical reagents, particularly detergents or acids, remove native cells by disrupting cell membranes and isolating the cellular components of the ECM (Gilbert et al., 2006). For example, peracetic acid (PAA) is commonly used because it removes nucleic acids with minimal effect on the ECM structure (Gilbert et al., 2008; Gao et al., 2015). Triton X-100, a non-ionic detergent, is the most efficient for the removal of cellular debris from tissues such as heart valves (Liao et al., 2008). Sodium dodecyl sulfate (SDS) is reported to be more effective than Triton X-100 to eliminate cells in the medullary regions of dense organs such as the kidney (Nakayama et al., 2010), and sodium deoxycholate (NaDOC), an anionic detergent, can completely remove the cytoplasmic proteins in dense tissues (Wang et al., 2014).

Decellularized kidneys using Triton X-100 retained growth factors and ECM components, although the cells were not properly removed. On the other hand, decellularization with SDS could sufficiently remove cells while preserving the ECM (Mathiesen et al., 2007; Tanemoto et al., 2008; Nakayama et al., 2010, 2011, 2013; Ross et al., 2012; Sullivan et al., 2012; Caralt et al., 2015). Choi et al. (2015), however, obtained opposite results regarding the comparison between the effects of SDS and Triton X-100 on porcine kidneys. They observed that a richer ECM protein and growth factor content were present in the Triton-treated scaffold than in the SDS-treated scaffold; additionally, cell viability, adherence, and proliferation were higher with the Triton-treated scaffold than with the SDS-treated scaffold (Choi et al., 2015). Furthermore, other researchers have demonstrated that the combination of the two agents produces better results (Sugawara et al., 2011). In view of these divergences, there is still a need to identify more suitable decellularizing agents to improve the quality of the obtained scaffolds (Table 1) (Ross et al., 2009, 2012; Peloso et al., 2013; Song et al., 2013).

ELEMENTS THAT INFLUENCE THE DECELLULARIZATION PROCESS

The decellularization processes require sensitive methods due to the fragility of the organs and their internal structural complexity. Therefore, it is necessary to develop techniques for decellularization and residual DNA removal simultaneously to preserve the integrity of the ECM. There are several factors that influence the process of decellularization, such as cell density, body weight, lipid content, the organ thickness, and the intrinsic properties of the substances employed to remove the cells (Ross et al., 2009). Furthermore, it is necessary to consider the mechanical forces involved in the process, such as the pressure of perfusion, flow rate, and possibility of the use of retrograde infusion of fluids (Lin et al., 2016). Another point to be considered is that the methods used in the organs of small animals (e.g., mice) have to be adapted to larger animals, such as monkeys and pigs, which resemble humans, at least regarding the size of the organ. In this sense, some studies have already demonstrated good results with the

decellularization of monkey's and pig's kidneys, with preservation of the ECM scaffolds (Badylak et al., 2009; Orlando et al., 2011b, 2012; Sullivan et al., 2012).

Regarding the types and concentrations of detergents employed in the decellularization process, we considered that each detergent exhibits a distinct pattern of action depending on the tissue involved (Baptista et al., 2009). There are two detergents widely used currently—Triton X-100 and SDS—at concentrations ranging from 0.1 to 5%, perfused alone or in combination (Baptista et al., 2011; Barakat et al., 2012; Sullivan et al., 2012; Nakayama et al., 2013). Recently, He et al. (2016) compared the success of rat kidney decellularization through SDS perfusion in different combinations of time of perfusion (4 and 8 h) and concentration of SDS (0.125, 0.25, 0.5, and 1.0%), with the best result obtained with 0.125% SDS perfused through 4 h. In this condition, histological and immunohistochemical evaluation were not different from other conditions, but growth factor maintenance was more efficient. Another recent approach to decrease SDS exposure time and improve the decellularization process of porcine kidneys employed a combination of freezing/thawing, low concentrations of SDS, incremental increases in flow rate under constant pressure, and applying osmotic shock to the cellular membranes. These procedures preserved the microstructure of the scaffold while still removed 99% of the DNA, enhanced cell–ECM interactions, and allowed the seeded cells to grow more rapidly when compared to kidneys decellularized only with SDS perfusion for longer period (Pooornejad et al., 2016a). This same group compared the effect of five different decellularization agents on porcine renal tissue (0.1 N NaOH, 1% PAA, 3% Triton X-100, 1% SDS, and 0.05% trypsin/EDTA). While the NaOH solution was the most efficient on cell removal and cell viability after recellularization, it damaged the ECM components, besides it also produced lots of caustic waste. This could be avoided with the use of HCl to neutralize NaOH. In turn, SDS led to less severe damage to ECM structure, but the cell viability and proliferation after recellularization were not as efficient as the NaOH solution. Triton X-100 and PAA preserved ECM structure and growth factors, although these reagents were not as effective as the SDS and NaOH on cell removal (Pooornejad et al., 2016b). In summary, the NaOH solution was considered the best choice if the intention is implantation of cells and rapid biodegradation of the scaffold. Nevertheless, adopting a multistep decellularization protocol using ionic and non-ionic detergent exposure would probably result in better preservation of a relatively intact structure.

DECELLULARIZATION ASSESSMENT

Maintaining the architecture and composition of the ECM is the largest challenge to the success of the decellularization process. With respect to the ECM composition, although many groups have demonstrated the retention of collagen, laminin, elastin, and fibronectin after decellularization (Caralt et al., 2015), the reduction or depletion of ECM proteins and growth factors has also been reported (Singh et al., 2010; Akhyari et al., 2011; Petersen et al., 2012; Wallis et al., 2012; Caralt et al., 2015). The

TABLE 1 | An overview of the kidney decellularization literature.

Source kidney	Methods						Overall time	Results	Reference
	Before perfusion	Decellularization solutions	Perfusion pressure	Perfusion flow rate	After perfusion	Threshold			
Goat	Heparinization	0.1% SDS; gradient of SDS (0.5%, 1.0%); 0.1% TritonX-100; 5 mM calcium chloride and magnesium sulfate	100 mmHg at 37°C	Not reported	0.0025% DNase; dH ₂ O + 1x PBS containing 10,000 U/mL penicillin G, 10 mg/mL streptomycin and 25 µg/mL amphotericin B at 1 mL/min constant perfusion	Time	5–6 days	Preserved the structure and composition of renal ECM and vascular structures within the scaffold No evidence of residual cellular components was found	Vishwakarma et al. (2014)
Human	dH ₂ O at a rate of approximately 12 mL/min for 12 h	0.5% SDS for 48 h	Not reported	12 mL/min	PBS 5 days at a flow rate of 6 mL/min	Not reported	7 days	SDS-based decellularization protocol completely cleared the cellular compartment in these kidneys, while the innate ECM framework retained its architecture and biochemical properties	Orlando et al. (2013)
Human	Placed on ice until decellularization PBS at the rate of 12 mL/min for 12 h	0.5% SDS	Not reported	12 mL/min	DNase for 6 h at a flow rate of 6 mL/h and then with PBS at the same flow rate for 5 days	Not reported	7–8 days	Discarded human kidneys are a suitable source of renal scaffolds because they maintain a well-preserved structure and function of the vasculature, as well as growth factors that are fundamental to achieve a satisfying recellularization of the scaffold <i>in vivo</i> due to their angiogenic properties.	Peloso et al. (2015)
Mouse	Physical decellularization: samples were washed in normal saline and stored for 1 week at -4°C. Chemical decellularization.	Nitrogen for 2 min. 1% SDS	Not reported.	Not reported.	PBS at 37°C PBS (24 h)	Time.	1–2 days.	Complete removal of cells and nuclei.	Rafiqdoust et al. (2015)

(Continued)

TABLE 1 | Continued

Source kidney	Methods					Overall time	Results	Reference	
	Before perfusion	Decellularization solutions	Perfusion pressure	Perfusion flow rate	After perfusion				Threshold
Mouse	Vessels were cannulated and attached to a peristaltic pump.	0.1% SDS 0.1% Triton X100 for 24–72 h 0.4% Sodium deoxycholate for 24–72 h ± 90 U/mL benzoylase for 2 h.	Not reported.	0.2 and 0.4 mL/min for 12, 24, 48 or 72 h	PBS PBS/PenStrep for 1 h.	Time.	1–2 days	Acellular kidney provided regionalized factors that are highly instructive, resulting in organized kidney structures within the acellular kidney.	Sambi et al. (2017)
Porcine	Vessels were cannulated and attached to a peristaltic pump, followed by overnight perfusion of ddH ₂ O.	1% of the detergent Triton X-100 and 0.1% ammonium hydroxide in ddH ₂ O.	Not reported.	Not reported.	10–60 mL/h for 24 h or until translucent. Perfused with ddH ₂ O prior to sterilization (gamma irradiation).	The removal of the cellular components is observable with the transparency/white color of the decellularized bioscaffolds.	2 days.	Preserved vascular network.	Baptista et al. (2009)
Porcine	Perfused with 10 USP units/mL Sodium heparin in 1x PBS for 15 min at 0.75 L/h.	0.5% SDS in 1x PBS, 0.25% SDS in 1x PBS, or 1% TritonX-100/0.1% Ammonium Hydroxide in 1x PBS were perfused through the kidneys for a total of 36 h.	Not reported.	0.75 L/h.	1x PBS for 48 h; 500 mL of DNase solution (0.0025 w/w% DNase in 1x PBS at neutral pH) overnight; Rinse with 1x PBS for 1 h; 10.0 kGy gamma irradiation to sterilize the decellularized scaffolds.	Time.	6–7 days.	Advantages for the use of 0.5% SDS in the decellularization of kidneys of a clinically relevant size.	Sullivan et al. (2012)
Porcine	Rinsed with heparinized PBS.	1% (v/v) SDS in ddH ₂ O.	Not reported.	Approximately 100 mL/min.	PBS solution was perfused for 24 h.	White appearance.	2–3 days.	Preservation of major architecture and vasculature.	Park and Woo (2012)

(Continued)

TABLE 1 | Continued

Source kidney	Methods						Overall time	Results	Reference
	Before perfusion	Decellularization solutions	Perfusion pressure	Perfusion flow rate	After perfusion	Threshold			
Porcine	PBS	1% Triton X-100 or 1% SDS.	Not reported.	Not reported.	dH ₂ O.	Transparency.	Not reported.	Verified that 1% Triton X-100 is a more suitable decellularizing agent than SDS regarding structural, biochemical integrity and biocompatibility of the scaffold.	Chae et al. (2014)
Porcine	Perfused with heparinized 1x PBS solution.	0.5% SDS.	80 mmHg.	Not reported.	dH ₂ O.	Time.	2–3 days.	Freeze porcine kidneys prior to decellularization to prevent spoilage by bacterial growth and after decellularization to prevent proteins from denaturing. The decellularized organs can then be preserved for months without cryoprotectants and thawed just prior to recellularization.	Poornejad et al. (2015)
Porcine	Perfusion of heparinized PBS.	dH ₂ O; 1% SDS; 1% Triton X-100.	Not reported.	10 mL/min.	PBS.	Translucency.	3–4 days.	Scaffolds maintain their basic components and show intact vasculature system.	Guan et al. (2015a)
Porcine	Saline solution.	1.0% Triton X-100; PBS; 0.25% or 0.75% SDS;	80 mmHg.	1 L/h.	PBS; DNase; 1% antibiotics/ antimycotics; Sterilized with 1% MIN-NCARE® (4.5% PAA and 22.0% hydrogen peroxide), or by irradiation with 12–16 kGy over 24–30 h.	Time.	4 days.	Maintenance of distinct vascular and collecting system compartments.	Willenberg et al. (2015)

(Continued)

TABLE 1 | Continued

Source kidney	Methods					Overall time	Results	Reference	
	Before perfusion	Decellularization solutions	Perfusion pressure	Perfusion flow rate	After perfusion				Threshold
Porcine	Heparinized (PBS) solution was perfused into the kidneys through the calcineinized artery to prevent thrombosis. The harvested kidneys were then preserved at -20°C .	Solutions of 0.1 N NaOH (pH 11.8–12), 1% (w/v) PAA (pH 2.6), 3% (w/v) Triton X-100 (pH 7.2), 1% (w/v) SDS (pH 8.1), and 0.05% Trypsin/ethylenediaminetetraacetic acid (EDTA).	Bench top shaker (70–80 r/min)	Bench top shaker (70–80 r/min)	Deionized (DI) water wash.	Time	24 h.	The NaOH solution induced the most efficient cell removal and resulted in the highest amount of cell viability and proliferation after recellularization, although it also produced the most significant damage to collagenous fiber networks. The SDS solution led to less severe damage to the ECM structure but it resulted in lower metabolic activity and less proliferation. PAA and Triton X-100 resulted in minimum disruption of ECMs and the most preserved glycosaminoglycans (GAGs) and FGF. However, these last two agents were not as efficient in removing cellular materials as NaOH and SDS, especially PAA, which left more than 80% of cellular material within the ECM.	Poornejad et al. (2016b)

(Continued)

TABLE 1 | Continued

Source kidney	Methods					Overall time	Results	Reference	
	Before perfusion	Decellularization solutions	Perfusion pressure	Perfusion flow rate	After perfusion				Threshold
Porcine	The kidneys were removed with special care to ensure that a sufficient length of renal artery was preserved. Heparinized PBS solution was perfused into the kidneys through a catheter to prevent thrombosis. The harvested kidneys were then preserved at -20°C until decellularization. After thawing overnight at 4°C , fat was stripped from the renal capsule, excess arterial tissue was excised, and the kidneys were cannulated via the renal artery with white nylon tubing.	Hypertonic solution (0.5 M NaCl in H_2O) was pumped into the kidneys for 30 min. 0.5% w/w SDS solution for 30 min, followed by DI water (hypotonic solution) for 30 min.	80 mmHg	Began at 10 mL/min and was incrementally increased every 30 min by 1.5 mL/min to approximately 40–50 mL/min.	DI water wash.	White kidney	2 days.	Preservation the microstructure while still removing 99% of the DNA.	Poornajad et al. (2016a)
Porcine Yorkshire	Washed twice with PBS.	1% Triton X-100 or 1% SDS containing 100 U/mL penicillin and 100 $\mu\text{g}/\text{mL}$ streptomycin. Samples were decellularized at 4°C in a shaking incubator (200 rpm) Sullivan et al. (2012)	Not reported.	Not reported.	DNase (30 $\mu\text{g}/\text{mL}$) in PBS for 1 h; Decellularized kidney scaffolds were cryo-embedded in optimum cutting temperature compound.	Transparency.	10–14 days.	Identified 1% Triton X-100 as a more suitable decellularizing agent for porcine renal ECM scaffolds prior to kidney regeneration.	Choi et al. (2015)

(Continued)

TABLE 1 | Continued

Source kidney	Methods						Overall time	Results	Reference
	Before perfusion	Decellularization solutions	Perfusion pressure	Perfusion flow rate	After perfusion	Threshold			
Porcine (Bama miniature)	Perfused with perfusable NaCl 8.3 g/L, KCl 0.5 g/L, HEPES 2.4 g/L, and EGTA (0.95 g/L). Rinsed twice with PBS and stored at -20°C until use.	ddH ₂ O; 1% SDS; Triton X-100; PAA; NaDOC.	Not reported.	15 mL/min.	PBS.	Time.	1-2 days.	Clearance of cellular components and xenotransgens, including DNA and protein and preservation of the ECM composition.	Wang et al. (2014)
Rat	Renal arteries were cannulated immediately after euthanization of the animal and perfused with PBS with vasodilator (10 mL of 10 μg/mL sodium nitroprusside in PBS, Sigma/UK, followed by 20 mL at 1 μg/mL) until a uniform blanching was observed, after which each kidney was perfused with 30 mL PBS without vasodilator.	SDS at differing concentrations and durations (1.0, 0.125, 0.25, and 0.5%).	Not reported.	10 mL/min	PBS for 1 h	Time.	4 hat 24 h	Improved preservation of both structural and functional components of the whole kidney ECM bioscaffold.	He et al. (2016)
Rat	Heparinized PBS for 15 min.	1% SDS for 12 h, ddH ₂ O for 12 min, 1% Triton X-100 for 30 min, PBS for 48 h, and antibiotic-containing PBS.	100 cmH ₂ O.	10-40 mL/min.	ddH ₂ O.	Time.	3 days.	No cell residue was found in the scaffolds under microscope.	Liu et al. (2015a)

(Continued)

TABLE 1 | Continued

Source kidney	Methods					Overall time	Results	Reference
	Before perfusion	Decellularization solutions	Perfusion pressure	Perfusion flow rate	After perfusion			
Rat	Anesthetized rats were systemically anti-coagulated with heparin, and cannulas were inserted in the renal artery and ureter. The kidney was arterially perfused <i>in situ</i> using a saline solution containing a vasodilator (nitroprusside) to remove the blood. The organ was observed to confirm uniform blanching indicative of even distribution of perfusate and was harvested.	NaDOC as the ionic detergent; Triton X-100 at 0.5, 3, 6, and 10% solutions; ddH ₂ O; DNase, 4% NaDOC; Use of SDS: 3% Triton X-100, DNase, repeat 3% Triton X-100, and then the 4% SDS. 0.05% sodium azide.	Approximately 100 mmHg (perfusion system was gravity based to).	Not reported.	ddH ₂ O.	Time.	5 days.	Both of the detergent-based perfusion protocols successfully produced acellular kidneys that were nearly transparent, yet retained the web-like appearance of the basement membrane. Ross et al. (2009)
Rat	Systemic heparin anticoagulation; Saline solution containing a vasodilator (nitroprusside); Continuous gravity-based perfusion.	Multiple sequential solutions that included Triton X-100 and SDS detergents, DNase, and deionized water rinses.	Approximately 100 mmHg.	Not reported.	ddH ₂ O.	Not reported.	Over 5 days.	New evidence for matrix-to-cell signaling in acellular whole organ scaffolds that induces differentiation of pluripotent precursor cells to endothelial lineage. Ross et al. (2012)

(Continued)

TABLE 1 | Continued

Source kidney	Methods					Overall time	Results	Reference
	Before perfusion	Decellularization solutions	Perfusion pressure	Perfusion flow rate	After perfusion			
Rat	Not reported.	1% Triton X-100; 1% Triton X-100 + 0,1% SDS; 1% Triton X-100 + Trypsin 0.02%-EGTA 0.05%.	Not reported.	1 mL/min; 5 mL/min	Not reported.	Not reported.	2 days. Only Triton/SDS and Trypsin-EGTA/Triton Protocols successfully removed cells while preserving the architecture and components of the ECM in rat kidneys. Triton/SDS Protocol retained a higher amount of FGF compared to the other protocols. Triton/SDS Protocol efficiently removed cells while maintaining scaffold structure and retaining growth factors that may be critical for transplant and reseeded of the scaffold with renal and endothelial progenitor cells.	Caralt et al. (2013)
Rat	Systemic heparinization; Perfusion of heparinized PBS at 30 mmHg arterial pressure for 15 min.	12 h of 1% SDS in ddH ₂ O, 15 min of ddH ₂ O, and 30 min of 1% Triton-X-100 in ddH ₂ O.	30 mmHg constant pressure.	Not reported.	Washed the kidney scaffolds with PBS containing 10,000 U/mL penicillin G, 10 mg/mL streptomycin, and 25 µg/mL amphotericin-B at 1.5 mL/min constant arterial perfusion for 96 h.	Not reported.	4 days. Yield acellular scaffolds with vascular, cortical, and medullary architecture, collecting system and ureters.	Song et al. (2013)
Rat	Kidney was perfused using a saline solution (NaCl 0.9%) containing a vasodilator (nitroprusside, 10 ⁻⁴ M).	1% SDS in PBS for 17 h at a flow rate of 0.4 mL/min;	Physiological range (from 62 ± 16–107 ± 23mmHg).	0.4 mL/min.	ddH ₂ O.	Not reported.	17 h. Rat kidneys can be efficiently decellularized to produce renal ECM scaffolds in a relatively short time and rapid recellularization of vascular structures and glomeruli.	Bonandrini et al. (2014)

(Continued)

TABLE 1 | Continued

Source kidney	Methods					Overall time	Results	Reference	
	Before perfusion	Decellularization solutions	Perfusion pressure	Perfusion flow rate	After perfusion				Threshold
Rat	50 U/mL heparin in 0.01 M PBS, pH 7.4 for 30 min.	0.1% TritonX-100 for 3 h, ddH ₂ O for 30 min, 0.8% (v/v) SDS for 3 h, and ddH ₂ O containing 100 U/mL penicillin and 100 mg/mL streptomycin for 24 h.	Not reported.	8 mL/min.	Kidney scaffolds were kept in 50 mL of ddH ₂ O containing the penicillin and streptomycin at 4 °C for less than 7 days.	Not reported.	8 days.	Decellularized kidney scaffolds could be used to promote renal recovery in the treatment of chronic kidney disease.	Yu et al. (2014)
Rat	Kidneys were harvested without previously administering anticoagulation medication to the animals. Kidneys were frozen at -80 °C in PBS.	ddH ₂ O for 10 min. 1st: SDS concentrations of 0.25, 0.5, 0.66, and 1% combined with a perfusion time of 0.5, 1, 2, and 4 h. 2nd: concentration of SDS was always 0.66% and the perfusion time was 1 h. After the first 30 min of perfusion with SDS, the kidneys were washed for 10 min with ddH ₂ O and then the organs were perfused for another 30 min with the SDS solution.	100 mmHg.	Not reported.	ddH ₂ O for 1 h. Decellularized organs were perfused for 1 h under sterile conditions with recirculated, sterile ddH ₂ O containing 200 U/mL of penicillin and 200 mg/mL of streptomycin.	Not reported.	5 h.	Novel standardized, time-efficient and reproducible protocol for the decellularization of solid tissues to derive a ready-to-use biomatrix within only 5 h.	Burgkart et al. (2014)
Rat	0.01 M PBS, pH 7.4, for 15 min.	0.5% SDS.	Not reported.	Approximately 2 mL/min.	PBS.	Time.	1-2 days.	Successfully produced renal scaffolds by decellularizing rat kidneys with 0.5% SDS, while still preserving the ECM 3D architecture, an intact vascular tree and biochemical components.	Guan et al. (2015b)

(Continued)

TABLE 1 | Continued

Source kidney	Methods						Overall time	Results	Reference
	Before perfusion	Decellularization solutions	Perfusion pressure	Perfusion flow rate	After perfusion	Threshold			
Rat	dH ₂ O.	Protocol 1: 1% Triton X-100; Protocol 2: 1% Triton X-100; 0.1% SDS; Protocol 3: 0.02% Trypsin-0.05% EGTA; 1% Triton X-100.	Not reported.	Not reported.	dH ₂ O.	Time.	1–2 days.	Triton and Triton/SDS preserved renal microarchitecture and retained matrix-bound basic FGF and vascular endothelial growth factor. Trypsin caused structural deterioration and growth factor loss. Triton/SDS-decellularized scaffolds maintained 3 h of leak-free blood flow in a rodent transplantation model and supported repopulation with human iPSC-derived endothelial cells and tubular epithelial cells <i>ex vivo</i> .	Carait et al. (2015)
Rat	Cold PBS was perfused until all blood was cleared. All organs were stored in PBS at -20°C. All organs were gradually thawed at room temperature.	1% Triton X-100, 1% Triton X-100, 0.1% SDS and 0.02% Trypsin-0.05% EGTA/1% Triton X-100 according to Carait et al. (2015)	Not reported according to Carait et al. (2015)	Not reported according to Carait et al. (2015)	Stored scaffolds in PBS at 4°C for a maximum of 2 weeks prior to use.	Transparency.	7 days.	Demonstrated non-invasive monitoring capabilities for tracking dynamic changes within scaffolds as the native cellular component is removed during decellularization and model human cells are introduced into the scaffold during recellularization and proliferate in maintenance culture.	Uzareki et al. (2015)
Rhesus monkeys (<i>Macaca mulatta</i>)	Washed with PBS.	1% SDS.	Not reported.	Not reported.	Washed with PBS and stored in 1% (v/v) penicillin-streptomycin in PBS at 4°C until use (2 months maximum).	Transparency.	10–14 days.	Decellularized scaffolds have an intrinsic spatial ability to influence hESC differentiation by physically shaping cells into tissue-appropriate structures and phenotypes, and additional approaches may be needed to ensure consistent recellularization throughout the matrix.	Nakayama et al. (2013)

(Continued)

TABLE 1 | Continued

Source kidney	Methods					Overall time	Results	Reference
	Before perfusion	Decellularization solutions	Perfusion pressure	Perfusion flow rate	After perfusion			
Rhesus monkeys (<i>Macaca mulatta</i>)	All tissues were placed in DMEM. Kidney sections were washed twice with PBS.	1% (v/v) SDS or 1% (v/v) Triton X-100 diluted in dH ₂ O at either 48°C or 37°C. Decellularization solution was changed 8 h after the initial tissue harvest and then every 48 h until the tissues were transparent.	Not reported.	Not reported.	Washed with PBS.	Transparency.	7–10 days. SDS was the most effective for decellularization of kidney sections. Triton X-100 was unable to completely decellularize the tissues and caused greater disruption of the basement membrane and connective tissue ECM.	Nakayama et al. (2010)
Rhesus monkeys (<i>Macaca mulatta</i>)	All tissues were placed in DMEM upon collection with processing conducted at the time of tissue harvest. Kidney sections were washed twice with PBS.	1% (v/v) SDS diluted in dH ₂ O at 4°C. The solution was changed 8 h after initial tissue harvest and then every 48 h until the tissue was transparent.	Not reported.	Not reported.	washed with PBS; 10% (v/v) penicillin/streptomycin (Gibco, Invitrogen) in PBS at 4°C until use.	Transparency.	7–10 days. Removal of cellular components while preserving the structural and functional properties of the native ECM.	Nakayama et al. (2011)

ECM, extracellular matrix; ddH₂O, double-distilled water; PBS, phosphate-buffered saline; SDS, sodium dodecyl sulfate; NaDOC, sodium deoxycholate; DNase, deoxyribonuclease; DMEM, Dulbecco's modified Eagle's medium; EGTA, ethylene glycol tetraacetic acid; FGF, fibroblast growth factor; hESCs, human embryonic stem cells; dH₂O, distilled water; NaCl, sodium chloride; KCl, potassium chloride; HEPES, 4-[2-hydroxyethyl]-1-piperazineethanesulfonic acid; PAA, peracetic acid; iPSC, induced pluripotent stem cell.

retention of the main components of the ECM, such as collagen and laminin, provides the preservation of the ultrastructure of the scaffold, which can facilitate repopulation by providing the necessary spatial orientation (Scarritt et al., 2015). To evaluate the ECM structure maintenance, a system for histological classification is usually applied to verify whether the fundamental characteristics of renal scaffolds were preserved after decellularization. This system may include assessment of the ECM structure of tubules, glomeruli, and vessels, as well as the level of removal of cells (Figures 1C,D). Transmission electron microscopy has also been used to demonstrate whether the structure of the glomerular basement membrane was preserved after decellularization (Goh et al., 2013; Orlando et al., 2013). As a further evaluation of the retention of ECM components, many researchers have employed the use of traditional engineering techniques such as atomic force microscopy and uni- or bi-axial mechanical tests to evaluate the biophysical properties of the decellularized organ. In many cases, decellularization affects the rigidity of the matrix due to the removal of cells and damage to ECM components (Ott et al., 2008, 2010; Nakayama et al., 2010; Price et al., 2010; Wainwright et al., 2010; Daly et al., 2012; Petersen et al., 2012; Goh et al., 2013). The evaluation of the growth factor retention rate may also be a pattern that indicates the biofunctionality of the ECM (Caralt et al., 2015). Recent studies have shown that preservation of the ECM induces pluripotent cells cultured in the decellularized scaffolds to differentiate into tissue-specific cells (Ross et al., 2009; Cortiella et al., 2010). This cell differentiation linked to ECM intrinsic properties allows the engineering of complex tissues. Moreover, the composition of the ECM is dynamic and constantly changing in response to the metabolic activity of living cells, which modulate their own niche (Badylak et al., 2011). Withal the *in silico* predication of the genes that encode the ECM components and cell proteins that interact with, or modify the ECM, resulted in a database called “*the matrisome*” (Naba et al., 2012; Randles et al., 2017). Proteomic analysis by the use of mass spectrometry analysis focused on the matrisome, allow a complete identification and quantification of the ECM components, and already represent powerful resources for researchers (Gessel et al., 2015; Hill et al., 2015; Calle et al., 2016).

In addition to the parenchymal structures, maintaining the acellular scaffold microvasculature is critical for subsequent recolonization. The perfusion of dyes followed by angiographic analyses with micro computed tomography or vascular corrosion are useful strategies to evaluate the structure of the vascular tree after decellularization and have been performed in kidneys (Figures 1A,B) (Ott et al., 2008; Shupe et al., 2010; Uygun et al., 2010; Baptista et al., 2011; Barakat et al., 2012; Sullivan et al., 2012; Bonvillain et al., 2013; Caralt et al., 2013; Goh et al., 2013; Mirmalek-Sani et al., 2013; Yu et al., 2014). The complete removal of the DNA from the ECM donor is important to prevent a possible inflammatory response in its implementation into the host after recellularization (Badylak et al., 2009; Gilbert et al., 2009). Currently, the techniques for evaluating the presence of DNA in the ECM include spectrophotometric analyses

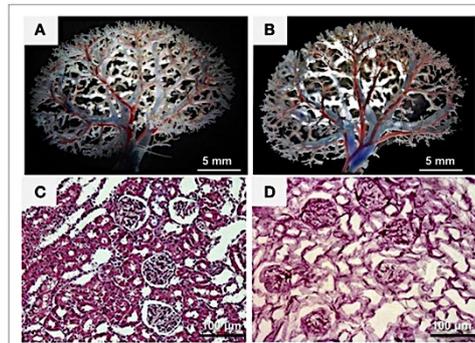


FIGURE 1 | Characterization of the decellularized kidney scaffolds. (A,B) Vascular corrosion casting showed a normal vascular tree of the decellularized kidney scaffold (B) compared with that of the intact kidney (A). (C,D) H&E staining showed the existence of blue-stained nuclei in the intact kidney (C) but not in the decellularized kidney scaffold (D). Reprinted and modified with permission from Yu et al. (2014).

(Rosario et al., 2008; Narayanan et al., 2009), histological stains (Bolland et al., 2007; Rosario et al., 2008; Gilbert et al., 2009), and immunohistochemical methods (Woods and Gratzner, 2005). The quantification of beta-actin gene (one of the main non-muscular cell components) is another reliable alternative method to assess the presence of DNA in the ECM (Kabsch et al., 1990). Furthermore, the beta-actin gene has been widely used as a positive control in polymerase chain reactions (PCRs) (Bellis et al., 2003) and is also configured as a pattern in gene tests due to its constitution and ubiquitous expression (Nygard et al., 2007).

The decellularization techniques developed until the present moment have not been able to remove 100% of the native cellular components without damage to the ECM structure and composition. The residual DNA content may cause cytocompatibility problems *in vitro* and adverse events in hosts during the reintroduction of cells *in vivo* (Nagata et al., 2010; Zhang et al., 2010). The threshold concentration of residual cellular components within the ECM, which is sufficient to cause the host response, depends on the (Lai et al., 2013) source of the ECM (United States Renal Data System, 2015), immune response of the receiver, and (Jha et al., 2013) environment in which the ECM will be installed. In this regard, the minimum criteria that reflect a satisfactory decellularization process involve displaying less than 50 ng of double-stranded DNA per mg of ECM (dry weight) with fragments lower than 200 base pairs and the absence of visible nuclear material on optical microscopy stained with 4',6-diamidino-2-phenylindole (DAPI) or hematoxylin (Figure 1) (Woods and Gratzner, 2005; Crapo et al., 2011). Thus far, there is no consensus regarding the use of a specific detergent because this can degrade collagen, even in similar tissues, thus decreasing the mechanical strength of the organ (Cartmell and Dunn, 2000; Woods and Gratzner, 2005).

SCAFFOLD STERILIZATION

Prior to use *in vitro* or *in vivo*, the ECM scaffold must be sterilized to remove all endotoxins and possible viral or bacterial DNA. The solvents or acidic solutions may be used for this process (Hodde and Hiles, 2002; Gorschewsky et al., 2005). However, these solutions can damage the ECM and affect the adhesion of cells during repopulation (Sun and Leung, 2008). The use of gamma irradiation or ethylene oxide is also reported, but these approaches also alter the ultrastructure of the ECM/scaffold, with the loss of collagen fibers and GAGs, decrease in cell proliferation and alterations in porosity and swelling properties (Pooornejad et al., 2016c). Furthermore, exposure to this type of process can activate immune responses from the receptor (Qiu et al., 2009). One alternative for the sterilization of the kidney scaffold without damage to the ECM is the infusion of antibiotic and antifungal solutions, such as sodium azide or a combination of penicillin, streptomycin, and amphotericin, generally diluted in sterile phosphate-buffered saline (PBS). Perfusion with sterile filtered 70% ethanol is also used before perfusion with antibiotics (Nakayama et al., 2010, 2011; Xu et al., 2014; Pooornejad et al., 2015). The kidney scaffold is usually perfused with the antimicrobial solution over a period of time to ensure that no microorganisms remain in the scaffold (Nakayama et al., 2010, 2011; Song et al., 2013; Bonandrini et al., 2014). Recently, Pooornejad et al., 2016c showed that a 0.2% PAA in 1 M NaCl solution was the best method for decontamination of porcine decellularized ECM over other sterilization solutions such as 70% ethanol and 0.2% PAA in 4% ethanol or gamma-irradiation.

CELL SOURCES FOR KIDNEY RECELLULARIZATION

The kidney is a complex organ that contains more than 26 types of cells derived from ureteric bud and the metanephrogenic mesenchyme (MM) (Al-Awqati and Oliver, 2002; Nishinakamura, 2008; Gouon-Evans, 2014). The renal corpuscle is composed of endothelial cells, mesangial cells, visceral epithelial cells, also known as podocytes, and parietal epithelial cells, besides the cells that comprise the juxtaglomerular apparatus, such as peripolar cells, juxtaglomerular granular cells, extraglomerular mesangial cells, and cells from the macula densa (Barajas, 1979). The renal proximal tubular cells are epithelial cells that can be distinguished in different cell types, according to the proximal tubular segment in which they are located. In rats, the proximal tubular segments are divided into S1, S2, and S3 segments, and the cells that comprise these segments have been well described by Maunsbach (1966). At the loop of Henle, the epithelial cells are also distinguished by their ultrastructural characteristics and their location within the different regions that form the medulla (Pannabecker, 2012). There are also cells that form the distal tubules, composed of morphologically distinct segments—the thick ascending limb of the loop of Henle, the macula densa, the distal convoluted tubule, and connecting tubules. Each of these segments presents different epithelial cells, with different functions related to their ultrastructural characteristics. Finally,

the cells that comprise the collecting duct are the principal cells, type A and type B intercalated cells, and cells that form the inner medullary collecting duct, in addition to the different types of interstitial cells (Little et al., 2007).

In view of this complexity and variety of cells that form the kidneys, different strategies have been used to recellularize this organ. An immortalized human renal cortical-tubular epithelial (RCTE) cell line seeded through the renal artery within a bioreactor has also formed tubular structures and was not found within arterioles, suggesting that cells could translocate into the parenchyma or peri-tubular space to rest on the basement membrane (Caralt et al., 2015).

Another approach to repopulate the kidney scaffold is based on the contribution to urine production from various epithelial cell phenotypes presented in different niches along the nephron (Song et al., 2013). The infusion of suspended human umbilical venous endothelial cells (HUVECs) *via* the renal artery and a combination of rat neonatal kidney cells (NKC) *via* the ureter is a promising strategy. These cells can be maintained in culture media supplemented with *in vivo* maturation signals such as glucocorticoids and catecholamines to accelerate *in vitro* nephrogenesis and the maturation of NKC in acellular kidney matrices. In this sense, repopulation of the renal scaffold with epithelial and endothelial cells with the preservation of glomerular, tubular, and vascular architecture was observed through histologic evaluation after approximately 4 days in culture (Song et al., 2013). HUVECs lined vascular channels throughout the entire scaffold cross section, and the spatial organization of the regenerated epithelium and endothelium resembled the native nephron, which could provide the anatomic basis for renal function, including the processes of water and solute filtration, secretion, and reabsorption (Song et al., 2013).

Primary adult renal cells isolated from kidney cortical tissue by a process of digestion have also been applied to kidney recellularization (Abolbashari et al., 2016). Prior to seeding into the kidney scaffold, the isolated cells were maintained in primary culture, and the expression of aquaporin 1, aquaporin 2, aquaporin 4, ezrin, and podocin was analyzed by immunostaining to identify the cell phenotypes. The majority of the cells were positive for aquaporin1 and ezrin (a protein localized at the brush border membrane of proximal tubules that cross-links plasma membrane proteins with the actin cytoskeleton), indicative of proximal tubular cells, while distal tubular cells and collecting duct cells, expressing aquaporin 2 and aquaporin 4, respectively, represented a small percentage of the total cell population, with very few cells expressing podocin. After the identification of the phenotypes that confirmed the presence of cells from different renal segments, the cells were seeded into the scaffold. Some functional determinations such as electrolyte and protein adsorption, hydrolase activity, and erythropoietin (EPO) production were accessed to evaluate the functional capacity of the engineered kidneys, and the results were encouraging. However, they did not focus on the full characterization of the cultured cells, and cells with vascular phenotypes were not used, leading to the need for future tests to be performed (Abolbashari et al., 2016).

Embryonic stem (ES) cells have been used for organ recellularization with good results (Ross et al., 2009, 2012; Bonandrini

et al., 2014). ES cells are especially interesting because of their pluripotency and ability to grow indefinitely. These cells have the potential to form any embryonic organ *in vivo*, and their capacity to differentiate into any of the adult renal cell types makes these cells great candidates for kidney recellularization (Keller, 2005). Pluripotent ES cells are usually maintained in culture medium in the presence of leukemia inhibitory factor, which reduces spontaneous cell differentiation, until the moment of the recellularization (Garreta et al., 2014). Infusion of the cells in the kidney scaffold through both the renal artery and ureter shows a pattern of distribution of the injected ES cells into tubular and vascular structures and their associated glomeruli, with multiplication of the cells (Song et al., 2013). Furthermore, evidence of embryonic cell differentiation toward epithelial and endothelial phenotypes was obtained by immunohistochemistry and fluorescence microscopy (Ross et al., 2009, 2012; Guan et al., 2015b). When the ES cells are infused only by the renal artery, the cells remain largely in the vascular network, with few cells housed on the tubular segments (Bonandrini et al., 2014).

Despite the good results obtained in applying ES cells for organ recellularization, ethical questions and the teratogenic potential of ES may limit the use of these cells for organ repopulation (Nowacki et al., 2014). One possible alternative is the use of autologous adult stem cells that do not require direct ethical questions, do not lead to immunologic responses, and can be obtained in minimally invasive processes. Bone marrow mesenchymal stem cells (BM-MSCs) have frequently been used for kidney repair and regeneration (Burgkart et al., 2014), but stem cells from other sources such as adipose tissue or amniotic fluid also exhibit promising applications (Hass et al., 2011; Liu et al., 2015b). Induced pluripotent stem cells (iPSCs) can be generated directly from adult somatic cells *via* the transduction of reprogramming factors and closely resemble ESCs been also suitable for kidney regeneration (Rogers, 2011; Hendry and Little, 2012; Usui et al., 2012). Some studies have achieved highly efficient differentiation of human iPSCs into intermediate mesoderm cells with potential to generate embryonic renal progenitors and adult renal cell types (Mae et al., 2013), as well as iPSC differentiation into podocytes with cytoplasmic contractile response to angiotensin II (AII) and functional ability to albumin intake (Song et al., 2012). The reconstitution of kidney structures *in vitro*, including efficiently vascularized glomeruli with podocytes, as well as renal proximal and distal tubules with clear lumen have already been generated from iPSCs differentiated to MM (Taguchi et al., 2014). A schematic review detailing the differentiation of MM from iPSCs was published from this same group of researchers (Taguchi and Nishinakamura, 2014). Furthermore, iPSC-derived endothelial cells injected through the renal artery of decellularized kidney were able to outlining branching vasculature and individual glomeruli (Caralt et al., 2015). It can be considered that patient-decellularized kidneys reseeded with patient-derived iPSCs differentiated to the renal precursors and vascular progenitors may represent the most promising recellularization option to the reconstruction of whole kidneys that can hereafter be used for autologous transplantation.

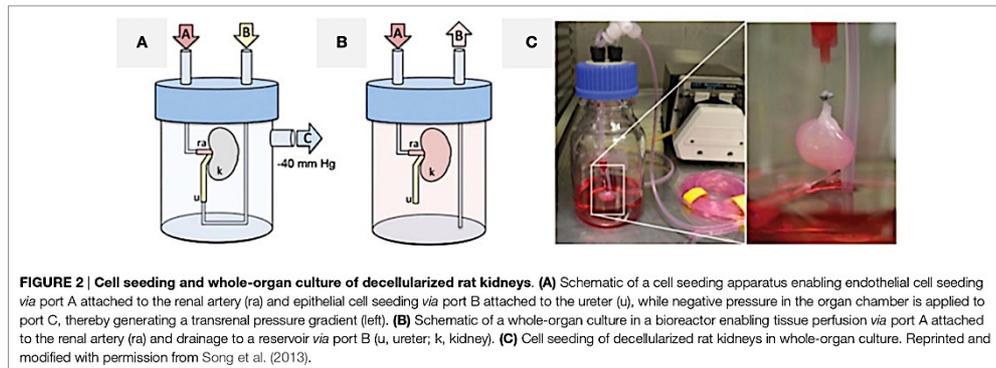
WHOLE-ORGAN RECELLULARIZATION

Kidney recellularization is usually made by the anterograde infusion of cells through the vasculature or retrograde infusion through the ureter or both (Ross, 2009; Ross et al., 2009, 2012; Song et al., 2013; Bonandrini et al., 2014). The cells can be manually injected (Ross et al., 2009, 2012), or they may be subject to infusion using a syringe pump (Bonandrini et al., 2014) or peristaltic pump (Song et al., 2013; Caralt et al., 2015), which allows for control of the flow rate of infusion. These latter options, coupled to a bioreactor, seem to be more adequate because they ensure the constant infusion of cells without apparent damage to the scaffold. In addition, maintaining a constant or pulsatile perfusion of cell culture medium allows the viability, nutrition, proliferation, migration, and differentiation of the recent seeded cells (Scarritt et al., 2015). Another alternative to seeding the renal scaffolds is the delivery of the cells into the cortical region of renal scaffolds using a needle. The distance between the injection sites and depth of injection has to be optimized to ensure that the whole organ is covered, with cells homogeneously injected into the cortex site (Abolbashari et al., 2016).

The first attempt to recellularize a whole kidney used the incubation of the reseeded organ with static media. This procedure allowed less reproducible growth, significant apoptosis occurred, and this approach did not consistently maintain viability beyond approximately 4 days. Better results were observed with transverse sectioning of the pre-seeded organ and culture of the slices in a multiwell dish, but this approach cannot be extrapolated to rebuild the organ for transplantation (Ross et al., 2009). Still, a peristaltic pump coupled to appropriate tubing could deliver a physiologically normal pressure profile, in a temperature-controlled incubator supplied by regulated medical-grade sterile gases. In this case, there was sufficient cell viability and proliferation with migration into glomeruli and other small vessels, extending from the afferent arterioles and glomerular tufts to the efferent arterioles and peritubular capillary networks (Ross et al., 2009, 2012). Other attempts to seed cells by applying pressure to the collecting system failed to reach the glomerulus, encouraging the development of a bioreactor for the perfusion of cells through the renal artery and retrograde through the ureter, with a vacuum pressure of 40 cmH₂O applied to the system (Figure 2). This approach ensured cell seeding with a transrenal gradient and culminating in cell dispersion throughout the entire kidney parenchyma (Song et al., 2013). Thereafter, other studies also used perfusion-based bioreactors for renal repopulation with considerable success (Bonandrini et al., 2014; Caralt et al., 2015; Abolbashari et al., 2016). A table with a summary of some methods and cell sources already used for kidney repopulation can be seen in the review published by Scarritt et al. (2015).

CHARACTERIZATION OF THE RESEDED KIDNEY STRUCTURE

The characterization of the reseeded kidney with respect to the ECM structure, cell adhesion, proliferation, migration, and differentiation, as well as the regeneration of a new kidney, that



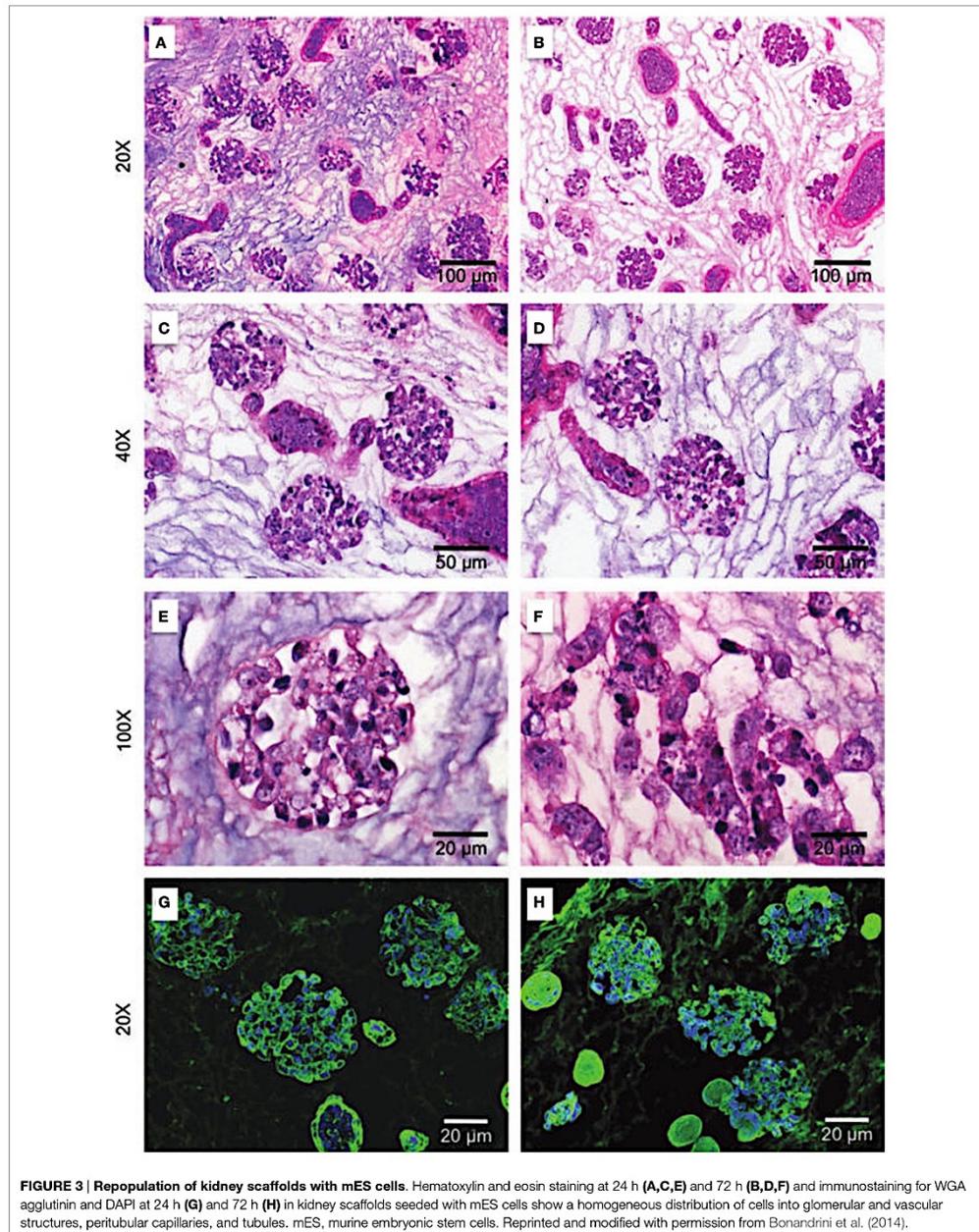
resembles the native structure is usually made by histological evaluation. Monitoring the distribution of the cells allows for observation not only of cell proliferation and migration through the scaffold but also the integrity of the vascular basement membranes based on the presence or absence of cells at the Bowman's space (Ross et al., 2009, 2012; Song et al., 2013; Caralt et al., 2015). Morphometric analysis is also described for repopulated kidney characterization, such as the analysis of the average glomerular diameter, Bowman's space, and glomerular capillary lumen (Song et al., 2013). Elastin staining gives the notion of vessel and artery integrity (Caralt et al., 2015). Transmission and scanning electron microscopy are also performed to evaluate the final structure of the rebuilt kidney, showing glomerular capillaries with engrafted podocytes and the formation of foot processes (pedicels) (Song et al., 2013; Caralt et al., 2015).

Histological staining with H&E performed for light microscopy allows the analysis of cell distribution, as well as the maintenance of ECM structure (Figure 3). Observations relative to the morphology of the engrafted cells can indicate their cytology features and assessment of the distribution, migration, and grouping tendencies, as well as cell-ECM interactions indicate the success of the chosen method (Ross et al., 2009; Song et al., 2013; Bonandrini et al., 2014; Caralt et al., 2015; Abolbashari et al., 2016). The use of GFP-stained cells for recellularization is also a strategic tool for the characterization of the distribution of the cells along the kidney scaffold by monitoring GFP expression by fluorescence microscopy (Ross et al., 2009, 2012). Other stains are also used to assess cell distribution, such as the periodic acid-Schiff (PAS) stain, in addition to fluorescein wheat germ agglutinin (WGA) and DAPI staining, which documents cellular nuclei in the scaffold (Figure 3) (Ross et al., 2009; Bonandrini et al., 2014; Caralt et al., 2015).

In addition to the histological stains, the evaluations of the expression of cell differentiation and proliferation markers by immunostaining or RT-PCR are also tools for the characterization of the rebuilt kidney. In this regard, there is a range of antibodies available for review of different cell types, resulting in repopulation of kidney scaffolds. Some of the proteins and

genes accessed for evaluation of cell differentiation are Oct-4, a marker of embryonic stemness, NCAM, a marker of mesoderm precursors, and the endothelial cell markers Tie-2 and CD3 (Bonandrini et al., 2014). Pan-cytokeratin immunostaining and staining of Pax-2 and Ksp-cadherin, a cell adhesion protein normally expressed in distal nephron tubular cells at later developmental stages, may also be useful in evaluating stem cell differentiation into epithelial tubular cells (Ross et al., 2009). Lectin-specific (BsLB4) staining for murine endothelial cells and the presence of VEGFR2 are indicators of the differentiation of ES cells into endothelial cells in the scaffold's glomeruli and blood vessels (Ross et al., 2009, 2012). Markers such as Wilms tumor WT-1, podocalyxin like-2, glial cell-derived neurotrophic factor (GDNF), LMX1B, nephrin, and synaptodinlike-2 are other indications of mature renal cells (Petrosyan et al., 2015). For a more accurate observation of the specific cells differentiated upon recellularization, analysis of the expression of podocin indicates a glomerular epithelial phenotype (Abolbashari et al., 2016), while the polarity of the cells with expression of (Na⁺)/(K⁺)-ATPase represents a proximal tubular phenotype (Song et al., 2013). E-cadherin expression can be used as a marker of the distal tubular phenotype, and the expression of β1-integrin indicates glomerular epithelial site-specific cell adhesion to ECM domains. Furthermore, as mentioned previously in the "Cell sources for kidney recellularization" section, the evaluation of the different aquaporins can also indicate the level of differentiation of the tubular cells in the different segments of the kidney (Song et al., 2013; Abolbashari et al., 2016). The expression of aquaporin1 together with ezrin indicates the differentiation of cells into proximal tubular cells, while distal tubular cells and collecting duct cells express aquaporin2 and aquaporin4, respectively (Hatano et al., 2013; Abolbashari et al., 2016).

Cell proliferation and viability are other important parameters to ensure that recellularization is successful. Cell viability is usually assessed by immunostaining of BAX, an apoptotic activator, or cleaved caspase-3, a critical executioner of apoptosis (Ross et al., 2009; Bonandrini et al., 2014). Another approach to assess cell apoptosis is TUNEL staining (Abolbashari et al., 2016). The



analysis of cell proliferation, in turn, is made by staining with Ki-67, a nuclear protein necessary for cellular proliferation (Bullwinkel et al., 2006; Ross et al., 2009; Abolbashari et al., 2016) and proliferating cell nuclear antigen (PCNA), a co-factor for DNA polymerase δ activity in eukaryotic cells, that acts as a scaffold for the recruitment of proteins involved in DNA repair, chromatin remodeling, and DNA replication (Moldovan et al., 2007; Bonandrini et al., 2014; Abolbashari et al., 2016). The PCNA/BAX ratio is also used to confirm the success of the cell seeding over time (Petrosyan et al., 2015).

Functional analysis of the rebuilt kidney is also performed. The electrolyte reabsorption can be monitored by sodium uptake assays, with slices from the recellularized kidney cortex incubated with fluorescent sodium dyes and imaged using a fluorescent microscope. For this purpose, ouabain may be used to inhibit $(Na^+)/(K^+)$ -ATPase on the cells, while normal kidney may be used as a positive control (Abolbashari et al., 2016). Albumin uptake can also be measured using the same methods adapted to sodium uptake, indicating the functionality of proximal tubular cells (Birn and Christensen, 2006). Amino acid transport is another important function performed by renal cells. This activity can be evaluated by accessing the activity of hydrolases, such as leucine aminopeptidase (LAP) and gamma glutamyltranspeptidase (GGT), which play significant roles in amino acid transfer (Meister, 1974; Abolbashari et al., 2016).

Secretome analysis is also an excellent approach to assess the functionality of the recellularized organ (Petrosyan et al., 2015). By analyzing the ability of the cells to secrete various proteins, it is possible to estimate the rate of differentiation of the seeded cells and their metabolic activities. Analysis of metalloproteinases and their inhibitors (MMPs and TIMPs) indicates the induction of cells to produce matrix modulators and their potential to repair and remodel the ECM. The secretion of growth factors (VEGF, TGF, PDGF) is related to different tissue processes, including matrix remodeling, immunomodulation, and angiogenesis. Cytokine (interleukins and GRO) and chemokine (MCP-1, RANTES, Fractalkine) secretion are indicative of multiple processes, including inflammation, angiogenesis, wound healing, and immunomodulation (Peloso et al., 2015; Petrosyan et al., 2015). Another pattern that can be observed to characterize renal function is the EPO production by renal cortical interstitial cells through real-time measurement of secreted EPO into the cell culture medium during bioreactor culture (Ullrich, 1979; Abolbashari et al., 2016).

Finally, transmission electron microscopy images may complement the analyses of cell functions, through the evaluation of the intensity of expression in the endoplasmic reticulum and Golgi apparatus, as well as the presence of secretory granules and vacuoles within the cells, which together are indicative of cellular activity and secretion, demonstrating the ability of cells to synthesize key molecules involved in tissue and organ homeostasis (Petrosyan et al., 2015). Alternatively, the development of non-invasive techniques for monitoring cell behavior such as surface scanning or multiphoton microscopy would be very important to improve the evaluation of the success of the recellularization process (Scarritt et al., 2015). Actually, some currently non-invasive techniques used in regenerative medicine may be used

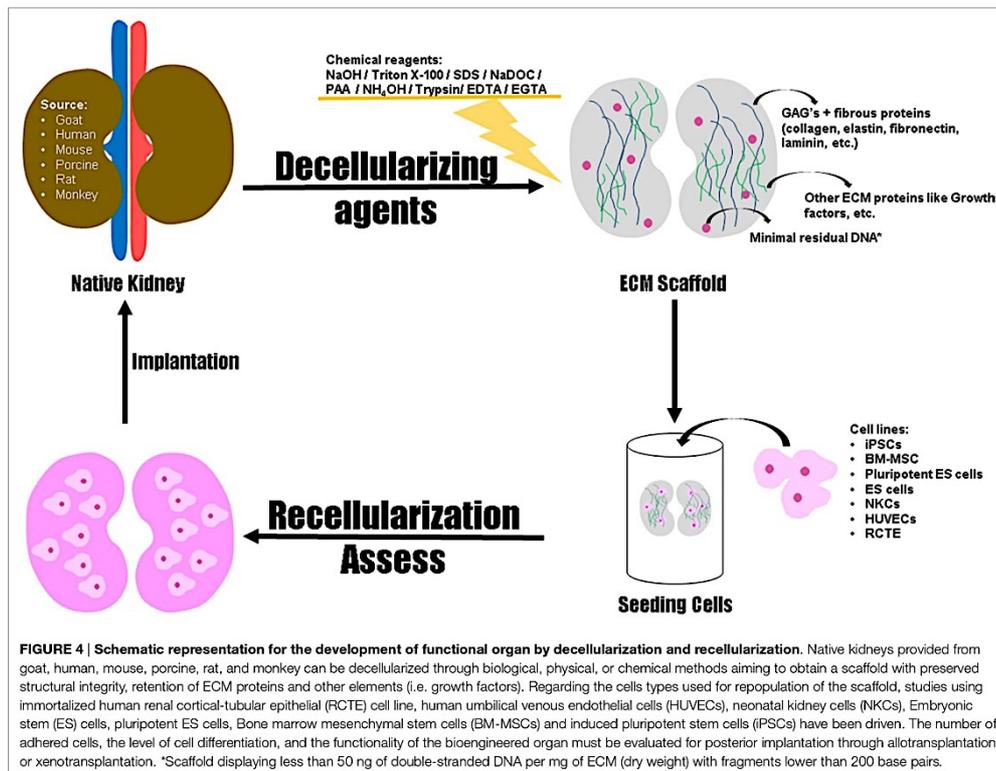
in tissue engineering, such as the resazurin perfusion assay, which allows the repetitive and rapid estimation of viable cell numbers during long-term *ex vivo* culture without destruction of the organ (Ren et al., 2015). Another non-invasive approach used in ECM scaffold remodeling evaluation is the use of a ^{19}F -MRI (magnetic resonance imaging) contrast agent in 1H -MRI scans, which can adequately monitor the distribution of transplanted cells while allowing an evaluation of the formation of new tissue (Bible et al., 2012).

FUTURE CHALLENGES

We have reviewed one of the promising technologies in regenerative therapies for entire organ recovery. Solid organ regeneration based on perfusion-decellularized native ECM scaffolds has enormous potential in patients with organ failure. The use of biologic scaffolds can represent a potential alternative in the field of tissue engineering and regenerative medicine since the employed methods for decellularization can achieve success in the removal of cells without damaging the ECM. It is now necessary to improve these methods to extrapolate them for large-scale experiments. **Figure 4** represents the development of functional organ by decellularization and recellularization, indicating the decellularizing agents, the ECM components to be evaluated post decellularization and the cell sources for recellularization of the organ.

Many of the present efforts aimed at progressive strategies for cell expansion and differentiation might deliver original solutions applicable to organ engineering in the foreseeable future. Considering the several types of cells that have been used in different approaches for kidney recellularization research, choosing the ideal cell source will determine the effectiveness of the new building organ when *in vivo* transplantation occurs. Until now, ES cells have seemed to be the most efficient cell source for kidney recellularization. On the other hand, there are some ethical issues that make ES cells an unsuitable option for human organ recellularization and transplantation. With these considerations in mind, there is a need for more studies regarding iPSCs or adult stem cells, such as bone marrow-derived stem cells or adipocyte-derived stem cells, which present no ethical issues but have not yet been used in transplantation post-recellularization. iPSCs represent an ideal alternative to the ES cells, presenting the same ability of ES to efficiently expand in culture, as well as their capacity to differentiate into multiple cell types, with the advantage of having no ethical problems.

Although several methods have been used to characterize the success of kidney regeneration after decellularization, these processes are often directed toward histological characterization; thus, there is a lack of information regarding the functionality of the new kidney. The newly formed organ should mimic the same biological functions of the native organ without impairing its functionality; and this is what is expected for the next decade (Peloso et al., 2016). The *in vitro* capacity of regenerated kidneys to filter a standardized perfusate, clear metabolites, reabsorb electrolytes and glucose, and generate concentrated urine was assessed by Song et al. (2013), and the results indicate a partial recovered function of endothelial cells, podocytes, and



tubular epithelial cells (Song et al., 2013). Their results could be related to incomplete seeding and the immature stage of seeded neonatal epithelial cells (FALK, 1955; Baum, 2009). Despite the functional immaturity observed through *in vitro* analysis, *in vivo* transplantation showed that regenerated kidney constructs provided urine production and clearance of metabolites, without the occurrence of bleeding or graft thrombosis (Song et al., 2013). However, this method has presently achieved only short-term functionality *in vivo* and only in rodent models. Until now, there has been no report of a mature complete regenerated kidney successfully transplanted into a donor with recovery of its functions, an observation that is a challenge in the field of kidney bioengineering at present. Recently, Caralt and colleagues investigated the ability of a decellularized kidney scaffold to hold sutures and support systemic arterial blood flow by implanting it into a rat recipient in an orthotopic position. Although there was an absence of clotting or major bleeding and the kidney scaffolds remained intact *in situ* for the duration of the study, these results cannot be extrapolated to a real transplantation, considering the absence of cells in the scaffolds (Caralt, 2015; Caralt et al., 2015).

In view of all of the advances observed in kidney bioengineering concerning organ decellularization and repopulation, there is a huge perspective regarding the confirmation of recovery of kidney function after transplantation. The expectation of researchers for the next 10 years is that the studies with decellularized and recellularized kidneys are in the preclinical phase, representing a high potential for translation compared to other tissue engineering approaches to kidney repair, such as renal organoids or 3D bioprinting (Peloso et al., 2016). Nonetheless, the adaptation of the methods described to date for use in human kidney regeneration and transplantation would change the current perspective related to the treatment of kidney diseases in the near future.

AUTHOR CONTRIBUTIONS

AD and GS: each author has made a valuable contribution to the preparation of this manuscript such as writing, literature review, and table layout. The authors AD and GS contributed equally to this work. BN: conception of this work, drafting the work, and revising it critically for all content.

FUNDING

The authors were supported by grants from Fundação de Amparo à Pesquisa e Inovação do Espírito Santo (EDITAL FAPES

Nº 006/2014-UNIVERSAL; process number 0606/2015; EDITAL FAPES/CNPq Nº 012/2014-DCR; process number 0832/2015); Rede Nordeste de Biotecnologia (RENORBIO) and Coordenação de Aperfeiçoamento de Pessoal de Nível Superior (CAPES).

REFERENCES

- Abecassis, M., Bridges, N. D., Clancy, C. J., Dew, M. A., Eldadah, B., Englesbe, M. J., et al. (2012). Solid-organ transplantation in older adults: current status and future research. *Am. J. Transplant.* 12, 2608–2622. doi:10.1111/j.1600-6143.2012.04245.x
- Abolbashari, M., Agcaoili, S. M., Lee, M.-K., Ko, I. K., Aboushwareb, T., Jackson, J. D., et al. (2016). Repopulation of porcine kidney scaffold using porcine primary renal cells. *Acta Biomater.* 29, 52–61. doi:10.1016/j.actbio.2015.11.026
- Abt, P. L., Fisher, C. A., and Singhal, A. K. (2006). Donation after cardiac death in the US: history and use. *J. Am. Coll. Surg.* 203, 208–225. doi:10.1016/j.jamcollsurg.2006.03.014
- Ahn, H. H., Kim, K. S., Lee, J. H., Lee, M. S., Song, I. B., Cho, M. H., et al. (2007). Porcine small intestinal submucosa sheets as a scaffold for human bone marrow stem cells. *Int. J. Biol. Macromol.* 41, 590–596. doi:10.1016/j.ijbiomac.2007.07.019
- Akhyari, P., Aubin, H., Gwanmesia, P., Barth, M., Hoffmann, S., Huelsmann, J., et al. (2011). The quest for an optimized protocol for whole-heart decellularization: a comparison of three popular and a novel decellularization technique and their diverse effects on crucial extracellular matrix qualities. *Tissue Eng. Part C Methods* 17, 915–926. doi:10.1089/ten.TEC.2011.0210
- Al-Awqati, Q., and Oliver, J. A. (2002). Stem cells in the kidney. *Kidney Int.* 61, 387–395. doi:10.1046/j.1523-1755.2002.00164.x
- Alberts, B., Johnson, A., Lewis, J., Raff, M., Roberts, K., and Walter, P. (2002). "The extracellular matrix of animals," in *Molecular Biology of the Cell*, 4th Edn. New York: Garland Science. Available at: <https://www.ncbi.nlm.nih.gov/books/NBK26810/>
- Anil Kumar, B. N., and Mattoo, S. K. (2015). Organ transplant & the psychiatrist: an overview. *Indian J. Med. Res.* 141, 408–416. doi:10.4103/0971-5916.159268
- Anil Kumar, M. S., Khan, S. M., Jaglan, S., Heifets, M., Moritz, M. J., Saeed, M. I., et al. (2006). Successful transplantation of kidneys from deceased donors with acute renal failure: three-year results. *Transplantation* 82, 1640–1645. doi:10.1097/01.tp.0000250908.62948.8f
- Badylak, S. F. (2002). The extracellular matrix as a scaffold for tissue reconstruction. *Semin. Cell Dev. Biol.* 13, 377–383. doi:10.1016/S1084952102000940
- Badylak, S. F. (2004). Xenogeneic extracellular matrix as a scaffold for tissue reconstruction. *Transpl. Immunol.* 12, 367–377. doi:10.1016/j.trim.2003.12.016
- Badylak, S. F., Freytes, D. O., and Gilbert, T. W. (2009). Extracellular matrix as a biological scaffold material: structure and function. *Acta Biomater.* 5, 1–13. doi:10.1016/j.actbio.2008.09.013
- Badylak, S. F., and Gilbert, T. W. (2008). Immune response to biologic scaffold materials. *Semin. Immunol.* 20, 109–116. doi:10.1016/j.smim.2007.11.003
- Badylak, S. F., Taylor, D., and Uygun, K. (2011). Whole-organ tissue engineering: decellularization and recellularization of three-dimensional matrix scaffolds. *Annu. Rev. Biomed. Eng.* 13, 27–53. doi:10.1146/annurev-bioeng-071910-124743
- Baptista, P. M., Orlando, G., Mirmalek-Sani, S.-H. H., Siddiqui, M., Atala, A., and Soker, S. (2009). Whole organ decellularization – a tool for bioscaffold fabrication and organ bioengineering. *Conf. Proc. IEEE Eng. Med. Biol. Soc.* 2009, 6526–6529. doi:10.1109/IEMBS.2009.5333145
- Baptista, P. M., Siddiqui, M. M., Lozier, G., Rodriguez, S. R., Atala, A., and Soker, S. (2011). The use of whole organ decellularization for the generation of a vascularized liver organoid. *Hepatology* 53, 604–617. doi:10.1002/hep.24067
- Barajas, L. (1979). Anatomy of the juxtaglomerular apparatus. *Am. J. Physiol.* 237, F333–F343.
- Barakat, O., Abbasi, S., Rodriguez, G., Rios, J., Wood, R. P., Ozaki, C., et al. (2012). Use of decellularized porcine liver for engineering humanized liver organ. *J. Surg. Res.* 173, e11–e25. doi:10.1016/j.jss.2011.09.033
- Barkan, D., Green, J. E., and Chambers, A. F. (2010). Extracellular matrix: a gate-keeper in the transition from dormancy to metastatic growth. *Eur. J. Cancer* 46, 1181–1188. doi:10.1016/j.ejca.2010.02.027
- Baum, M. (2009). Postnatal developmental renal physiology: a study of historic significance. *Am. J. Physiol. Renal. Physiol.* 296, F667–F668. doi:10.1152/ajprenal.00037.2009
- Bellis, C., Ashton, K. J., Freney, L., Blair, B., and Griffiths, L. R. (2003). A molecular genetic approach for forensic animal species identification. *Forensic Sci. Int.* 134, 99–108. doi:10.1016/S0379-0738(03)00128-2
- Bible, E., Dell'acqua, F., Solanky, B., Balducci, A., Crapo, P. M., Badylak, S. F., et al. (2012). Non-invasive imaging of transplanted human neural stem cells and ECM scaffold remodeling in the stroke-damaged rat brain by 19 F-and diffusion-MRI. *Biomaterials* 33, 2858–2871. doi:10.1016/j.biomaterials.2011.12.033
- Birn, H., and Christensen, E. I. (2006). Renal albumin absorption in physiology and pathology. *Kidney Int.* 69, 440–449. doi:10.1038/sj.ki.5000141
- Bolland, F., Korossis, S., Wilshaw, S.-P., Ingham, E., Fisher, J., Kearney, J. N., et al. (2007). Development and characterisation of a full-thickness acellular porcine bladder matrix for tissue engineering. *Biomaterials* 28, 1061–1070. doi:10.1016/j.biomaterials.2006.10.005
- Bonandrini, B., Figliuzzi, M., Papadimou, E., Morigi, M., Perico, N., Casiraghi, F., et al. (2014). Recellularization of well-preserved acellular kidney scaffold using embryonic stem cells. *Tissue Eng. Part A* 20, 1486–1498. doi:10.1089/ten.TEA.2013.0269
- Bonvillain, R. W., Scarritt, M. E., Pashos, N. C., Mayeux, J. P., Meshberger, C. L., Betancourt, A. M., et al. (2013). Nonhuman primate lung decellularization and recellularization using a specialized large-organ bioreactor. *J. Vis. Exp.* 82, e50825. doi:10.3791/50825
- Bosman, F. T., and Stamenkovic, I. (2003). Functional structure and composition of the extracellular matrix. *J. Pathol.* 200, 423–428. doi:10.1002/path.1437
- Brown, B., Lindberg, K., Reing, J., Stolz, D. B., and Badylak, S. F. (2006). The basement membrane component of biologic scaffolds derived from extracellular matrix. *Tissue Eng.* 12, 519–526. doi:10.1089/ten.2006.12.519
- Bullwinkel, J., Baron-Lühr, B., Lüdemann, A., Wohlenberg, C., Gerdes, J., and Scholzen, T. (2006). Ki-67 protein is associated with ribosomal RNA transcription in quiescent and proliferating cells. *J. Cell. Physiol.* 206, 624–635. doi:10.1002/jcp.20494
- Burgkart, R., Tron, A., Proding, P., Culmes, M., Tübel, J., van Griensven, M., et al. (2014). Decellularized kidney matrix for perfused bone engineering. *Tissue Eng. Part C Methods* 20, 553–561. doi:10.1089/ten.TEC.2013.0270
- Caldas, H. C., Hayashi, P. C., and Abbud-Filho, M. (2011). Repairing the chronic damaged kidney: the role of regenerative medicine. *Transplant. Proc.* 43, 3573–3576. doi:10.1016/j.transproceed.2011.10.053
- Calle, E. A., Hill, R. C., Leiby, K. L., Le, A. V., Gard, A. L., Madri, J. A., et al. (2016). Targeted proteomics effectively quantifies differences between native lung and detergent-decellularized lung extracellular matrices. *Acta Biomater.* 46, 91–100. doi:10.1016/j.actbio.2016.09.043
- Caralt, M. (2015). Present and future of regenerative medicine: liver transplantation. *Transplant. Proc.* 47, 2377–2379. doi:10.1016/j.transproceed.2015.08.029
- Caralt, M., Jacob, S., Obergfell, K., Akgun, B., Bijonowski, B., Abecassis, M., et al. (2013). A critical evaluation of kidney extracellular matrix after perfusion decellularization as a structural basis for renal tissue engineering. *J. Tissue Eng. Regen. Med.* 6, 1–429. doi:10.1002/term.1586
- Caralt, M., Uzarski, J. S., Jacob, S., Obergfell, K. P., Berg, N., Bijonowski, B. M., et al. (2015). Optimization and critical evaluation of decellularization strategies to develop renal extracellular matrix scaffolds as biological templates for organ engineering and transplantation. *Am. J. Transplant.* 15, 64–75. doi:10.1111/ajt.12999
- Cartmell, J. S., and Dunn, M. G. (2000). Effect of chemical treatments on tendon cellularity and mechanical properties. *J. Biomed. Mater. Res.* 49, 134–140. doi:10.1002/(SICI)1097-4636(200001)49:1<134::AID-JBM17>3.0.CO;2-D
- Centers for Disease Control and Prevention (CDC). (2014). *National Chronic Kidney Disease Fact Sheet: General Information and National Estimates on Chronic Kidney Disease in the United States*. Atlanta, GA: Centers for Disease

- Control and Prevention. Available at: http://www.cdc.gov/diabetes/pubs/pdf/kidney_factsheet.pdf (accessed September 21, 2015).
- Chae, S. Y., Chun, S. Y., Park, M., Jang, Y.-J., Kim, J. R., Oh, S. H., et al. (2014). Development of renal extracellular matrix (ECM) scaffold for kidney regeneration. *Tissue Eng. Regen. Med.* 11, 1–7. doi:10.1007/s13770-013-1125-6
- Cheng, X., Liu, F., Zhang, Y., and Jiang, Y. (2013). Cloning and expression of a urate oxidase and creatinine hydrolase fusion gene in *Escherichia coli*. *Ren. Fail.* 35, 275–278. doi:10.3109/0886022X.2012.745787
- Choi, S. H., Chun, S. Y., Chae, S. Y., Kim, J. R., Oh, S. H., Chung, S. K., et al. (2015). Development of a porcine renal extracellular matrix scaffold as a platform for kidney regeneration. *J. Biomed. Mater. Res. A* 103, 1391–1403. doi:10.1002/jbm.a.35274
- Choi, Y. C., Choi, J. S., Kim, B. S., Kim, J. D., Yoon, H. I., and Cho, Y. W. (2012). Decellularized extracellular matrix derived from porcine adipose tissue as a xenogeneic biomaterial for tissue engineering. *Tissue Eng. Part C Methods* 18, 866–876. doi:10.1089/ten.tec.2012.0009
- Cooper, D. K. C., Gollackner, B., and Sachs, D. H. (2002). Will the pig solve the transplantation backlog? *Annu. Rev. Med.* 53, 133–147. doi:10.1146/annurev.med.53.082901.103900
- Cooper, G. M. (2000). "Cell walls and the extracellular matrix," in *The Cell: A Molecular Approach*, 2nd Edn. Sunderland, MA: Sinauer Associates. Available at: <https://www.ncbi.nlm.nih.gov/books/NBK9874/>
- Cortiella, J., Niles, J., Cantu, A., Bretler, A., Pham, A., Vargas, G., et al. (2010). Influence of acellular natural lung matrix on murine embryonic stem cell differentiation and tissue formation. *Tissue Eng. Part A* 16, 2565–2580. doi:10.1089/ten.tea.2009.0730
- Crapo, P. M., Gilbert, T. W., and Badylak, S. F. (2011). An overview of tissue and whole organ decellularization processes. *Biomaterials* 32, 3233–3243. doi:10.1016/j.biomaterials.2011.01.057
- Cruzado, J. M., Bestard, O., Riera, L., Torras, J., Gil-Vernet, S., Serón, D., et al. (2007). Immunosuppression for dual kidney transplantation with marginal organs: the old is better yet. *Am. J. Transplant.* 7, 639–644. doi:10.1111/j.1600-6143.2007.01671.x
- Daly, K. A., Liu, S., Agrawal, V., Brown, B. N., Johnson, S. A., Medberry, C. J., et al. (2012). Damage associated molecular patterns within xenogeneic biologic scaffolds and their effects on host remodeling. *Biomaterials* 33, 91–101. doi:10.1016/j.biomaterials.2011.09.040
- De Serres, S. A., Caumartin, Y., Noël, R., Lachance, J.-G., Côté, I., Naud, A., et al. (2010). Dual-kidney transplants as an alternative for very marginal donors: long-term follow-up in 63 patients. *Transplantation* 90, 1125–1130. doi:10.1097/TP0b013e3181f8f2b8
- Debout, A., Foucher, Y., Trébern-Launay, K., Legendre, C., Kreis, H., Mourad, G., et al. (2015). Each additional hour of cold ischemia time significantly increases the risk of graft failure and mortality following renal transplantation. *Kidney Int.* 87, 343–349. doi:10.1038/ki.2014.304
- Dew, M. A., Switzer, G. E., Goycoolea, J. M., Allen, A. S., DiMartini, A., Kormos, R. L., et al. (1997). Does transplantation produce quality of life benefits? A quantitative analysis of the literature. *Transplantation* 64, 1261–1273. doi:10.1097/00007890-199711150-00006
- FALK, G. (1955). Maturation of renal function in infant rats. *Am. J. Physiol.* 181, 157–170.
- Farney, A. C., Hines, M. H., al-Geizawi, S., Rogers, J., and Stratta, R. J. (2011). Lessons learned from a single center's experience with 134 donation after cardiac death donor kidney transplants. *J. Am. Coll. Surg.* 212, 440–451; discussion 451–453. doi:10.1016/j.jamcollsurg.2010.12.033
- Farney, A. C., Rogers, J., Orlando, G., al-Geizawi, S., Buckley, M., Farooq, U., et al. (2013). Evolving experience using kidneys from deceased donors with terminal acute kidney injury. *J. Am. Coll. Surg.* 216, 645–655; discussion 655–656. doi:10.1016/j.jamcollsurg.2012.12.020
- Faulk, D. M., Wildemann, J. D., and Badylak, S. F. (2014a). Decellularization and cell seeding of whole liver biologic scaffolds composed of extracellular matrix. *J. Clin. Exp. Hepatol.* 5, 69–80. doi:10.1016/j.jceh.2014.03.043
- Faulk, D. M., Johnson, S. A., Zhang, L., and Badylak, S. F. (2014b). Role of the extracellular matrix in whole organ engineering. *J. Cell. Physiol.* 229, 984–989. doi:10.1002/jcp.24532
- Fernández-Lorente, L., Riera, L., Bestard, O., Carrera, M., Gomà, M., Porta, N., et al. (2012). Long-term results of biopsy-guided selection and allocation of kidneys from older donors in older recipients. *Am. J. Transplant.* 12, 2781–2788. doi:10.1111/j.1600-6143.2012.04153.x
- Fissell, W. H., Manley, S., Westover, A., Humes, H. D., Fleischman, A. J., and Roy, S. (2006). Differentiated growth of human renal tubule cells on thin-film and nanostructured materials. *ASAIO J.* 52, 221–227. doi:10.1097/01.mat.0000205228.30516.9c
- Fissell, W. H., and Roy, S. (2009). The implantable artificial kidney. *Semin. Dial.* 22, 665–670. doi:10.1111/j.1525-139X.2009.00662.x
- Franquesa, M., Flaquer, M., Cruzado, J. M., and Grinyó, J. M. (2013). Kidney regeneration and repair after transplantation. *Curr. Opin. Organ Transplant* 18, 191–196. doi:10.1097/MOT.0b013e32835f0771
- Freytes, D. O., Martin, J., Velankar, S. S., Lee, A. S., and Badylak, S. F. (2008). Preparation and rheological characterization of a gel form of the porcine urinary bladder matrix. *Biomaterials* 29, 1630–1637. doi:10.1016/j.biomaterials.2007.12.014
- Gagliardini, E., Conti, S., Benigni, A., Remuzzi, G., and Remuzzi, A. (2010). Imaging of the porous ultrastructure of the glomerular epithelial filtration slit. *J. Am. Soc. Nephrol.* 21, 2081–2089. doi:10.1681/ASN.2010020199
- Gao, R., Wu, W., Xiang, J., Lv, Y., Zheng, X., Chen, Q., et al. (2015). Hepatocyte culture in autologous decellularized spleen matrix. *Organogenesis* 11, 16–29. doi:10.1080/15476278.2015.1011908
- Garreta, E., Melo, E., Navajas, D., and Farre, R. (2014). Low oxygen tension enhances the generation of lung progenitor cells from mouse embryonic and induced pluripotent stem cells. *Physiol. Rep.* 2, e12075. doi:10.14814/phy2.12075
- Genovese, F., Manresa, A. A., Leeming, D. J., Karsdal, M. A., and Boor, P. (2014). The extracellular matrix in the kidney: a source of novel non-invasive biomarkers of kidney fibrosis? *Fibrogenesis Tissue Repair* 7, 4. doi:10.1186/1755-1536-7-4
- Gessel, M., Spraggins, J. M., Voziyani, P., Hudson, B. G., and Caprioli, R. M. (2015). Decellularization of intact tissue enables MALDI imaging mass spectrometry analysis of the extracellular matrix. *J. Mass Spectrom.* 50, 1288–1293. doi:10.1002/jms.3696
- Gilbert, T. W. (2012). Strategies for tissue and organ decellularization. *J. Cell. Biochem.* 113, 2217–2222. doi:10.1002/jcb.24130
- Gilbert, T. W., Freund, J. M., and Badylak, S. F. (2009). Quantification of DNA in biologic scaffold materials. *J. Surg. Res.* 152, 135–139. doi:10.1016/j.jss.2008.02.013
- Gilbert, T. W., Sellaro, T. L., and Badylak, S. F. (2006). Decellularization of tissues and organs. *Biomaterials* 27, 3675–3683. doi:10.1016/j.biomaterials.2006.02.014
- Gilbert, T. W., Stewart-Akers, A. M., Simmons-Byrd, A., and Badylak, S. F. (2007). Degradation and remodeling of small intestinal submucosa in canine achilles tendon repair. *J. Bone Joint Surg. Am.* 89, 621–630. doi:10.2106/JBJS.E.00742
- Gilbert, T. W., Wognum, S., Joyce, E. M., Freytes, D. O., Sacks, M. S., and Badylak, S. F. (2008). Collagen fiber alignment and biaxial mechanical behavior of porcine urinary bladder derived extracellular matrix. *Biomaterials* 29, 4775–4782. doi:10.1016/j.biomaterials.2008.08.022
- Goh, S. K., Bertera, S., Olsen, P., Candiello, J. E., Halfter, W., Uechi, G., et al. (2013). Perfusion-decellularized pancreas as a natural 3D scaffold for pancreatic tissue and whole organ engineering. *Biomaterials* 34, 6760–6772. doi:10.1016/j.biomaterials.2013.05.066
- Gong, J., Sagiv, O., Cai, H., Tsang, S. H., and Del Priore, L. V. (2008). Effects of extracellular matrix and neighboring cells on induction of human embryonic stem cells into retinal or retinal pigment epithelial progenitors. *Exp. Eye Res.* 86, 957–965. doi:10.1016/j.exer.2008.03.014
- Gorschewsky, O., Klakow, A., Riechert, K., Pitzl, M., and Becker, R. (2005). Clinical comparison of the Tutoplast allograft and autologous patellar tendon (bone-patellar tendon-bone) for the reconstruction of the anterior cruciate ligament: 2- and 6-year results. *Am. J. Sports Med.* 33, 1202–1209. doi:10.1177/0363546504271510
- Gouon-Evans, V. (2014). The race for regeneration: pluripotent-stem-cell-derived 3D kidney structures. *Cell Stem Cell* 14, 5–6. doi:10.1016/j.stem.2013.12.004
- Guan, Y., Liu, S., Liu, Y., Sun, C., Cheng, G., Luan, Y., et al. (2015a). Porcine kidneys as a source of ECM scaffold for kidney regeneration. *Mater. Sci. Eng. C* 56, 451–456. doi:10.1016/j.msec.2015.07.007
- Guan, Y., Liu, S., Sun, C., Cheng, G., Kong, F., Luan, Y., et al. (2015b). The effective bioengineering method of implantation decellularized renal extracellular matrix scaffolds. *Oncotarget* 6, 36126–36138. doi:10.18632/oncotarget.5304

- Habka, D., Mann, D., Landes, R., and Soto-Gutierrez, A. (2015). Future economics of liver transplantation: a 20-year cost modeling forecast and the prospect of bioengineering autologous liver grafts. *PLoS ONE* 10:e0131764. doi:10.1371/journal.pone.0131764
- Hall, I. E., Schröppel, B., Doshi, M. D., Ficek, J., Weng, F. L., Hasz, R. D., et al. (2015). Associations of deceased donor kidney injury with kidney discard and function after transplantation. *Am. J. Transplant.* 15, 1623–1631. doi:10.1111/ajt.13144
- Hammerman, M. R. (2002). Xenotransplantation of developing kidneys. *Am. J. Physiol. Renal. Physiol.* 283, F601–F606. doi:10.1152/ajprenal.00126.2002
- Hanna, J. H., Saha, K., and Jaenisch, R. (2010). Pluripotency and cellular reprogramming: facts, hypotheses, unresolved issues. *Cell* 143, 508–525. doi:10.1016/j.cell.2010.10.008
- Hass, R., Kasper, C., Böhm, S., and Jacobs, R. (2011). Different populations and sources of human mesenchymal stem cells (MSC): a comparison of adult and neonatal tissue-derived MSC. *Cell Commun. Signal.* 9, 12. doi:10.1186/1478-811X-9-12
- Hatano, R., Fujii, E., Segawa, H., Mukaisho, K., Matsubara, M., Miyamoto, K., et al. (2013). Ezrin, a membrane cytoskeletal cross-linker, is essential for the regulation of phosphate and calcium homeostasis. *Kidney Int.* 83, 41–49. doi:10.1038/ki.2012.308
- He, M., and Callanan, A. (2013). Comparison of methods for whole-organ decellularization in tissue engineering of bioartificial organs. *Tissue Eng. Part B Rev.* 19, 194–208. doi:10.1089/ten.teb.2012.0340
- He, M., Callanan, A., Lagaras, K., Steele, J. A. M., and Stevens, M. M. (2016). Optimization of SDS exposure on preservation of ECM characteristics in whole organ decellularization of rat kidneys. *J. Biomed. Mater. Res. B Appl. Biomater.* 1–9. doi:10.1002/jbm.b.33668
- Heilman, R. L., Smith, M. L., Kurian, S. M., Huskey, J., Batra, R. K., Chakkera, H. A., et al. (2015). Transplanting kidneys from deceased donors with severe acute kidney injury. *Am. J. Transplant.* 15, 2143–2151. doi:10.1111/ajt.13260
- Hendry, C. E., and Little, M. H. (2012). Reprogramming the kidney: a novel approach for regeneration. *Kidney Int.* 82, 138–146. doi:10.1038/ki.2012.68
- Hill, R. C., Calle, E. A., Dzieciatkowska, M., Niklason, L. E., and Hansen, K. C. (2015). Quantification of extracellular matrix proteins from a rat lung scaffold to provide a molecular readout for tissue engineering. *Mol. Cell. Proteomics* 1, 961–973. doi:10.1074/mcp.M114.045260
- Hodde, J., and Hiles, M. (2002). Virus safety of a porcine-derived medical device: evaluation of a viral inactivation method. *Biotechnol. Bioeng.* 79, 211–216. doi:10.1002/bit.10281
- Hollister, S. J. (2005). Porous scaffold design for tissue engineering. *Nat. Mater.* 4, 518–524. doi:10.1038/nmat1421
- Howard, R. J., Schold, J. D., and Cornell, D. L. (2005). A 10-year analysis of organ donation after cardiac death in the United States. *Transplantation* 80, 564–568. doi:10.1097/01.tp.0000168156.79847.46
- Hutton, J. (1999). The economics of immunosuppression in renal transplantation: a review of recent literature. *Transplant. Proc.* 31, 1328–1332. doi:10.1016/S0041-1345(98)02017-X
- Hynes, R. O. (2009). The extracellular matrix: not just pretty fibrils. *Science* 326, 1216–1219. doi:10.1126/science.1176009
- Jha, V., Garcia-Garcia, G., Iseki, K., Li, Z., Naicker, S., Plattner, B., et al. (2013). Chronic kidney disease: global dimension and perspectives. *Lancet* 382, 260–272. doi:10.1016/S0140-6736(13)60687-X
- Johnson, D. W., Herzig, K., Purdie, D., Brown, A. M., Rigby, R. J., Nicol, D. L., et al. (2000). A comparison of the effects of dialysis and renal transplantation on the survival of older uremic patients. *Transplantation* 69, 794–799. doi:10.1097/00007890-200003150-00020
- Johnson, L. B., Kuo, P. C., Schweitzer, E. J., Ratner, L. E., Klassen, D. K., Hoehn-Saric, E. W., et al. (1996). Double renal allografts successfully increase utilization of kidneys from older donors within a single organ procurement organization. *Transplantation* 62, 1581–1583. doi:10.1097/00007890-199612150-00009
- Kabsch, W., Mannherz, H. G., Suck, D., Pai, E. F., and Holmes, K. C. (1990). Atomic structure of the actin:DNase I complex. *Nature* 347, 37–44. doi:10.1038/347037a0
- Kayler, L. K., Garzon, P., Magliocca, J., Fujita, S., Kim, R. D., Hemming, A. W., et al. (2009). Outcomes and utilization of kidneys from deceased donors with acute kidney injury. *Am. J. Transplant.* 9, 367–373. doi:10.1111/j.1600-6143.2008.02505.x
- Kayler, L. K., Magliocca, J., Zendejas, I., Srinivas, T. R., and Schold, J. D. (2011). Impact of cold ischemia time on graft survival among ECD transplant recipients: a paired kidney analysis. *Am. J. Transplant.* 11, 2647–2656. doi:10.1111/j.1600-6143.2011.03741.x
- Keane, T. J., Londono, R., Turner, N. J., and Badyal, S. F. (2012). Consequences of ineffective decellularization of biologic scaffolds on the host response. *Biomaterials* 33, 1771–1781. doi:10.1016/j.biomaterials.2011.10.054
- Keller, G. (2005). Embryonic stem cell differentiation: emergence of a new era in biology and medicine. *Genes Dev.* 19, 1129–1155. doi:10.1101/gad.1303605
- Kim, S. M., Ahn, S., Min, S. I., Park, D., Park, T., Min, S. K., et al. (2013). Cold ischemic time is critical in outcomes of expanded criteria donor renal transplantation. *Clin. Transplant.* 27, 132–139. doi:10.1111/ctr.12034
- Klein, A. S., Messersmith, E. E., Ratner, L. E., Kochik, R., Baliga, P. K., and Ojo, A. O. (2010). Organ donation and utilization in the United States, 1999–2008. *Am. J. Transplant.* 10, 973–986. doi:10.1111/j.1600-6143.2009.03008.x
- Koorn, J. P., Joles, J. A., and Gerritsen, K. G. (2015). Creating a wearable artificial kidney: where are we now? *Expert Rev. Med. Devices* 12, 373–376. doi:10.1586/17434440.2015.1053466
- Krause, D., and Cantley, L. G. (2005). Bone marrow plasticity revisited: protection or differentiation in the kidney tubule? *J. Clin. Invest.* 115, 1705–1708. doi:10.1172/JCI25540
- Lai, C.-F., Tsai, H.-B., Hsu, S.-H., Chiang, C.-K., Huang, J.-W., and Huang, S.-J. (2013). Withdrawal from long-term hemodialysis in patients with end-stage renal disease in Taiwan. *J. Formos. Med. Assoc.* 112, 589–599. doi:10.1016/j.jfma.2013.04.009
- Levey, A. S., and Coresh, J. (2012). Chronic kidney disease. *Lancet* 379, 165–180. doi:10.1016/S0140-6736(11)60178-5
- Li, B., Cohen, A., Hudson, T. E., Motlagh, D., Amrani, D. L., and Duffield, J. S. (2010). Mobilized human hematopoietic stem/progenitor cells promote kidney repair after ischemia/reperfusion injury. *Circulation* 121, 2211–2220. doi:10.1161/CIRCULATIONAHA.109.928796
- Liao, J., Joyce, E. M., and Sacks, M. S. (2008). Effects of decellularization on the mechanical and structural properties of the porcine aortic valve leaflet. *Biomaterials* 29, 1065–1074. doi:10.1016/j.biomaterials.2007.11.007
- Lih, E., Park, K. W., Chun, S. Y., Kim, H., Kwon, T. G., Joung, Y. K., et al. (2016). Biomimetic porous PLGA scaffolds incorporating decellularized extracellular matrix for kidney tissue regeneration. *ACS Appl. Mater. Interfaces* 8, 21145–21154. doi:10.1021/acsami.6b03771
- Lin, Y.-Q., Wang, L.-R., Pan, L.-L., Wang, H., Zhu, G.-Q., Liu, W.-Y., et al. (2016). Kidney bioengineering in regenerative medicine: an emerging therapy for kidney disease. *Cytotherapy* 18, 186–197. doi:10.1016/j.jcyt.2015.10.004
- Little, M. H., Brennan, J., Georgas, K., Davies, J. A., Davidson, D. R., Baldock, R. A., et al. (2007). A high-resolution anatomical ontology of the developing murine genitourinary tract. *Gene Expr. Patterns* 7, 680–699. doi:10.1016/j.modgep.2007.03.002
- Liu, R., Gao, J., Yang, Y., Zeng, W. (2015a). Preparation of rat whole-kidney acellular matrix via peristaltic pump. *Urol J* 12, 2457–2461.
- Liu, J., Yu, F., Sun, Y., Jiang, B., Zhang, W., Yang, J., et al. (2015b). Concise reviews: characteristics and potential applications of human dental tissue-derived mesenchymal stem cells. *Stem Cells* 33, 627–638. doi:10.1002/stem.1909
- Lu, H., Hoshiba, T., Kawazoe, N., Koda, I., Song, M., and Chen, G. (2011). Cultured cell-derived extracellular matrix scaffolds for tissue engineering. *Biomaterials* 32, 9658–9666. doi:10.1016/j.biomaterials.2011.08.091
- Mae, S.-I., Shono, A., Shiota, F., Yasuno, T., Kajiwara, M., Gotoda-Nishimura, N., et al. (2013). Monitoring and robust induction of nephrogenic intermediate mesoderm from human pluripotent stem cells. *Nat. Commun.* 4, 1367. doi:10.1038/ncomms2378
- Matas, A. J., Smith, J. M., Skeans, M. A., Thompson, B., Gustafson, S. K., Stewart, D. E., et al. (2015). OPTN/SRTR 2013 Annual Data Report: Kidney. *Am. J. Transplant.* 15(Suppl. 2), 1–34. doi:10.1111/ajt.13195
- Matthiesen, T., Ott, H. C., Goh, S.-K., Kren, S. M., and Taylor, D. A. (2007). Abstract 428: creating biocompatible 3-D scaffolds for engineering cardiovascular tissues: heart, lung, and kidney. *Circulation* 116, IL_70-c.
- Maunsbach, A. B. (1966). Observations on the segmentation of the proximal tubule in the rat kidney. *J. Ultrastruct. Res.* 16, 239–258. doi:10.1016/S0022-5320(66)80019-9

- McKee, R., and Wingert, R. (2016). Repopulating decellularized kidney scaffolds: an avenue for ex vivo organ generation. *Materials (Basel)* 9, 190. doi:10.3390/ma9030190
- Mecham, R. P. (2001). "Overview of extracellular matrix," in *Current Protocols in Cell Biology*. Hoboken, NJ: John Wiley & Sons, Inc., Unit 10.1.
- Meister, A. (1974). They-glutamyl cycle. *Ann. Intern. Med.* 81, 247. doi:10.7326/0003-4819-81-2-247
- Merion, R. M., Ashby, V. B., Wolfe, R. A., Distant, D. A., Hulbert-Shearon, T. E., Metzger, R. A., et al. (2005). Deceased-donor characteristics and the survival benefit of kidney transplantation. *JAMA* 294, 2726–2733. doi:10.1001/jama.294.21.2726
- Mirmalek-Sani, S.-H., Sullivan, D. C., Zimmerman, C., Shupe, T. D., and Petersen, B. E. (2013). Immunogenicity of decellularized porcine liver for bioengineered hepatic tissue. *Am. J. Pathol.* 183, 558–565. doi:10.1016/j.ajpath.2013.05.002
- Moini, M., Schilsky, M. L., and Tichy, E. M. (2015). Review on immunosuppression in liver transplantation. *World J. Hepatol.* 7, 1355–1368. doi:10.4254/wjh.v7.i10.1355
- Moldovan, G.-L., Pfander, B., and Jentsch, S. (2007). PCNA, the maestro of the replication fork. *Cell* 129, 665–679. doi:10.1016/j.cell.2007.05.003
- Moroni, F., and Mirabella, T. (2014). Decellularized matrices for cardiovascular tissue engineering. *Am. J. Stem Cells* 3, 1–20.
- Murray, C. J. L., Abraham, J., Ali, M. K., Alvarado, M., Atkinson, C., Baddour, L. M., et al. (2013). The state of US health, 1990–2010: burden of diseases, injuries, and risk factors. *JAMA* 310, 591–608. doi:10.1001/jama.2013.13805
- Naba, A., Clauser, K. R., Hoersch, S., Liu, H., Carr, S. A., and Hynes, R. O. (2012). The matrisome: in silico definition and in vivo characterization by proteomics of normal and tumor extracellular matrices. *Mol. Cell. Proteomics* 11, M111.014647. doi:10.1074/mcp.M111.014647
- Nagata, S., Hanayama, R., and Kawane, K. (2010). Autoimmunity and the clearance of dead cells. *Cell* 140, 619–630. doi:10.1016/j.cell.2010.02.014
- Nakayama, K. H., Batchelder, C. A., Lee, C. I., and Tarantal, A. F. (2010). Decellularized rhesus monkey kidney as a three-dimensional scaffold for renal tissue engineering. *Tissue Eng. Part A* 16, 2207–2216. doi:10.1089/ten.TEA.2009.0602
- Nakayama, K. H., Batchelder, C. A., Lee, C. I., and Tarantal, A. F. (2011). Renal tissue engineering with decellularized rhesus monkey kidneys: age-related differences. *Tissue Eng. Part A* 17, 2891–2901. doi:10.1089/ten.TEA.2010.0714
- Nakayama, K. H., Lee, C. C. I., Batchelder, C. A., and Tarantal, A. F. (2013). Tissue specificity of decellularized rhesus monkey kidney and lung scaffolds. *PLoS ONE* 8:e64134. doi:10.1371/journal.pone.0064134
- Naranjo, T. Á., Noguera-Salvá, R., and Fariñas Guerrero, F. (2009). Extracellular matrix: morphology, function and biotensegrity (part I). *Rev. Esp. Patol.* 42, 249–261.
- Narayanan, K., Leck, K.-J., Gao, S., and Wan, A. C. A. (2009). Three-dimensional reconstituted extracellular matrix scaffolds for tissue engineering. *Biomaterials* 30, 4309–4317. doi:10.1016/j.biomaterials.2009.04.049
- National Kidney and Urologic Diseases Information Clearinghouse. (2012). Kidney disease statistics for the United States. *Natl. Inst. Health* 12, 1–16.
- Ng, S. L. J., Narayanan, K., Gao, S., and Wan, A. C. A. (2011). Lineage restricted progenitors for the repopulation of decellularized heart. *Biomaterials* 32, 7571–7580. doi:10.1016/j.biomaterials.2011.06.065
- Nguyen, D. M., and El-Serag, H. B. (2010). The epidemiology of obesity. *Gastroenterol. Clin. North Am.* 39, 1–7. doi:10.1016/j.gtc.2009.12.014
- Nishinakamura, R. (2008). Stem cells in the embryonic kidney. *Kidney Int.* 73, 913–917. doi:10.1038/sj.ki.5002784
- Nowacki, M., Kloskowski, T., Pokrywczyńska, M., Nazarewski, L., Jundziłł, A., Pietkun, K., et al. (2014). Is regenerative medicine a new hope for kidney replacement? *J. Artif. Organs* 17, 123–134. doi:10.1007/s10047-014-0767-z
- Nygard, A.-B., Jørgensen, C. B., Cirera, S., and Fredholm, M. (2007). Selection of reference genes for gene expression studies in pig tissues using SYBR green qPCR. *BMC Mol. Biol.* 8:67. doi:10.1186/1471-2199-8-67
- O'Brien, F. J. (2011). Biomaterials & scaffolds for tissue engineering. *Mater. Today* 14, 88–95. doi:10.1016/S1369-7021(11)70058-X
- Ofenbauer, A., Sebinger, D. D. R., Prewitz, M., Gruber, P., and Werner, C. (2015). Dewaxed ECM: a simple method for analyzing cell behaviour on decellularized extracellular matrices. *J. Tissue Eng. Regen. Med.* 9, 1046–1055. doi:10.1002/term.1658
- Ojo, A. O., Hanson, J. A., Meier-Kriesche, H., Okechukwu, C. N., Wolfe, R. A., Leichtman, A. B., et al. (2001). Survival in recipients of marginal cadaveric donor kidneys compared with other recipients and wait-listed transplant candidates. *J. Am. Soc. Nephrol.* 12, 589–597.
- Orandi, B. J., Luo, X., Massie, A. B., Garonzik-Wang, J. M., Lonze, B. E., Ahmed, R., et al. (2016). Survival benefit with kidney transplants from HLA-incompatible live donors. *N. Engl. J. Med.* 374, 940–950. doi:10.1056/NEJMoa1508380
- Orlando, G., Booth, C., Wang, Z., Totonelli, G., Ross, C. L., Moran, E., et al. (2013). Discarded human kidneys as a source of ECM scaffold for kidney regeneration technologies. *Biomaterials* 34, 5915–5925. doi:10.1016/j.biomaterials.2013.04.033
- Orlando, G., Farney, A. C., Iskandar, S. S., Mirmalek-Sani, S.-H., Sullivan, D. C., Moran, E., et al. (2012). Production and implantation of renal extracellular matrix scaffolds from porcine kidneys as a platform for renal bioengineering investigations. *Ann. Surg.* 256, 363–370. doi:10.1097/SLA.0b013e31825a02ab
- Orlando, G., Wood, K. J., Stratta, R. J., Yoo, J. J., Atala, A., and Soker, S. (2011a). Regenerative medicine and organ transplantation: past, present, and future. *Transplantation* 91, 1310–1317. doi:10.1097/TP.0b013e318219ebb5
- Orlando, G., Baptista, P., Birchall, M., De Coppi, P., Farney, A., Guimaraes-Souza, N. K., et al. (2011b). Regenerative medicine as applied to solid organ transplantation: current status and future challenges. *Transpl. Int.* 24, 223–232. doi:10.1111/j.1432-2277.2010.01182.x
- Ott, H. C., Clippinger, B., Conrad, C., Schuetz, C., Pomerantseva, I., Ikononou, L., et al. (2010). Regeneration and orthotopic transplantation of a bioartificial lung. *Nat. Med.* 16, 927–933. doi:10.1038/nm.2193
- Ott, H. C., Matthiesen, T. S., Goh, S.-K., Black, L. D., Kren, S. M., Netoff, T. I., et al. (2008). Perfusion-decellularized matrix: using nature's platform to engineer a bioartificial heart. *Nat. Med.* 14, 213–221. doi:10.1038/nm1684
- Pannabecker, T. L. (2012). Structure and function of the thin limbs of the loop of henle. *Compr. Physiol.* 2, 2063–2086. doi:10.1002/cphy.c110019
- Park, K. M., and Woo, H. M. (2012). Porcine bioengineered scaffolds as new frontiers in regenerative medicine. *Transplant. Proc.* 44, 1146–1150. doi:10.1016/j.transproceed.2012.03.043
- Pascual, J., Zamora, J., and Pirsch, J. D. (2008). A systematic review of kidney transplantation from expanded criteria donors. *Am. J. Kidney Dis.* 52, 553–586. doi:10.1053/j.ajkd.2008.06.005
- Peloso, A., Katari, R., Patel, T., Hemal, S., Zambon, J. P., Salvatori, M., et al. (2013). Considerations on the development of a model of kidney bioengineering and regeneration in rats. *Expert Rev. Med. Devices* 10, 597–601. doi:10.1586/17434440.2013.827528
- Peloso, A., Petrosyan, A., Da Sacco, S., Booth, C., Zambon, J. P., O'Brien, T., et al. (2015). Renal extracellular matrix scaffolds from discarded kidneys maintain glomerular morphometry and vascular resilience and retains critical growth factors. *Transplantation* 99, 1807–1816. doi:10.1097/TP.0000000000000811
- Peloso, A., Tamburrini, R., Edgar, L., Wilm, B., Katari, R., Perin, L., et al. (2016). Extracellular matrix scaffolds as a platform for kidney regeneration. *Eur. J. Pharmacol.* 790, 21–27. doi:10.1016/j.ejphar.2016.07.038
- Petersen, T. H., Calle, E. A., Colehour, M. B., and Niklason, L. E. (2012). Matrix composition and mechanics of decellularized lung scaffolds. *Cells Tissues Organs* 195, 222–231. doi:10.1159/000324896
- Petrosyan, A., Orlando, G., Peloso, A., Wang, Z., Farney, A. C., Rogers, J., et al. (2015). Understanding the bioactivity of stem cells seeded on extracellular matrix scaffolds produced from discarded human kidneys: a critical step towards a new generation bio-artificial kidney. *Issues* 1. Available at: http://www.researchgate.net/profile/Astgik_Petrosyan/publication/273451480_Understanding_the_bioactivity_of_stem_cells_seeded_on_extracellular_matrix_scaffolds_produced_from_discarded_human_kidneys_a_critical_step_towards_a_new_generation_bio-artificial_kidney
- Poornajad, N., Frost, T. S., Scott, D. R., Elton, B. B., Reynolds, P. R., Roeder, B. L., et al. (2015). Freezing/thawing without cryoprotectant damages native but not decellularized porcine renal tissue. *Organogenesis* 11, 30–45. doi:10.1080/15476278.2015.1022009
- Poornajad, N., Momtahan, N., Salehi, A. S. M., Scott, D. R., Fronk, C. A., Roeder, B. L., et al. (2016a). Efficient decellularization of whole porcine kidneys improves reseeded cell behavior. *Biomed. Mater.* 11, 25003. doi:10.1088/1748-6041/11/2/025003
- Poornajad, N., Schaumann, L. B., Buckmiller, E. M., Momtahan, N., Gassman, J. R., Ma, H. H., et al. (2016b). The impact of decellularization agents on renal tissue extracellular matrix. *J. Biomater. Appl.* 31, 521–533. doi:10.1177/0885328216656099

- Poorejad, N., Nielsen, J. J., Morris, R. J., Gassman, J. R., Reynolds, P. R., Roeder, B. L., et al. (2016c). Comparison of four decontamination treatments on porcine renal decellularized extracellular matrix structure, composition, and support of human renal cortical tubular epithelium cells. *J. Biomed. Appl.* 30, 1154–1167. doi:10.1177/0885328215615760
- Port, F. K., Bragg-Gresham, J. L., Metzger, R. A., Dykstra, D. M., Gillespie, B. W., Young, E. W., et al. (2002). Donor characteristics associated with reduced graft survival: an approach to expanding the pool of kidney donors. *Transplantation* 74, 1281–1286. doi:10.1097/01.TP.0000034060.18738.0B
- Price, A. P., England, K. A., Matson, A. M., Blazar, B. R., and Panoskaltis-Mortari, A. (2010). Development of a decellularized lung bioreactor system for bioengineering the lung: the matrix reloaded. *Tissue Eng. Part A* 16, 2581–2591. doi:10.1089/ten.tea.2009.0659
- Qiu, Q.-Q., Leamy, P., Brittingham, J., Pomerleau, J., Kabaria, N., and Connor, J. (2009). Inactivation of bacterial spores and viruses in biological material using supercritical carbon dioxide with sterilant. *J. Biomed. Mater. Res. Part B Appl. Biomater.* 91, 572–578. doi:10.1002/jbm.b.31431
- Rafighdoust, A., Shahri, N. M., and Baharara, J. (2015). Decellularized kidney in the presence of chondroitin sulfate as a natural 3D scaffold for stem cells. *Iran J. Basic Med. Sci.* 18, 788–798.
- Ramage, L. (2011). Integrins and extracellular matrix in mechanotransduction. *Cell Health Cytoskeleton* 4, 1. doi:10.2147/CHC.S21829
- Rana, A., Gruessner, A., Agopian, V. G., Khalpey, Z., Riaz, I. B., Kaplan, B., et al. (2015). Survival benefit of solid-organ transplant in the United States. *JAMA Surg.* 150, 252–259. doi:10.1001/jamasurg.2014.2038
- Rana, D., Zreiqat, H., Benkirane-Jessel, N., Ramakrishna, S., and Ramalingam, M. (2017). Development of decellularized scaffolds for stem cell-driven tissue engineering. *J. Tissue Eng. Regen. Med.* 11, 942–965. doi:10.1002/term.2061
- Randles, M., Humphries, M. J., and Lennon, R. (2017). Proteomic definitions of basement membrane composition in health and disease. *Matrix Biol.* 57–58, 12–28. doi:10.1016/j.matbio.2016.08.006
- Reing, J. E., Brown, B. N., Daly, K. A., Freund, J. M., Gilbert, T. W., Hsiang, S. X., et al. (2010). The effects of processing methods upon mechanical and biologic properties of porcine dermal extracellular matrix scaffolds. *Biomaterials* 31, 8626–8633. doi:10.1016/j.biomaterials.2010.07.083
- Ren, X., Tapias, L. F., Jank, B. J., Mathisen, D. J., Lanuti, M., and Ott, H. C. (2015). Ex vivo non-invasive assessment of cell viability and proliferation in bio-engineered whole organ constructs. *Biomaterials* 52, 103–112. doi:10.1016/j.biomaterials.2015.01.061
- Reticker-Flynn, N. E., Malta, D. F. B., Winslow, M. M., Lamar, J. M., Xu, M. J., Underhill, G. H., et al. (2012). A combinatorial extracellular matrix platform identifies cell-extracellular matrix interactions that correlate with metastasis. *Nat. Commun.* 3, 1122. doi:10.1038/ncomms2128
- Rogers, I. (2011). Induced pluripotent stem cells from human kidney. *J. Am. Soc. Nephrol.* 22, 1179–1180. doi:10.1681/ASN.2011050501
- Roodnat, J. I., Mulder, P. G. H., Van Riemsdijk, I. C., IJzermans, J. N. M., van Gelder, T., and Weimar, W. (2003). Ischemia times and donor serum creatinine in relation to renal graft failure. *Transplantation* 75, 799–804. doi:10.1097/01.TP.0000056632.00848.8D
- Rosario, D. J., Reilly, G. C., Ali Salah, E., Glover, M., Bullock, A. J., and Macneil, S. (2008). Decellularization and sterilization of porcine urinary bladder matrix for tissue engineering in the lower urinary tract. *Regen. Med.* 3, 145–156. doi:10.2217/17460751.3.2.145
- Rose, W., Wood, J. D., Simmons-byrd, A., and Spievack, A. R. (2009). Effect of a xenogeneic urinary bladder injectable bioscaffold on lameness in dogs with osteoarthritis of the coxofemoral joint (Hip): a randomized, double blinded controlled trial. *Int. J. Appl. Res. Vet. Med.* 7, 13–22.
- Ross, E. A. (2009). "Kidney regeneration using stem cells and acellular whole organ scaffolds: perspective and recent developments" in *World Congress on Medical Physics and Biomedical Engineering, September 7–12, 2009, Munich, Germany*, 936–939.
- Ross, E. A., Abrahamson, D. R., St John, P., Clapp, W. L., Williams, M. J., Terada, N., et al. (2012). Mouse stem cells seeded into decellularized rat kidney scaffolds endothelialize and remodel basement membranes. *Organogenesis* 8, 49–55. doi:10.4161/org.20209
- Ross, E. A., Williams, M. J., Hamazaki, T., Terada, N., Clapp, W. L., Adin, C., et al. (2009). Embryonic stem cells proliferate and differentiate when seeded into kidney scaffolds. *J. Am. Soc. Nephrol.* 20, 2338–2347. doi:10.1681/ASN.2008111196
- Roy, S., Goldman, K., Marchant, R., Zydny, A., Brown, D., Fleischman, A., et al. (2011). Implanted renal replacement for end-stage renal disease. *Panminerva Med.* 53, 155–166.
- Sambi, M., Chow, T., Whiteley, J., Li, M., Chua, S., Raileanu, V., et al. (2017). Acellular mouse kidney ECM can be used as a three-dimensional substrate to test the differentiation potential of embryonic stem cell derived renal progenitors. *Stem Cell Rev.* doi:10.1007/s12015-016-9712-2
- Scarritt, M. E., Pashos, N. C., and Bunnell, B. A. (2015). A review of cellularization strategies for tissue engineering of whole organs. *Front. Bioeng. Biotechnol.* 3:43. doi:10.3389/fbioe.2015.00043
- Shupe, T., Williams, M., Brown, A., Willenberg, B., and Petersen, B. E. (2010). Method for the decellularization of intact rat liver. *Organogenesis* 6, 134–136. doi:10.4161/org.6.2.11546
- Singh, P., Carraher, C., and Schwarzbauer, J. E. (2010). Assembly of fibronectin extracellular matrix. *Annu. Rev. Cell Dev. Biol.* 26, 397–419. doi:10.1146/annurev-cellbio-100109-104020
- Song, B., Smink, A. M., Jones, C. V., Callaghan, J. M., Firth, S. D., Bernard, C. A., et al. (2012). The directed differentiation of human iPS cells into kidney podocytes. *PLoS ONE* 7:e46453. doi:10.1371/journal.pone.0046453
- Song, J. J., Guyette, J. P., Gilpin, S. E., Gonzalez, G., Vacanti, J. P., and Ott, H. C. (2013). Regeneration and experimental orthotopic transplantation of a bioengineered kidney. *Nat. Med.* 19, 646–651. doi:10.1038/nm.3154
- Song, J. J., and Ott, H. C. (2011). Organ engineering based on decellularized matrix scaffolds. *Trends Mol. Med.* 17, 424–432. doi:10.1016/j.molmed.2011.03.005
- Stratta, R. J., Rohr, M. S., Sundberg, A. K., Farney, A. C., Hartmann, E. L., Moore, P. S., et al. (2006). Intermediate-term outcomes with expanded criteria deceased donors in kidney transplantation: a spectrum or specter of quality? *Ann. Surg.* 243, 594–601; discussion 601–603. doi:10.1097/01.sla.0000216302.43776.1a
- Sugawara, M., Ichimura, S., Kokubo, K., Shimbo, T., Hirose, M., Kobayashi, H., et al. (2011). Transplantation: basic science and immune-tolerance. *Clin. Kidney J.* 4, 4.s2.42. doi:10.1093/ndpplus/4.s2.42
- Suh, J. H., and Miner, J. H. (2013). The glomerular basement membrane as a barrier to albumin. *Nat. Rev. Nephrol.* 9, 470–477. doi:10.1038/nrneph.2013.109
- Sullivan, D. C., Mirmalek-Sani, S.-H., Deegan, D. B., Baptista, P. M., Aboushwareb, T., Atala, A., et al. (2012). Decellularization methods of porcine kidneys for whole organ engineering using a high-throughput system. *Biomaterials* 33, 7756–7764. doi:10.1016/j.biomaterials.2012.07.023
- Sun, W. Q., and Leung, P. (2008). Calorimetric study of extracellular tissue matrix degradation and instability after gamma irradiation. *Acta Biomater.* 4, 817–826. doi:10.1016/j.actbio.2008.02.006
- Swetha, G., Chandra, V., Phadnis, S., and Bhonde, R. (2011). Glomerular parietal epithelial cells of adult murine kidney undergo EMT to generate cells with traits of renal progenitors. *J. Cell. Mol. Med.* 15, 396–413. doi:10.1111/j.1582-4934.2009.00937.x
- Taguchi, A., Kaku, Y., Ohmori, T., Sharmin, S., Ogawa, M., Sasaki, H., et al. (2014). Redefining the in vivo origin of metanephric nephron progenitors enables generation of complex kidney structures from pluripotent stem cells. *Cell Stem Cell* 14, 53–67. doi:10.1016/j.stem.2013.11.010
- Taguchi, A., and Nishinakamura, R. (2014). Nephron reconstitution from pluripotent stem cells. *Kidney Int.* 87, 1–7. doi:10.1038/ki.2014.358
- Tanemoto, M., Toyohara, T., Abe, T., and Ito, S. (2008). MAGI-1a functions as a scaffolding protein for the distal renal tubular basolateral K⁺ channels. *J. Biol. Chem.* 283, 12241–12247. doi:10.1074/jbc.M707738200
- Teodori, L., Costa, A., Marzio, R., Perniconi, B., Coletti, D., Adamo, S., et al. (2014). Native extracellular matrix: a new scaffolding platform for repair of damaged muscle. *Front. Physiol.* 5:218. doi:10.3389/fphys.2014.00218
- Tien, J., and Nelson, C. M. (2014). Microstructured extracellular matrices in tissue engineering and development: an update. *Ann. Biomed. Eng.* 42, 1413–1423. doi:10.1007/s10439-013-0912-5
- Tonelli, M., Wiebe, N., Knoll, G., Bello, A., Browne, S., Jadhav, D., et al. (2011). Systematic review: kidney transplantation compared with dialysis in clinically relevant outcomes. *Am. J. Transplant.* 11, 2093–2109. doi:10.1111/j.1600-6143.2011.03686.x
- Ullrich, K. J. (1979). Sugar, amino acid, and NA⁺ cotransport in the proximal tubule. Available at: <http://www.annualreviews.org/doi/pdf/10.1146/annurev.ph.41.030179.001145>

- United States Renal Data System. (2015). CKD in the United States: an overview of the USRDS Annual Data Report, volume 1. *Am. J. Kidney Dis.* 66, S1–S10. doi:10.1053/j.ajkd.2015.04.017
- USRDS. (2016). Chapter 7: transplantation. *Am. J. Kidney Dis.* 67, S227–S238. doi:10.1053/j.ajkd.2016.02.018
- Usui, J., Kobayashi, T., Yamaguchi, T., Knisely, A. S., Nishinakamura, R., and Nakauchi, H. (2012). Generation of kidney from pluripotent stem cells via blastocyst complementation. *Am. J. Pathol.* 180, 2417–2426. doi:10.1016/j.ajpath.2012.03.007
- Uygun, B. E., Soto-Gutierrez, A., Yagi, H., Izamis, M.-L., Guzzardi, M. A., Shulman, C., et al. (2010). Organ reengineering through development of a transplantable recellularized liver graft using decellularized liver matrix. *Nat. Med.* 16, 814–820. doi:10.1038/nm.2170
- Uzarski, J. S., Bijonowski, B. M., Wang, B., Ward, H. H., Wandinger-Ness, A., Miller, W. M., et al. (2015). Dual-purpose bioreactors to monitor noninvasive physical and biochemical markers of kidney and liver scaffold recellularization. *Tissue Eng. Part C Methods* 21, 1032–1043. doi:10.1089/ten.tec.2014.0665
- Uzarski, J. S., Xia, Y., Belmonte, J. C. I., and Wertheim, J. A. (2014). New strategies in kidney regeneration and tissue engineering. *Curr. Opin. Nephrol. Hypertens.* 23, 399–405. doi:10.1097/01.mnh.0000447019.66970.ea
- Valapour, M., Skeans, M. A., Heubner, B. M., Smith, J. M., Schnitzler, M. A., Hertz, M. I., et al. (2014). OPTN/SRTR 2012 Annual Data Report: kidney. *Am. J. Transplant.* 14, 11–44. doi:10.1111/ajt.12579
- Vavken, P., Joshi, S., and Murray, M. M. (2009). TRITON-X is most effective among three decellularization agents for ACL tissue engineering. *J. Orthop. Res.* 27, 1612–1618. doi:10.1002/jor.20932
- Vishwakarma, S. K., Bhavani, P. G., Bardia, A., Abkari, A., Murthy, G. S., Venkateshwarulu, J., et al. (2014). Preparation of natural three-dimensional goat kidney scaffold for the development of bioartificial organ. *Indian J. Nephrol.* 24, 372–375. doi:10.4103/09714065.133008
- Vogetseder, A., Picard, N., Gaspert, A., Walch, M., Kaissling, B., and Le Hir, M. (2008). Proliferation capacity of the renal proximal tubule involves the bulk of differentiated epithelial cells. *Am. J. Physiol. Cell Physiol.* 294, C22–C28. doi:10.1152/ajpcell.00227.2007
- Vorotnikova, E., McIntosh, D., Dewilde, A., Zhang, J., Reing, J. E., Zhang, L., et al. (2010). Extracellular matrix-derived products modulate endothelial and progenitor cell migration and proliferation in vitro and stimulate regenerative healing in vivo. *Matrix Biol.* 29, 690–700. doi:10.1016/j.matbio.2010.08.007
- Wainwright, J. M., Czajka, C. A., Patel, U. B., Freytes, D. O., Tobita, K., Gilbert, T. W., et al. (2010). Preparation of cardiac extracellular matrix from an intact porcine heart. *Tissue Eng. Part C Methods* 16, 525–532. doi:10.1089/ten.tec.2009.0392
- Wallis, J. M., Borg, Z. D., Daly, A. B., Deng, B., Ballif, B. A., Allen, G. B., et al. (2012). Comparative assessment of detergent-based protocols for mouse lung de-cellularization and re-cellularization. *Tissue Eng. Part C Methods* 18, 420–432. doi:10.1089/ten.tec.2011.0567
- Wang, Y., Bao, J., Wu, Q., Zhou, Y., Li, Y., Wu, X., et al. (2014). Method for perfusion decellularization of porcine whole liver and kidney for use as a scaffold for clinical-scale bioengineering grafts. *Xenotransplantation*. Available at: <http://www.ncbi.nlm.nih.gov/pubmed/25291435>
- Wen, D., Ni, L., You, L., Zhang, L., Gu, Y., Hao, C.-M., et al. (2012). Upregulation of nestin in proximal tubules may participate in cell migration during renal repair. *Am. J. Physiol. Renal. Physiol.* 303, F1534–F1544. doi:10.1152/ajprenal.00083.2012
- Willenberg, B. J., Oca-Cossio, J., Cai, Y., Brown, A. R., Clapp, W. L., Abrahamson, D. R., et al. (2015). Repurposed biological scaffolds: kidney to pancreas. *Organogenesis* 11, 47–57. doi:10.1080/15476278.2015.1067354
- Wolfe, R. A., Ashby, V. B., Milford, E. L., Ojo, A. O., Ettenger, R. E., Agodoa, L. Y. C., et al. (1999). Comparison of mortality in all patients on dialysis, patients on dialysis awaiting transplantation, and recipients of a first cadaveric transplant. *N. Engl. J. Med.* 341, 1725–1730. doi:10.1056/NEJM19991203412303
- Wolfe, R. A., Roys, E. C., and Merion, R. M. (2010). Trends in organ donation and transplantation in the United States, 1999–2008. *Am. J. Transplant.* 10, 961–972. doi:10.1111/j.1600-6143.2010.03021.x
- Woods, T., and Gratzner, P. F. (2005). Effectiveness of three extraction techniques in the development of a decellularized bone-anterior cruciate ligament-bone graft. *Biomaterials* 26, 7339–7349. doi:10.1016/j.biomaterials.2005.05.066
- Xia, Y., Friedmann, P., Cortes, C. M., Lubetzky, M. L., and Kayler, L. K. (2015). Influence of cold ischemia time in combination with donor acute kidney injury on kidney transplantation outcomes. *J. Am. Coll. Surg.* 221, 532–538. doi:10.1016/j.jamcollsurg.2015.05.003
- Xu, H., Xu, B., Yang, Q., Li, X., Ma, X., Xia, Q., et al. (2014). Comparison of decellularization protocols for preparing a decellularized porcine annulus fibrosus scaffold. *PLoS ONE* 9:e86723. doi:10.1371/journal.pone.0086723
- Yagi, H., Fukumitsu, K., Fukuda, K., Kitago, M., Shinoda, M., Obara, H., et al. (2013). Human-scale whole-organ bioengineering for liver transplantation: a regenerative medicine approach. *Cell Transplant.* 22, 231–242. doi:10.3727/096368912X654939
- Yamanaka, S., and Blau, H. M. (2010). Nuclear reprogramming to a pluripotent state by three approaches. *Nature* 465, 704–712. doi:10.1038/nature09229
- Yokoo, T., and Kawamura, T. (2009). Xenobiotic kidney organogenesis: a new avenue for renal transplantation. *J. Nephrol.* 22, 312–317.
- Yokote, S., Yamanaka, S., and Yokoo, T. (2012). De novo kidney regeneration with stem cells. *J. Biomed. Biotechnol.* 2012, 453519. doi:10.1155/2012/453519
- Yu, Y. L., Shao, Y. K., Ding, Y. Q., Lin, K. Z., Chen, B., Zhang, H. Z., et al. (2014). Decellularized kidney scaffold-mediated renal regeneration. *Biomaterials* 35, 6822–6828. doi:10.1016/j.biomaterials.2014.04.074
- Zhang, Q., Raoof, M., Chen, Y., Sumi, Y., Sursal, T., Junger, W., et al. (2010). Circulating mitochondrial DAMPs cause inflammatory responses to injury. *Nature* 464, 104–107. doi:10.1038/nature08780

Conflict of Interest Statement: The authors declare that the research was conducted in the absence of any commercial or financial relationships that could be construed as a potential conflict of interest.

The reviewer, MH, and handling editor declared their shared affiliation, and the handling editor states that the process nevertheless met the standards of a fair and objective review.

Copyright © 2017 Destefani, Sirtoli and Nogueira. This is an open-access article distributed under the terms of the Creative Commons Attribution License (CC BY). The use, distribution or reproduction in other forums is permitted, provided the original author(s) or licensor are credited and that the original publication in this journal is cited, in accordance with accepted academic practice. No use, distribution or reproduction is permitted which does not comply with these terms.

5. CAPÍTULO 2

Artigo II

TIME OPTIMIZATION IN RAT KIDNEY DECELLULARIZATION PROCESS: ECM CHARACTERIZATION BY MASS SPECTROMETRY

Time optimization in rat kidney decellularization process: ECM characterization by mass spectrometry

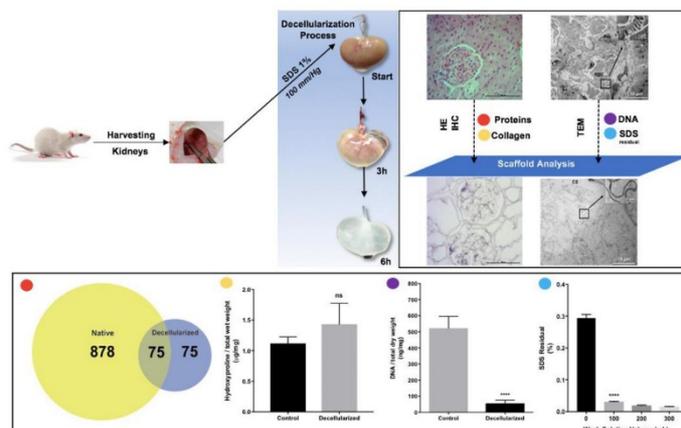
Received 12th October 2018,
Accepted 00th January 20xx

DOI: 10.1039/x0xx00000x

www.rsc.org/

A. C. Destefani^{a,b}, G. M. Sirtoli^b, F. G. Amorim^{a,b,c}, G. H. Taufner^{a,b}, T. E. C. Zanardo^{a,b}, I. F. Lima^d, L. K. Iwaj^d and B. V. Nogueira^{a,b*}

Whole rat kidney decellularization was obtained by a reduced time (6 hours) and concentration of ionic detergent solutions (SDS, 1%) perfusion through the renal artery. At the end of this stage, the kidney scaffolds showed translucent physical features and preserved vascular conduits. Histochemical analysis and electron microscopy revealed glomerulus with the preserved basal membrane (GBM), beside tubular and vascular network without cell debris residue and DNA. Proteomic analysis identified majority proteins preservation related to extracellular matrix (ECM) compounds. Thus, the using of low concentration of SDS for 6 hours promotes a successful decellularization process that removed the cells and DNA and protecting extracellular matrix with minimum SDS residue.



Introduction

Chronic Kidney Disease (CKD) is currently one of the world's primary concerns regarding public health expenditures and patient recovery following dialysis or kidney transplant procedures¹. Millions of people with chronic kidney disease that subsequently develop into kidney failure who need transplantation to survive. In the United States, there are about 26 million Americans in these conditions, and the number of new cases of kidney failure exceeds 90,000 annually and \$14 billion in costs involved with treatment strategies^{2,3}. In the Europe Union (EU) approximately 45,000 people were still waiting for a kidney transplant⁴. The demand for organs continues to exceed the supply strongly in EU. CKD is characterized by a progressive loss of renal function due mainly

^aGraduate Program in Biotechnology/RENORBIO of Federal University of Espírito Santo (UFES), Brazil

^bLaboratory of Cellular Ultrastructure, Department of Morphology, Federal University of Espírito Santo (UFES), Brazil

^cPharmaceutical Sciences Graduate Program, Vila Velha University, Vila Velha, ES, Brazil

^dSpecial Laboratory of Applied Toxinology (LETA), Center of Toxins, Immune-Response and Cell Signaling (CeTICS), Instituto Butantan, São Paulo, Brazil.

*Corresponding author **Breno Valentim Nogueira**

Laboratory of Cellular Ultrastructure Carlos Alberto Redins, Department of Morphology, CCS/UFES, Av. Marechal Campos, 1468, CEP: 29.043-900. Brazil. E-mail: brenovalentim@gmail.com, Tel/Fax. +55 27-3335-7365; 27-3335-7367 Electronic Supplementary Information (ESI) available: [details of any supplementary information available should be included here]. See DOI: 10.1039/x0xx00000x

to increased levels of toxic waste circulating in the blood which lead the individual to various complications such as increased blood pressure, anaemia, bone fragility, nutritional deficiency and nervous system damage⁵. It is known that CKD can be caused by diabetes, increased blood pressure and other less recurrent disorders. Current treatments for renal failure consist of dialysis and transplantation⁶. About dialysis, this does not promote the cure of renal failure and the costs involved for the maintenance of the sections are onerous, in addition to that patients need to perform the dialysis treatment for life and until they can receive a new organ transplanted⁷. About kidney transplantation, this comes from organs donated by living or deceased (cadaver) donor and requires receptor-compatible blood type and tissue in order to reduce the risk of immunological rejection⁸. Moreover, the treatment requires waiting, sometimes too much, for patients of a compatible tissue/organ, and administration of anti-rejection medications which are expensive and may cause increased susceptibility to disease⁹. Globally, the shortage of organs for transplants have increasingly stimulated the urgent interest to obtain technologies that involve the tissue regeneration in patients affected by different diseases¹⁰.

A proposed alternative would be to use tissue bioengineering aimed at restoring a compromised organ, under the aspect of renal functions, into a viable and transplantable organ. In this scenario, the use of the patient's stem cells is useful to recolonise a kidney in which some damages impaired renal physiology. Hole organ decellularization has emerged as a promisor alternative for the shortage of organs for transplantation¹¹. Using biological, physical or chemical reagents, it is possible to remove the cells of organs, preserving the extracellular matrix (ECM) components, which may be used as a scaffold for tissue recellularization and complete organ reconstruction. Several studies have used rat kidney to conduct decellularization process in a total time ranging from 17h to days^{12,13}.

Here we propose an improvement decellularization process with reduction of time detergent perfusion (6h) and consequently ECM components preservation (Proteomics Analysis by Mass Spectrometry), reduced cell debris and DNA residues allowing ensuing cells repopulation.

Experimental

Organ Source

Thirty-Two Wistar male adult rats with 60 to 90 days of life were used, weighing 268 ± 7 g reared in the animal facility at the Center for Health Sciences of the Federal University of Espírito Santo (UFES). The animals were kept in cages in the light/dark cycle environment (12h/12h), with controlled temperature ($22 \pm 2^\circ\text{C}$) and humidity ($60 \pm 5\%$), water and received water and food (Nuvilab CR-1, Quimtia S/A) *ad libitum*. The use of the animals was carried out following standards established by national and international scientific entities (Committee of Ethics in Research with Animals - CEUA/UFES n° 033/2014 and 042/2016).

Before sacrifice, the animals were anaesthetized with intraperitoneal (i.p.) administration of anaesthetic solution overdose containing Ketamine (Quetamina®, Vetnil) 90mg/kg and Xylazine (Rompun®, Bayer) 10mg/kg intraperitoneally. After visual confirmation of complete anaesthetic induction the animals were heparinised (saline solution: NaCl 0,9% and Heparin [Hepamax-s, Blausiegel] 1:1000) gravitationally at 100 ± 10 mmHg for 5 min¹⁴. A laparotomy and sternotomy were performed to access the kidneys. The extracted kidneys were segregated into two groups, namely, Control (native) and Decellularized.

Decellularization Process

The kidney was released from the surrounding fat, mobilised, extracted, weighed (wet) and stored in fixative solution at 2°C - 8°C for further histological analysis in a fixative volume 20 times that of the organ¹⁵.

For the decellularized group, the left/right kidney (randomly) was released from the surrounding fat, mobilized and the renal artery was cannulated with a silicone cannula (Micro-Renathane - 0,040 mm OD X 0,025 mm ID; Braintree) with a narrowed lumen by heating and secured with a 4.0 silk thread suture. The kidney was extracted, weighed, packed in a decellularization apparatus and the cannula was connected to a peristaltic pump (Gilson®) which provided a constant control of perfusion pressure (100 ± 10 mmHg), as measured by inserted nanometer (BD®) in line at the infusion line, and flow rate of 1.0 ± 0.1 mL/min. A solution of 0.1 M PBS pH 7.2 heparinised 1:1000 was perfused for 30 min, and the perfusate was depleted. Sodium dodecyl sulfate (SDS; Sigma Aldrich®) solution was then perfused at 1% for 6 hours. At the end of this time, a solution of 0.1 M PBS pH 7.2 for 30 min and 4% paraformaldehyde fixative solution in 0.1 M PBS pH 7.2 was also perfused for 30 minutes. The kidney was weighed (wet) and stored in fixative solution at 2°C - 8°C for further histological analysis in a fixative volume 20 times that of the organ.

Microscopic Analysis

The kidneys were previously dehydrated in alcoholic solutions (70%: 12h; 80%: 1h; 90%:1h; 100%: 1h, 3 times); 100% alcohol solution and xylene (1/1): 1 hour; xylol: 1 h, 3 times; treated with histological paraffin; sectioned at $5 \mu\text{m}$ in a microtome (Leica® LM2125RT); and hydrated (xylol: 5 min, 3 times; 100% alcohol solution and xylene (1/1) for 5 min; alcohol: 100% for 5 min, 3 times; running water for 10 minutes). The sections were stained for Cytoplasm and Nuclei by Hematoxylin and Eosin (HE) staining; Collagen Fibers by Picro Sirius staining; Non-sulphated Glycosaminoglycans (GAG's) by Alcian Blue staining in pH 2.5; Sulphated Glycosaminoglycans (GAG's) by Alcian Blue staining in pH 0.5; Glycoproteins (GLPs) by Periodic Schiff Acid (PAS) staining. The images were obtained through an Olympus® AX70 light microscope coupled to the AxioCam Zeiss® ERc5s camera interfaced to the Axio Vision® LE version 4.8.2.0 software under a 40X objective by a single operator. The images were analyzed using Image J software version 1.51j8. Mean area values were corrected by the retraction index (22.67%) of the renal scaffold (data not shown).

Transmission Electron Microscopy (TEM)

Three controls and three decellularized kidneys were used. The samples were fixed with 2.5% glutaraldehyde in PBS (pH 7.4) for 24 h at 4 °C, washed and postfixed with 1% OsO₄ buffered with 0.1 mol/L PBS for 2h. All samples were dehydrated in a graded series of ethanol and embedded in Epon. Ultrathin sections (90 nm) were double-stained with uranyl acetate and lead citrate and then examined with JEM-1400 (JEOL®, JEM-1400, USA, Inc.).

GBM Thickness Analysis

Three controls and three decellularized kidneys were used for GBM evaluation. For quantitative analysis, ten sections of electronic micrographs were selected for each animal/group. Five random areas of each electron micrograph obtained at appropriate magnification ($\pm 17,000\times$) were selected on a standardized scale of 0.5 μm . Thus, the mean glomerular basement membrane (GBM) thickness can be obtained for each image. All images were analyzed using previously calibrated Image J software.

GBM Thickness Analysis

Three controls and three decellularized kidneys were used for GBM evaluation. For quantitative analysis, ten sections of electronic micrographs were selected for each animal/group. Five random areas of each electron micrograph obtained at appropriate magnification ($\pm 17,000\times$) were selected on a standardized scale of 0.5 μm . Thus, the mean glomerular basement membrane (GBM) thickness can be obtained for each image. All images were analyzed using previously calibrated Image J software.

Immunohistochemistry

For immunohistochemical analysis, anti-fibronectin (Abcam®) and anti-laminin (Abcam®) primary antibody at 1:100 and 1:100 dilution was used, respectively. Initially, control tissue (n=5) and decellularized tissue (n=5) samples were submitted to a deparaffinization process. Then termed endogenous peroxidase blockade was performed using hydrogen peroxide. Subsequently, protein block was performed, and 40 μL of anti-fibronectin and anti-laminin primary antibody were added to the sections. The slides were incubated with HRP secondary antibody (Nichirei Biosciences Inc., Japan) 1:100. For the revelation of the reaction, was used diaminobenzidine (DAB) (Spring Bioscience®, Germany) 1:50. The slides were washed in running water and dehydrated in alcohol to be subsequently mounted in DPX.

Hydroxyproline Quantification

Briefly, after the decellularization, the organs were divided into small pieces, proceeding with dehydration in 30%, 50%, 70%, 90% alcohol and three baths in 100% ethanol, with 15 min times each bath and then taken to a critical point (CO₂). The samples were immediately weighed after drying. After that, a portion of known weight (about 10 mg) was removed, fractionated into smaller portions, hydrolysed with 7N NaOH;

acidified with 3.5M H₂SO₄, submitted to a chloramine-T solution and Ehrlich reagent. The spectrophotometer was read at 560 nm.

Sulphated GAG's Quantification

Samples and blank (8M guanidine-HCl), 50 μL of 8M guanidine-HCl solution were added to standard, sample and blank aliquots. SAT reagent (0.3% H₂SO₄/0.75% Triton X-100) was added. The microtubes stand for 15 minutes; then 750 μL of Alcian Blue reagent was added and remained overnight at 4°C. The tubes were centrifuged at 12,000 $\times g$ for 15 minutes, and the supernatant was discarded. We added 500 μL of DMSO in each tube to resuspend the pellet and kept them in constant agitation for 15 minutes. Subsequently, we centrifuged again at 12,000 $\times g$ for 15 minutes and discarded the supernatant. We finally added 500 μL of Gu-Prop-H₂O reagent and resuspended the pellet. Samples were aliquoted into 96-well plates and read at 605 nm in plate reader¹⁶.

Proteomics Analysis

Samples Preparation

Extraction of proteins from the extracellular matrix.

The following protocol was performed based on Barallobre-Barreiro et al.¹⁷, with modification. Decellularized and native tissues were kept frozen until the use. 100 mg of each sample were cut one by one to avoid the complete thawing of the tissues and placed them into 1.5 mL tubes. Prior partial decellularization was performed for the native organs for the removal of plasma contaminants and minimize the cellular proteins contamination. For that, the native tissues were washed five times with PBS, following by a second wash with NaCl buffer (0.5 M NaCl, ten mM Tris-HCl and 25 mM EDTA, pH 7.5) at ten times (v:w) the tissue weight. Samples were vortexed at room temperature for 1 h at minimum speed (600 rpm) and then centrifuged at 16,000 $\times g$ for 10 min. The supernatants were discarded, and 1% SDS (w/v) was added to the pellet at ten times (v:w) the tissue weight. The tubes were vortexed at room temperature for 4 h at minimum speed. After that, the tubes were centrifuged at 16,000 $\times g$ for 10 min, the supernatants were discarded, and the pellets were washed with double distilled water (ddH₂O). After that, we performed ECM protein extraction with guanidine hydrochloride buffer (GuHCl, 4 M guanidine hydrochloride, 50 mM sodium acetate and 25 mM EDTA, pH 5.8 with proteinase inhibitors). From now on, we proceeded the experiments with both samples (decellularized and native tissues). Samples were incubated in a GuHCl buffer for 48h at room temperature and vortexed vigorously to enhance mechanical disruption of the ECM components. Then, the supernatants were transferred to new tubes and centrifuged at 16,000 $\times g$ for 10 min at 4 °C and store at -20 °C until use. Protein concentration was estimated by ultraviolet absorbance at 280 nm using an extinction coefficient of 1.1 of 0.1% mg/mL solution¹⁸. An aliquot of 100 μg of protein for each sample was precipitated with ten times the volume of ethanol and incubated overnight at -20 °C.

In-solution Trypsin Digestion

Proteins of each sample were denatured using 6 M urea and 2 M thiourea (final concentrations), followed by reduction by adding 100 mM dithiothreitol (DTT, final concentration: 10 mM) and incubation at 37 °C for 1 h. After that, the samples were alkylated with 0.5 M iodoacetamide (final concentration: 50 mM) and incubated in the dark for 1 h. The materials were precipitated with cold acetone at six times the volume of the sample and incubated overnight at -20 °C. The solutions were centrifuged at 14,000 $\times g$ for 25 min, and the supernatants were aspirated without disturbing the precipitated pellet. Protein pellets were dried using a vacuum concentrator for 30 min at room temperature. Pellets were resuspended with 20 μ L of 0.1 M ammonium bicarbonate buffer, pH 8.2, containing trypsin (1:50 trypsin: protein) and digested overnight at 37 °C. Digestions were stopped by addition of 10% trifluoroacetic acid (TFA, the final concentration of 1% TFA). Digested peptide samples were purified using a Pierce™ C18 Tips of 100 μ L bed (ThermoFisher Scientific, Waltham, MA, USA) according to the manufacturer's recommendations for LC-MS/MS and eluted in 0.1% TFA/50% acetonitrile/50% ddH₂O. Samples were dried in a vacuum concentrator for 30 min at room temperature and subjected to LC-MS/MS analysis.

Mass Spectrometry (MS) Analysis

Mass spectrometry analysis was performed on an LTQ-Orbitrap Velos mass spectrometer (ThermoFisher Scientific, Waltham, MA, USA) coupled to an EASY-nLC II liquid chromatography (ThermoFisher Scientific, Waltham, MA, USA). A gradient segmented was performed with 50 min of 5 to 30% solvent B (0.1% formic acid in acetonitrile) followed by a 20 min of 30 to 95% of solvent B at a flow rate of 200 μ L/min in-house prepared pre-column (ID 100 μ m \times OD 360 μ m) packed with 5 cm of C18 10 μ m Jupiter beads (Phenomenex Inc., Torrance, CA, USA). This pre-column was attached to an in-house fritted-tip analytical column (ID 75 μ m \times OD 360 μ m) packed with 15 cm of C18 5 μ m AQUA beads (Phenomenex Inc., Torrance, CA, USA). Data were acquired in a data-dependent acquisition mode where the top five precursor ions in each cycle were selected for fragmentation by collision-induced dissociation excluded for 90 seconds, with a nanospray voltage set to 2.3kV and the source temperature set to 250 °C. Ion trap injection time was set to 100 ms and FT-MS injection time was set to 100 ms with a resolution of 30,000 across an m/z of 300-1800.

MS Data Analysis

Protein identification was performed with "Rattus norvegicus" package from UniProt database downloaded in July 2018 (36,879 sequences). Carbamidomethylation was set as fixed modification, while oxidation (M) were set as variable modification, with maximum mixed cleavages at three. Parent mass and fragment mass error tolerance were set at 10 ppm and 0.5 Da, respectively. False discovery rate (FDR) of 1% and unique peptide ≥ 1 were used for filtering out inaccurate proteins for the PEAKS search. A $-10\lg P > 20$ (equivalent to a p -value of 0.01) indicates that the detected proteins are relatively high in confidence as it targets very few decoys matches above that threshold. The label-free quantifications were performed

in the same software using PEAKQ analysis that considers the most three abundant unique peptides for protein label-free quantification. For that, we considered the retention time between 10 and 95 min, and for peptide features, we applied quality ≥ 8 , peptide ID count ≥ 1 , charge between 1-10 and at least three assured samples. For protein filters, we used FDR of 1%, fold change ≥ 1.5 , unique peptides ≥ 1 , PEAKQ as a significant method and we applied the total ion current (TIC) of the samples to calculate the normalization factors.

MS Gene Ontology Annotation

To classify the identified proteins regarding molecular function, biological process and cellular component, we use the public NCBI Blast service (QBLast) blastp algorithm¹⁹ (e-value 1e-3).

DNA Residual Content Quantification

The kidneys were cut into small pieces and the samples were submitted to gradual inclusion in 30%, 50%, 70%, 90% ethanol and three baths in 100% ethanol, with 15 min times each bath and then brought to critical point (CO₂); after the complete cycle of the critical point the dry weight was obtained. Samples were placed in 1.5mL conical tubes according to DNeasy kit (Qiagen®, Germany). Then 180 μ L of ATL buffer and 20 μ L of proteinase K were added and vortexed. Tubes were incubated in a water bath at 56°C overnight for complete tissue lysis. After, 200 μ L of AL buffer was followed and vortexed and incubated at 56°C for 10 min; 200 μ L of 100% ethanol was added and vortexed again. The mixture was pipetted onto a mini spin column of the DNeasy kit and collected in 2mL tubes, then centrifuged at 6,000 $\times g$ for 1 min. The tube liquid was discarded and inserted into a new 2mL tube to then add 500 μ L of the AW1 buffer in the column and centrifuge at 6,000 $\times g$ for 1 min. Repeatedly, the remaining liquid was discarded, and a new tube inserted. Then, 500 μ L of the AW2 buffer was added to the column and centrifuged for 3 min at 20,000 $\times g$. The mini-column was transferred to a conical tube and DNA was eluted by adding 200 μ L of AE buffer to the centre of the column and incubated at room temperature for 1 min and then centrifuged for 1 min at 6,000 $\times g$. The samples were quantified in Nanodrop 2000 (Thermo Scientific®) by spectrophotometric analysis²⁰.

Perfusate SDS Traces Quantification

The Methylene Blue (MB) colourimetry assay was performed for the SDS traces quantification²¹. The calibration curve was constructed assuming a final volume of 2 mL (volume of the spectrophotometer cuvette). A 2% SDS concentration solution was obtained in deionized water. 0.04 g SDS or 40 mg (SOLUTION A) was weighed for a final volume of 2 mL; 1 mL of SOLUTION A was aliquoted, and 1 mL of 0.0125% of MB (Solution B) which was previously prepared in deionized water (w/v) was added (SOLUTION C, 1% SDS). From the SOLUTION C serial dilutions were performed at 9 points with deionized water: 1%, 0.5%, 0.25%, 0.125%, 0.0625%, 0.03125%, 0.015625%; for the determination of SDS traces in the Perfusate, 5.0 μ L of effluent was aliquoted, the samples were vortexed with SOLUTION B in the ratio 1:100 (sample: SOLUTION B, v/v), i.e. 495.0 μ L of SOLUTION B was added to

each well, the samples were vortexed, and chloroform was added 1:2 (sample: chloroform, v/v); vortexed for 1 minute. The final volume per microtube was: 5.0 μ L sample + 495.0 μ L of SOLUTION B + 1.0 mL chloroform, totalling 1.5 mL per microtube. The solutions were then incubated for 30 min at room temperature; 150 μ L of the lower layer (chloroform) was extracted. The readings were performed in a spectrophotometer at a wavelength of 650 nm in triplicate. For the blank were used MB and chloroform in the ratio 1:2 (MB: chloroform, v/v).

Statistical analysis

Data were analyzed using GraphPad Prism® 7.00 software. Regarding normality by Shapiro-Wilk test, data were analyzed by Student's *t*-test for unpaired samples. Significant values were considered when $p < 0.05$. Values expressed as Mean \pm Standard Error Mean (SEM). For proteomics analyses raw data were processed with Peaks Studio 8.5 software²². Gene Ontology annotations are assigned to the sequences using Blast2Go 5.2.0 software²³.

Results and Discussion

One the primary objective of decellularization of a native tissue is the preservation of the structural integrity of the ECM components, specifically the components that will allow cellular functionality after the repopulation process, e.g., basal lamina. The basal lamina is a trellis of macromolecules, functionally crucial for the cell²⁴. This structure delimits the epithelial tissue of the underlying connective tissue. In the case of the kidney, this structure is founding in glomerular membrane filtration, and its preservation is crucial for repopulation process²⁵. It is a matrix rich in proteins and polysaccharides such as collagen type IV, laminin, fibronectin, entactin and heparin sulphated²⁶. Here, to the decellularization process, we used 1% SDS solution under the control of flow rate (1.0 mL/min) and pressure (100 mmHg) in contrast with other study wich not used/informed this conditions^{14,27,28}. This process revealed the preservation of important ECM components by mass spectrometry which was corroborated by other analyzes. It is known that throughout the process of decellularization there is the modulation of diverse metabolic routes with the production of pro-apoptotic factors²⁹. Thus, the shorter the time from organ withdrawal to its repopulation is one of the critical variables in this process. On the other hand, there is no point in increasing the perfusion pressure to try to advance the process because it can damage the components of the extracellular matrix. The use of quality and appropriate detergent also assists in obtaining a suitable scaffold.

An example of the importance of regulate perfusion pressure was related to the histological analysis of the area to **collagen fibres** (Control: 13.51 \pm 0.20; Desc.: 12.74 \pm 0.44 - Mean Area [μ m²], $p=0.5632$) (table 1). The Sirius Red staining can be used to detect the general distribution and preservation of collagen throughout the ECM³⁰. Type I collagen fibres are known to be strongly birefringent yellow-red fibres under polarized light, whereas type III collagen fibres are poorly

birefringent and greenish³¹. For example, this staining may be used in the cartilage of the knee joint³², in hepatic tissue³³ and in kidneys³⁴ to evaluate the alignment of collagen fibres under the effect of SDS. Additionally, immunohistochemistry analysis was observed the specific presence of fibronectin and laminin (fig. 3). The data presented were corroborated by the spectrophotometry quantification of hydroxyproline (Control: 1.119 \pm 0.1059; Desc.: 1.433 \pm 0.3423 - Total wet weight [μ g/mg], $p=0.4062^{ns}$) (table 2). It is known that the amino acid hydroxyproline is present in very few proteins, namely in collagen. By this feature, the quantification of collagen in a tissue sample can be made indirectly from the quantification of hydroxyproline therein.

Levels of other important ECM components have also been detected, such as, **non-sulphated GAG's** (Control: 9.28 \pm 0.21; Desc.: 3.91 \pm 0.11 - Mean Area [μ m²], $p<0.0001$), **Sulphated GAG's** (Control: 6.34 \pm 0.58; Desc.: 3.73 \pm 0.25 - Mean Area [μ m²], $p<0.0001$) and **GLP's** (Control: 6.99 \pm 0.30; Desc.: 1.72 \pm 0.15 - Mean Area [μ m²], $p<0.0001$) (table 1). The significant reduction of these components may be due to the high affinity to the chemical groups present in the SDS when it is in aqueous solution. It is known that SDS forms ions that can solubilize sulphated radicals like chondroitin sulphated, heparin sulphated, hyaluronic acid, mucins, glycoproteins, glycogen and other polysaccharides³⁵. Also, SDS complexes to other molecules by the high positive charge conferred by Na⁺. In case of sulphated GAG's the data presented were corroborated by the spectrophotometry quantification (Control: 33533 \pm 3551; Desc.: 3176 \pm 517 - Total dry weight [μ g], $p<0.0001$) (table 2).

The kidney has elegant and moderately tortuous three-dimensional structures that efficiently direct the distribution and filtration of blood, metabolites, ions and water reabsorption; besides the collection and removal of urine filtrate. The preservation of native renal extracellular architectures may play a vital role in the generation of a newly functioning tissue, facilitating the correct anatomical arrangement of the cell population. Other decellularized organ matrices were used to generate functional organs, such as a contractile heart, a lung capacity of performing oxygen and carbon dioxide exchanges, and a liver that secretes albumin³⁶. The kidney scaffolds produced with this research maintained their general shape with a visually identifiable vascular tree. Also, all relevant structures of the glomerular, tubular and collector tube remained intact and appeared continuous with regular sizes and segmentation. It has been suggested that preserved morphology improves cell growth in decellularized scaffolds³⁷. The morphology of the scaffold was performed using macroscopic visualization (fig. 1), blades of stained tissues (fig. 2) and TEM (fig. 4). However, there are other avenues for characterization that can increase understanding of the topic. Validation of the integrity of the vascular system can be performed with Evans blue dye injected or with contrast for computed tomography (microCT)³⁸. Given histology, the identification of discontinuities can be improved by using specific dyes that increase the contrast of the basement membrane, such as PAS or Jones Silver³⁹. The scaffold was produced with a protocol where SDS was employed at a

concentration of 1%⁴⁰. This protocol is superior in the preservation of ECM when compared to more aggressive methods, such as, for example, sodium deoxycholate (NaDOC) and NaOH³⁰. The TEM is another imaging modality commonly used to evaluate cell morphology and cell-cell interaction with ECM, often with the use of heavy metal immunostaining. As an example, TEM has been employed to examine pulmonary ECM, to check elastin and collagen fibres in explanted acellular tissue engineering constructs; besides the evaluation of the size, grouping and spacing of collagen bundles in decellularized pulmonary valves in pigs⁴¹. Studies have used TEM and perfusate particles to examine the glomerular filtration properties of decellularized kidneys⁴². In our study, we also used TEM to measure GBM thickness in decellularized kidneys for the first time in the literature according to our best knowledge. In the control group, it measured 239.8 ± 2.3 nm; in the decellularized group we obtained a mean of 232.3 ± 2.2 nm. There was no significant statistical difference ($p = 0.0604$) corroborating the idea that the decellularization process did not compromise this essential renal component (fig. 4)⁴³. The 3D were preserved and GBM was visible by SEM (data not showed). Ultimately, it may be beneficial to replicate these experiments with the repopulated scaffold produced by SDS to ensure that filtration does not decrease and that the ultrastructure of the basement membrane is minimally damaged.

The final step in any decellularization protocol is the washing of the newly decellularized scaffold to remove cytotoxic chemicals. In cell toxicity studies, viability was preserved when there was less than 0.50% SDS remaining in the scaffolds⁴⁴. In recent literature, the rinsing of organ scaffolds that were subsequently implanted or cultured ranged from 1 hour to 5 days⁴⁵; usually washing is performed with PBS⁴⁶. In the present study, the perfusion time of lavage solution with 0.1 M PBS pH 7.2 was 30 min. After 300 mL of washing solution the perfused remaining merely 0.01% of SDS (figure 1). Our finding is significant for the literature regarding the process of optimization and success of the recellularization.

One of the main advantages of using decellularized tissue as an implantable tissue engineering scaffold is the marked reduction of the host's negative immune response as compared to an entire organ transplant^{47,48}. It has been suggested that the cause is the removal of cellular antigens and the conservation of the protein structures of ECM intra- and inter- various species⁴⁹. Also, it has been demonstrated that the decellularization process will allow xenotransplantation requiring less and less dependence on human donors⁵⁰. Histochemistry by HE was used for the microscopic detection of DNA like in other studies of decellularization; this has the advantage of showing localized areas of low decellularization about the entire extracellular anatomy⁵¹. In contrast, some groups employ fluorescence histochemistry using 4', 6-diamino-2-phenylindole (DAPI)⁵². DAPI interacts directly with nuclei and can be used on histological slides or living cells. Quantitative methods using DNA isolation and measurement technology are standardized concerning the total mass or total proteins. It has not been able to make an adequate mapping of its location³⁶.

Only HE staining is comparatively insensitive and that a combination of criteria should be established for DNA removal verification. These include obtaining a scaffold containing less than 50 ng of double-stranded DNA (dsDNA) per mg ECM - dry weight⁵³; with DNA fragments less than 200 base pairs (bp) and absence of visible nuclear compounds in tissue sections stained with DAPI or HE²⁰. In our study, the control (native) group presented DNA levels in the order of 573 ± 57.77 ng per mg of dry organ weight. The decellularized group obtained a DNA concentration of 56.91 ± 26.38 ng per mg of dry organ weight. When comparing the groups, there was a statistically significant difference ($p = 0.0148$) (fig. 1). It is important to note that these criteria are proposed as a basis for the constructive remodelling of the environment in the acceptor but must be verified, modified and expanded according to the specific tissues and implant sites⁵³.

Proteomics analyses blasted 1,103 sequences/proteins (953 native and 150 decellularized groups, respectively) and shared 75 sequences between groups (fig. 5). This sequences were related with ECM, such as, Collagen alpha-1(I) chain; collagen alpha-1(IV) chain; collagen alpha-1(XVIII) chain isoform X3; collagen alpha-2(I) chain; collagen alpha-2(IV) chain; collagen alpha-2(VI) chain isoform X1; Collagen alpha-1(I) chain; collagen alpha-1(IV) chain; collagen alpha-1(XII) chain isoform X1; collagen alpha-2(I) chain; collagen alpha-2(IV) chain; fibronectin isoform X1; laminin subunit alpha-1; laminin subunit alpha-1; laminin subunit beta-1 isoform X1; laminin subunit gamma-1; nidogen-1; nidogen-2 isoform X1; collagen alpha-1(XVIII) chain isoform X3. Regarding the **extracellular matrix organization and basement membrane** we found 56 protein preserved, such as, vitronectin, versican core protein isoform X1, TGFBI, nidogen-2 isoform X1, nephronectin isoform X3, MFAP5, laminin, fibronectin, dystroglycan, dermatopontin, collagen (IV, VI, I, XVIII, XI, III), clusterin, (Hspg2), aggrecan core protein. Were showed other cluster proteins linked to **signal transduction** (Vitronectin, tubulointerstitial nephritis antigen-like, ATP synthase subunit beta, mitochondrial, aminopeptidase N); **cell adhesion** (collagen, laminin); **collagen fibril organization** (collagen); **angiogenesis** (TGFBI, junction plakoglobin, fibronectin isoform X1, collagen alpha-2(IV) chain, collagen alpha-1(XVIII) chain isoform X3, annexin A2, aminopeptidase N, alpha-dystroglycan, alpha-3 type IV collagen); **aging** (low-density lipoprotein receptor-related protein 2, Elongation factor 1-alpha 1, clusterin) (fig. 6). This protein profile is great and very necessary to a successful scaffold cells repopulation and maintenance of them⁵⁴. All the proteins identified in this analysis are described in material supplementary with their respective intensity and expression ratio between the groups.

The decellularization protocol developed in this research resulted in a progressive reduction of eosinophilic protein debris in the scaffolds produced, as visualized by HE histology. It has been reported that an overall reduction in residual cellular material results in better cell growth in the implanted scaffolds³⁷. At the beginning of our experiments, the tissue surrounding the renal corpuscles was cleared while the outer marrow was congested with protein aggregation. We could interpret that, during decellularization, the cell lysates of the glomerular capsules and the proximal tubules travelled downstream at a rate exceeding the lysates of the more distal tubular pathways

(data not showed). In response, the decellularization protocol was adjusted to increase the rate of release of cell lysates or improve the solubility of the aggregated proteins. One caveat to the use of HE histochemistry is that there is no structural differentiation between cellular or extracellular proteins.

Therefore, other contemporary protocols have incorporated techniques to recognize specific antigens to verify the removal of cellular debris⁵⁵. These techniques include immunohistochemistry (IHC), immunoblot protein (Western blot) and enzyme-linked immunosorbent assay (ELISA). Immunohistochemistry allows visualization of associated structures while Western Blot and ELISA provide a certain level of quantification. The ELISA is the most accurate, but comparatively the most expensive⁵⁶.

Conclusions

Here we show an optimization decellularization process concern to the reduction of detergent time perfusion described previously in the literature. The scaffold was achievable for a subsequent repopulation at where the microarchitecture of the decellularized kidney was maintained, in addition to the renal glomerular filtration membrane. The preservation of GMB and its desirable thickness is a significant finding because it contributes substantially to the filling of a gap not yet focused on the literature. Therewithal, minimal levels of DNA have been detected which can mitigate immunogenic responses. By mass spectrometric assay, important ECM structures and compounds were preserved enabling, posterior, cell repopulation. Further studies are needed to verify if this structure is, in fact, able to adhere, migrate and differentiate cells into a new kidney. This finding is fundamental to support studies in renal scaffold transplantation including CKD approach.

Conflicts of interest

There are no conflicts to declare.

Acknowledgements

The authors were supported by grants from Fundação de Amparo à Pesquisa e Inovação do Espírito Santo (EDITAL FAPES Nº 006/2014-UNIVERSAL: process number 0606/2015; EDITAL FAPES/CNPq Nº 012/2014-DCR: process number 0832/2015; EDITAL FAPES/CAPEs PROFIX 009/2014-63/2017 process number 79522882/17); Rede Nordeste de Biotecnologia (RENORBIO), Coordenação de Aperfeiçoamento de Pessoal de Nível Superior (CAPES), National Council for Scientific and Technological Development (CNPq, process number 150037/2018-0) and Fundação de Amparo à Pesquisa do Estado de São Paulo (FAPESP, Nº 2013/07467-1, 2016/04000-3 and 2017/17943-6).

References

- 1 USRDS, *CKD in the United States: An Overview of the USRDS Annual Data Report, Volume 1*, 2015, vol. 66.
- 2 J. Coresh, E. Selvin, L. A. Stevens, J. Manzi, J. W. Kusek, P. Eggers, F. Van Lente and A. S. Levey, *JAMA*, 2007, **298**, 2038–47.
- 3 USRDS, *Chapter 7: Transplantation*, 2016, vol. 67.
- 4 R. Bouwman, T. Wiegers, S. van Schoten, R. Coppen and R. Friele, *Study on the uptake and impact of the EU Action Plan on Organ Donation and Transplantation (2009-2015) in the EU Member States*, 2017.
- 5 Y.-L. Chiu, K.-L. Chien, S.-L. Lin, Y.-M. Chen, T.-J. Tsai and K.-D. Wu, *Nephron. Clin. Pract.*, 2008, **109**, c109-18.
- 6 D. W. Johnson, K. Herzog, D. Purdie, A. M. Brown, R. J. Rigby, D. L. Nicol and C. M. Hawley, *Transplantation*, 2000, **69**, 794–9.
- 7 R. A. Wolfe, V. B. Ashby, E. L. Milford, A. O. Ojo, R. E. Ettenger, L. Y. C. Agodoa, P. J. Held and F. K. Port, *N. Engl. J. Med.*, 1999, **341**, 1725–1730.
- 8 K. Takahashi and S. Yamanaka, *Cell*, 2006, **126**, 663–76.
- 9 M. Sugawara, S. Ichimura, K. Kokubo, T. Shimbo, M. Hirose and H. Kobayashi, *Clin. Kidney J.*, 2011, **4**, 4.s2.42-4.s2.42.
- 10 X. Ren and H. C. Ott, *Pflügers Arch. - Eur. J. Physiol.*, 2014.
- 11 B. Bonandrini, M. Figliuzzi, E. Papadimou, M. Morigi, N. Perico, F. Casiraghi, C. Dipl, F. Sangalli, S. Conti, A. Benigni, A. Remuzzi and G. Remuzzi, *Tissue Eng. Part A*, 2014, **20**, 1486–1498.
- 12 M. Caralt, J. S. Uzarski, S. Iacob, K. P. Obergfell, N. Berg, B. M. Bijonowski, K. M. Kiefer, H. H. Ward, A. Wandinger-Ness, W. M. Miller, Z. J. Zhang, M. M. Abecassis and J. A. Wertheim, *Am. J. Transplant.*, 2015, **15**, 64–75.
- 13 A. C. Destefani, G. M. Sirtoli and B. V. Nogueira, *Front. Bioeng. Biotechnol.*, 2017, **5**, 34.
- 14 E. a Ross, M. J. Williams, T. Hamazaki, N. Terada, W. L. Clapp, C. Adin, G. W. Ellison, M. Jorgensen and C. D. Batich, *J. Am. Soc. Nephrol.*, 2009, **20**, 2338–47.
- 15 M. Srinivasan, D. Sedmak and S. Jewell, *Am. J. Pathol.*, 2002, **161**, 1961–71.
- 16 M. Karlsson and S. Björnsson, *Methods Mol. Biol.*, 2001, **171**, 159–73.
- 17 J. Barallobre-Barreiro, F. Baig, M. Fava, X. Yin and M. Mayr, *J. Vis. Exp.*, DOI:10.3791/55674.
- 18 J. Barallobre-Barreiro, R. Oklu, M. Lynch, M. Fava, F. Baig, X. Yin, T. Barwari, D. N. Potier, H. Albadawi, M. Jahangiri, K. E. Porter, M. T. Watkins, S. Misra, J. Stoughton and M. Mayr, *Cardiovasc. Res.*, 2016, **110**, 419–430.
- 19 S. F. Altschul, W. Gish, W. Miller, E. W. Myers and D. J. Lipman, *J. Mol. Biol.*, 1990, **215**, 403–410.
- 20 N. Poornejad, N. Momtahan, A. S. M. Salehi, D. R. Scott, C. A. Fronk, B. L. Roeder, P. R. Reynolds, B. C. Bundy and A. D. Cook, *Biomed. Mater.*, 2016, **11**, 025003.
- 21 E. Castrén, T. Sillat, S. Oja, A. Noro, A. Laitinen, Y. T. Kontinen, P. Lehenkari, M. Hukkanen and M. Korhonen, *Stem Cell Res. Ther.*, 2015, **6**, 167.
- 22 B. Ma, K. Zhang, C. Hendrie, C. Liang, M. Li, A. Doherty-Kirby and G. Lajoie, *Rapid Commun. Mass Spectrom.*, 2003, **17**, 2337–2342.
- 23 S. Götz, R. Arnold, P. Sebastián-León, S. Martín-Rodríguez,

- P. Tischler, M.-A. Jehl, J. Dopazo, T. Rattei and A. Conesa, *Bioinformatics*, 2011, **27**, 919–924.
- 24 A. J. Groffen, M. A. Ruegg, H. Dijkman, T. J. van de Velden, C. A. Buskens, J. van den Born, K. J. Assmann, L. A. Monnens, J. H. Veerkamp and L. P. van den Heuvel, *J. Histochem. Cytochem.*, 1998, **46**, 19–27.
- 25 M. Abolbashi, S. M. Agcaolli, M.-K. Lee, I. K. Ko, T. Aboushwareb, J. D. Jackson, J. J. Yoo and A. Atala, *Acta Biomater.*, 2016, **29**, 52–61.
- 26 F. Genovese, A. a Manresa, D. J. Leeming, M. A. Karsdal and P. Boor, *Fibrogenesis Tissue Repair*, 2014, **7**, 4.
- 27 M. He, A. Callanan, K. Lagaras, J. A. M. Steele and M. M. Stevens, *J. Biomed. Mater. Res. B. Appl. Biomater.*, 2016, **00**, 1352–1360.
- 28 J. S. Uzarski, B. M. Bijonowski, B. Wang, H. H. Ward, A. Wandinger-Ness, W. M. Miller and J. A. Wertheim, *Tissue Eng. Part C Methods*, 2015, **21**, 1032–1043.
- 29 I. Fischer, M. Westphal, B. Rossbach, N. Bethke, K. Hariharan, I. Ullah, P. Reinke, A. Kurtz and H. Stachelscheid, *Biomed. Mater.*, 2017, **12**, 045005.
- 30 N. Poornejad, L. B. Schaumann, E. M. Buckmiller, N. Momtahan, J. R. Gassman, H. H. Ma, B. L. Roeder, P. R. Reynolds and A. D. Cook, *J. Biomater. Appl.*, 2016, **31**, 521–533.
- 31 A.-M. Kajbafzadeh, N. Sabetkish, S. Sabetkish, S. M. Tavangar, R. S. Hossein Beigi, M. A. Talebi, A. Akbarzadeh and L. Nikfarjam, *Biotech. Histochem.*, 2015, **90**, 111–23.
- 32 A. Pinheiro, A. Cooley, J. Liao, R. Prabhu and S. Elder, *J. Orthop. Res.*, 2016, **34**, 1037–46.
- 33 W. Ren, L. Y. Zhou, Y. Zhang, N. B. Li and H. Q. Luo, *Sensors Actuators B Chem.*, 2016, **223**, 24–29.
- 34 Y. Wang, J. Bao, Q. Wu, Y. Zhou, Y. Li, X. Wu, Y. Shi, L. Li and H. Bu, *Xenotransplantation*, 2015, **22**, 48–61.
- 35 M. Kilcoyne, J. Q. Gerlach, M. P. Farrell, V. P. Bhavanandan and L. Joshi, *Anal. Biochem.*, 2011, **416**, 18–26.
- 36 H. C. Ott, B. Clippinger, C. Conrad, C. Schuetz, I. Pomerantseva, L. Ikonomou, D. Kotton and J. P. Vacanti, *Nat. Med.*, 2010, **16**, 927–33.
- 37 T. W. Hudson, S. Zawko, C. Deister, S. Lundy, C. Y. Hu, K. Lee and C. E. Schmidt, *Tissue Eng.*, 2004, **10**, 1641–1651.
- 38 T. H. Petersen, E. A. Calle, L. Zhao, E. J. Lee, L. Gui, M. B. Raredon, K. Gavrilov, T. Yi, Z. W. Zhuang, C. Breuer, E. Herzog and L. E. Niklason, *Science*, 2010, **329**, 538–41.
- 39 D. B. JONES, *Am. J. Pathol.*, 1957, **33**, 313–29.
- 40 A. Remuzzi, M. Figliuzzi, B. Bonandrini, S. Silvani, N. Azzollini, R. Nossa, A. Benigni and G. Remuzzi, *Sci. Rep.*, 2017, **7**, 43502.
- 41 P. Sarathchandra, R. T. Smolenski, A. H. Y. Yuen, A. H. Chester, S. Goldstein, A. E. Heacox, M. H. Yacoub and P. M. Taylor, *J. Surg. Res.*, 2012, **176**, 376–385.
- 42 R. B. N. K. Brendel, E. Meezan, *Proc. First Int. Symp. Biol. Chem. Basement Membr.*
- 43 A. Peloso, L. Urbani, P. Cravedi, R. Katari, P. Maghsoudlou, M. E. A. Fallas, V. Sordi, A. Citro, C. Purroy, G. Niu, J. P. McQuilling, S. Sittadjody, A. C. Farney, S. S. Iskandar, J. P. Zambon, J. Rogers, R. J. Stratta, E. C. Opara, L. Piemonti, C. M. Furdulj, S. Soker, P. De Coppi and G. Orlando, *Ann. Surg.*, 2015, **XX**, 1.
- 44 S. Cebotari, I. Tudorache, T. Jaekel, A. Hilfiker, S. Dorfman, W. Ternes, A. Haverich and A. Lichtenberg, *Artif. Organs*, 2010, **34**, 206–10.
- 45 A. Soto-Gutierrez, H. Yagi, B. E. Uygun, N. Navarro-Alvarez, K. Uygun, N. Kobayashi, Y.-G. Yang and M. L. Yarmush, *Cell Transplant.*, 2010, **19**, 655–65.
- 46 K. H. Nakayama, C. a. Batchelder, C. I. Lee and A. F. Tarantal, *Tissue Eng. Part A*, 2010, **16**, 2207–2216.
- 47 E. Rieder, A. Nigisch, B. Dekan, M. T. Kasimir, F. Mühlbacher, E. Wolner, P. Simon and G. Weigel, *Biomaterials*, 2006, **27**, 5634–5642.
- 48 E. Rieder, G. Seebacher, M. T. Kasimir, E. Eichmair, B. Winter, B. Dekan, E. Wolner, P. Simon and G. Weigel, *Circulation*, 2005, **111**, 2792–2797.
- 49 T. W. Gilbert, T. L. Sellaro and S. F. Badylak, *Biomaterials*, 2006, **27**, 3675–3683.
- 50 A. J. Allman, T. B. McPherson, L. C. Merrill, S. F. Badylak and D. W. Metzger, *Tissue Eng.*, 2002, **8**, 53–62.
- 51 J. De Kock, L. Ceelen, W. De Spiegelaere, C. Casteleyn, P. Claes, T. Vanhaecke and V. Rogiers, *Arch. Toxicol.*, 2011, **85**, 607–12.
- 52 S. Heyner, M. J. Tucker, W. Wang, J. Gill, D. P. Wolf, P. M. Wassarman and J. M. Walker, *Kidney Research*, Springer New York, New York, NY, 2016, vol. 1397.
- 53 P. M. Crapo, T. W. Gilbert and S. F. Badylak, *Biomaterials*, 2011, **32**, 3233–3243.
- 54 L. Hobeika, M. T. Barati, D. J. Caster, K. R. McLeish and M. L. Merchant, *Kidney Int.*, 2017, **91**, 501–511.
- 55 J. Cortiella, J. Niles, A. Cantu, A. Brettler, A. Pham, G. Vargas, S. Winston, J. Wang, S. Walls and J. E. Nichols, *Tissue Eng. Part A*, 2010, **16**, 2565–2580.
- 56 E. Engvall and P. Perlmann, *Immunochemistry*, 1971, **8**, 871–874.

Table 1: Mean area measurement of the Collagen, Sulphated/Non-sulphated GAG's and GLP's by histological analysis.

	<i>Control (native)</i>	<i>Decellularized</i>	<i>p value</i>
Collagen Fibers (μm^2)	13.51 \pm 0.20	12.74 \pm 0.44	0.5632 ^{ns}
Non-sulphated GAG's (μm^2)	9.28 \pm 0.21	3.91 \pm 0.11	<0.0001
Sulphated GAG's (μm^2)	6.34 \pm 0.58	3.93 \pm 0.25	<0.0001
GLP's (μm^2)	6.99 \pm 0.30	1.72 \pm 0.15	<0.0001

GAG's: glycosaminoglycans; GLP's: glycoproteins; Student's *t*-test.

Table 2: Hydroxyproline and Sulphated GAG's spectrophotometry quantification.

	<i>Control (native)</i>	<i>Decellularized</i>	<i>p value</i>
Hydroxyproline ($\mu\text{g}/\text{mg}$)	1.119 \pm 0.1059	1.433 \pm 0.3423	0.4062
Sulphated GAG's ($\mu\text{g}/\text{mg}$)	33,533 \pm 3,551	3,176 \pm 517	<0.0001
Preservation content	\approx 100%	\approx 9,47%	

GAG's: glycosaminoglycans; Student's *t*-test.

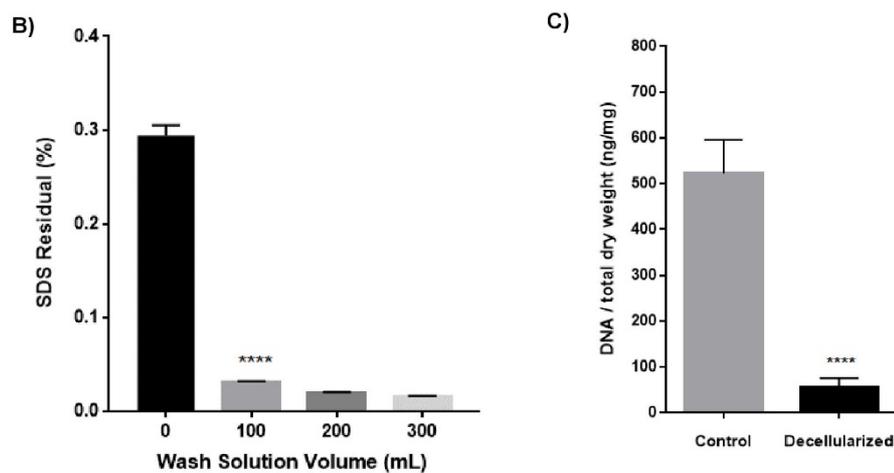
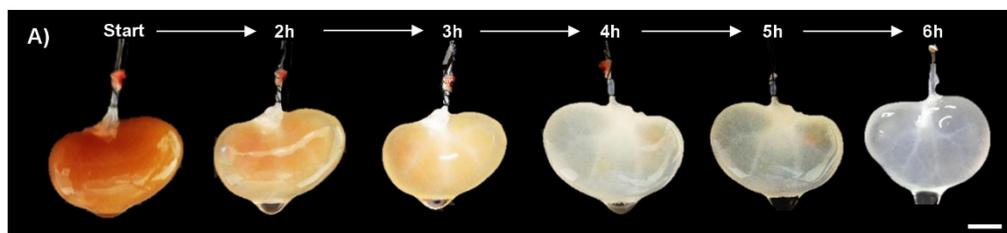
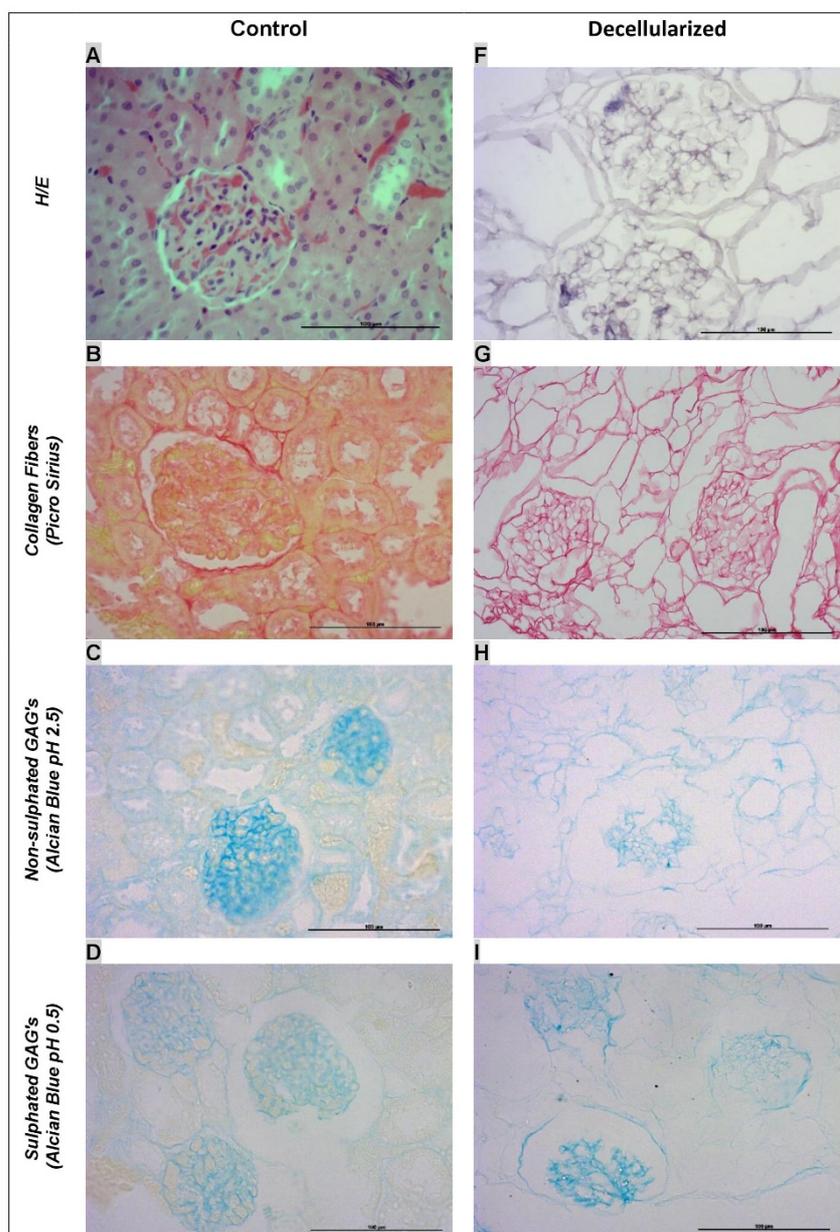


Fig. 1 A) Macroscopic analysis of the renal decellularization process. The gradual loss of organ colouration over time was observed by the perfusion of 1% SDS detergent. It is also noted that vasculature and three-dimensional architecture was preserved. Scale bar = 1 cm. Time in hours (h) **B)** showed the amount of SDS (%) remained in perfused immediately before the PBS solution perfusion (0.0 mL) and after (100, 200 and 300 mL). Note that SDS concentration ($0.293 \pm 0.0115\%$) decrease significantly after the first 100mL of PBS was solution ($0.031 \pm 0.0010\%$; $p < 0.0001$). As more PBS was the solution was perfused amounts of SDS reach $0.019 \pm 0.0009\%$ (200 mL) and $0.015 \pm 0.0008\%$ (300 mL). **C)** DNA Residual the control (native) showed $573.00 \pm 57.77 \text{ ng/mg}$ while decellularized group represent $56.91 \pm 26.38 \text{ ng/mg}$ of DNA by total dry weight ($p < 0.0001$).



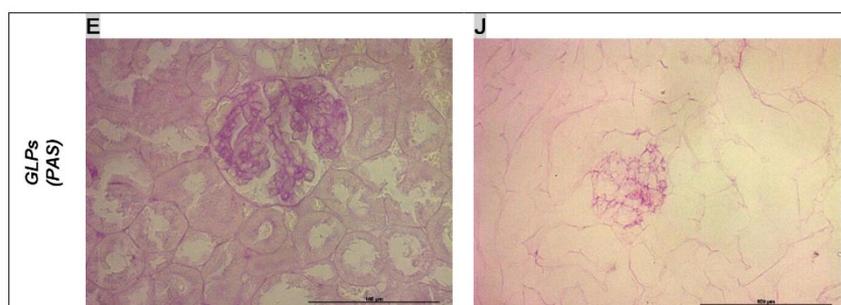


Fig. 2 Histological analysis of collagen fibres, sulphated and non-sulphated GAG's and glycoproteins. Native kidneys relative to the control group (A-E), were stained by different techniques, according to the figure. Similarly, the decellularized (F-J) kidneys were submitted to the same procedure. Note the absence of cells and undetectable levels of cellular debris. Scale bar 100 µm. GAG's: glycosaminoglycans; GLP's: glycoproteins; PAS: Periodic Acid Schiff.

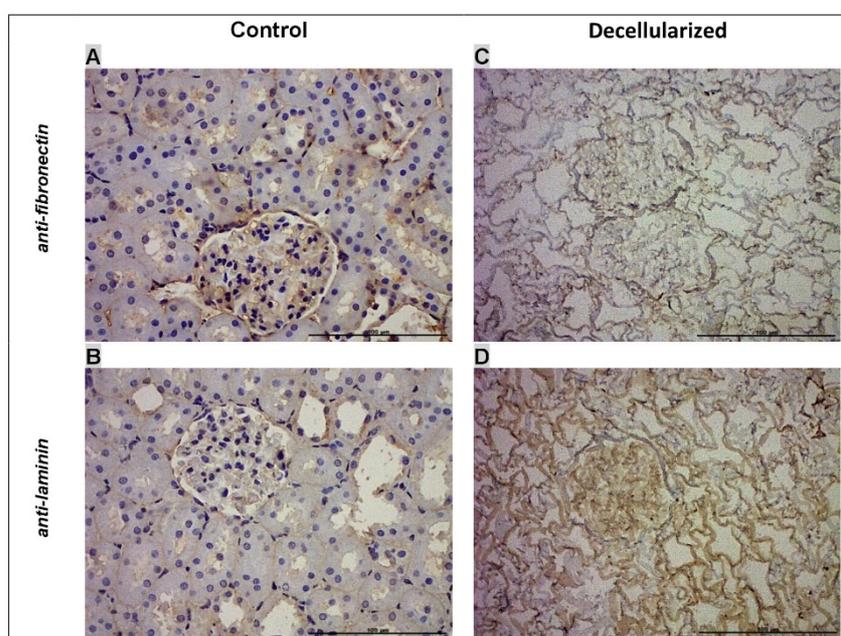


Fig. 3 Anti-fibronectin and anti-laminin. Native kidneys relative to the control group (A-B), were submitted to immunohistochemistry, according to figure. Similarly, the decellularized (C-D) kidneys were submitted to the same procedure. Laminins and fibronectins structure were widely preserved. Notwithstanding, proteomic analysis it has been demonstrated that there is the presence of collagen subunits. Scale bar 100 µm.

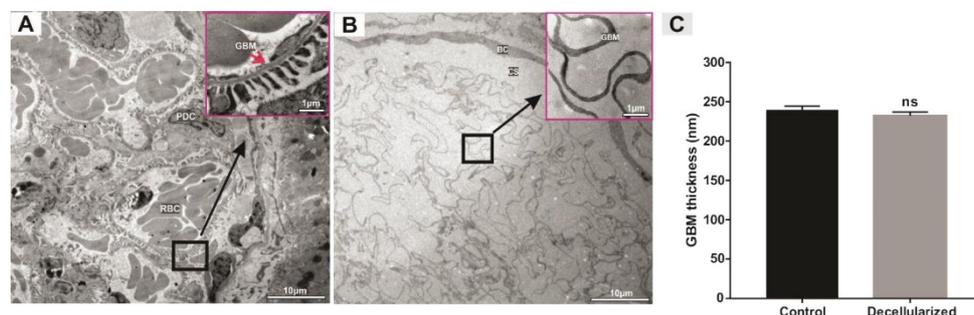


Fig. 4 Ultrastructural renal evaluation. Native (A) and decellularized (B) renal tissue can be observed using TEM. Capillaries were aligned by fenestrated endothelial cells (A). The integrity of the filtration membrane and the absence of cells were shown in addition to MEC (B) fibres. It should be noted that the glomerular basement membrane was preserved in the decellularized tissue and the GBM thickness was not different between native and decellularized groups (C). For TEM 10 μm scale bars with a magnification of 17.000X and 3.87 kV. Student's *t*-test. Red blood cells (RBC), capsular space (CS), basal glomerular membrane (GBM), podocytes (PDC) and Bowman's capsule (BC).

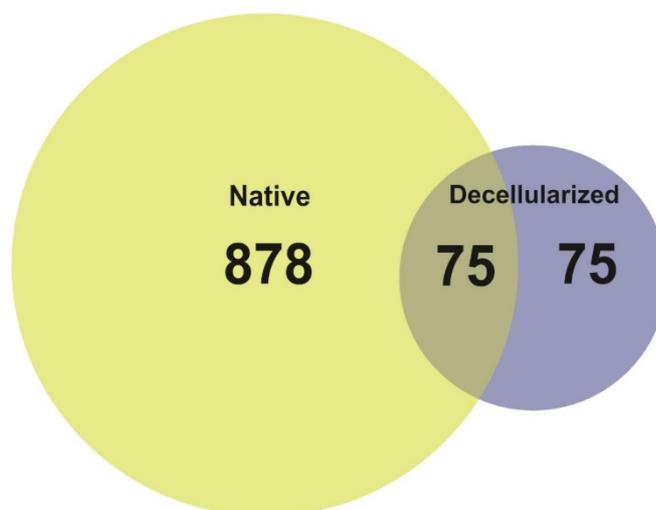


Fig. 5 Proteomics Analysis. The Venn diagram shows the total sequences obtain after the blastp algorithm. Were blast 1,103 sequences/proteins (953 native and 150 decellularized groups, respectively) and shared 75 sequences between groups. This sequences were related with ECM, such as, Collagen alpha-1(I) chain; collagen alpha-1(IV) chain; collagen alpha-1(XVIII) chain isoform X3; collagen alpha-2(I) chain; collagen alpha-2(IV) chain; collagen alpha-2(VI) chain isoform X1; Collagen alpha-1(I) chain; collagen alpha-1(IV) chain; collagen alpha-1(XII) chain isoform X1; collagen alpha-2(I) chain; collagen alpha-2(IV) chain; fibronectin isoform X1; laminin subunit alpha-1; laminin subunit alpha-1; laminin subunit beta-1 isoform X1; laminin subunit gamma-1; nidogen-1; nidogen-2 isoform X1; collagen alpha-1(XVIII) chain isoform X3.

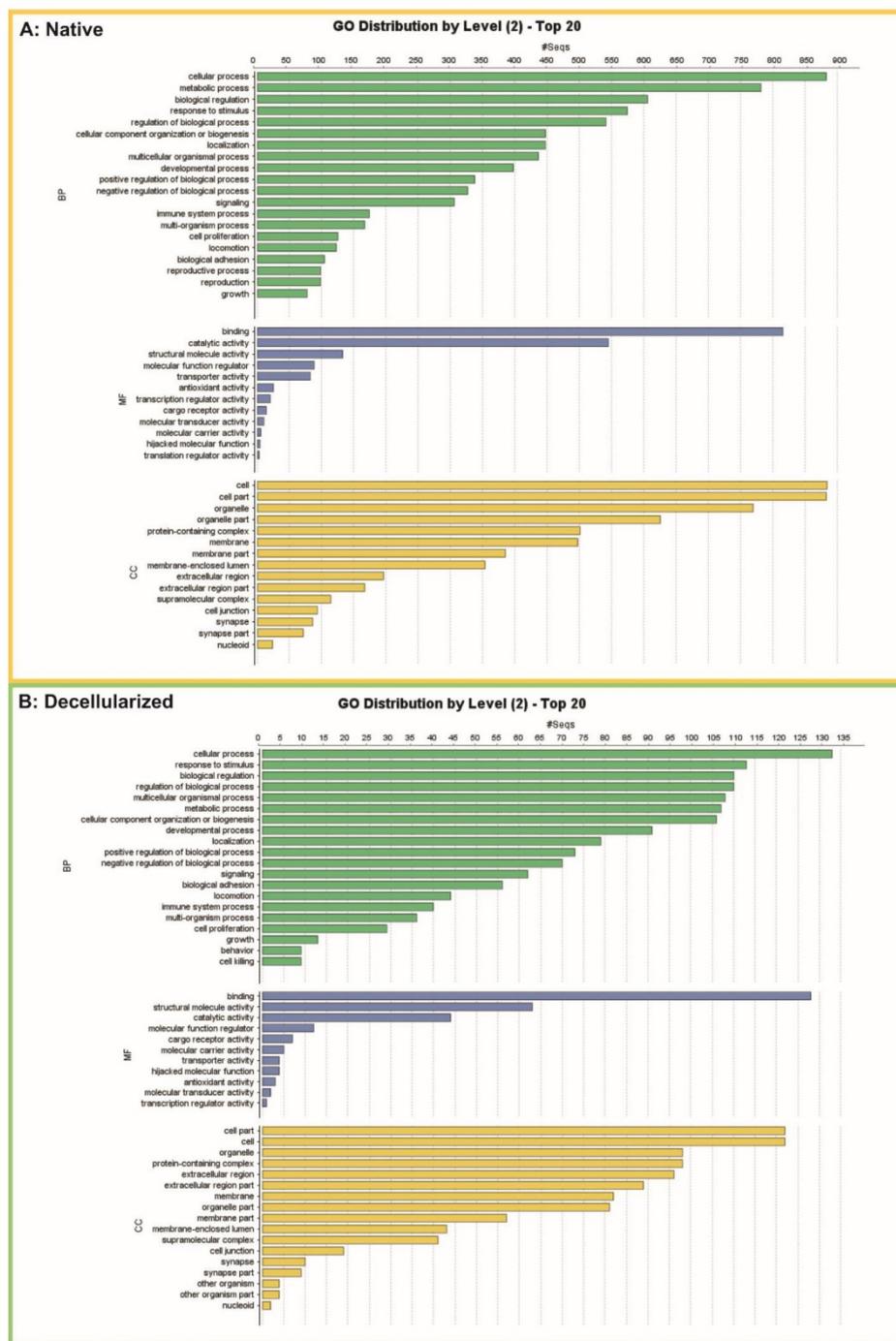


Fig. 6 Proteomics Analysis –Gene Ontology by Level (2) – Top 20 Sequences. Were founded extracellular matrix organization and basement membrane compounds; cluster proteins linked to signal transduction; cell adhesion; collagen fibril organization; angiogenesis proteins; ageing proteins and decellularized (B) according to native (A). BP: biological process. MF: molecular function; CC: cellular component.

Supplementary materials

Table 1: Native Sequences



Native_blast2go_go
_table_20180802_11;

Table 2: Decellularized Sequences



Dec_blast2go_go_t
able_20180730_1825

Table 3: Proteomics Analysis: Sequences presents in Native and Decellularized tissue.

SEQNAME	DESCRIPTION	NATIVE	DEC.
SP P63039 CH60_RAT	60 kDa heat shock protein, mitochondrial	X	X
SP P06761 BIP_RAT	78 kDa glucose-regulated protein	X	X
SP P60711 ACTB_RAT	actin, cytoplasmic 1	X	X
TR A0A0G2K3K2 A0A0G2K3K2_RAT	actin, cytoplasmic 1	X	X
SP P63259 ACTG_RAT	actin, cytoplasmic 2	X	X
TR D4A2F1 D4A2F1_RAT	agrin isoform X1	X	X
TR F1LPF2 F1LPF2_RAT	agrin isoform X1	X	X
SP P25304 AGRIN_RAT	agrin isoform X7	X	X
SP P01946 HBA_RAT	alpha-globin	X	X
TR B1H216 B1H216_RAT	alpha-globin	X	X
SP P15684 AMPN_RAT	aminopeptidase N	X	X
SP Q07936 ANXA2_RAT	annexin A2	X	X
SP P15999 ATPA_RAT	ATP synthase subunit alpha, mitochondrial	X	X
SP P10719 ATPB_RAT	ATP synthase subunit beta, mitochondrial	X	X
TR G3V6D3 G3V6D3_RAT	ATP synthase subunit beta, mitochondrial	X	X
TR F1LTJ5 F1LTJ5_RAT	basement membrane-specific heparan sulfate proteoglycan core protein	X	X
SP P05371 CLUS_RAT	clusterin	X	X
TR G3V836 G3V836_RAT	clusterin	X	X
TR Q6P7S6 Q6P7S6_RAT	clusterin	X	X
SP P02454 CO1A1_RAT	Collagen alpha-1(I) chain	X	X
TR F1MA59 F1MA59_RAT	collagen alpha-1(IV) chain	X	X
TR D3ZUL3 D3ZUL3_RAT	collagen alpha-1(VI) chain	X	X
TR A0A0G2KAJ7 A0A0G2KAJ7_RAT	collagen alpha-1(XII) chain isoform X1	X	X
TR F1LR02 F1LR02_RAT	collagen alpha-1(XVIII) chain isoform X3	X	X
TR A0A0G2KAN1 A0A0G2KAN1_RAT	collagen alpha-2(I) chain	X	X
TR F1M6Q3 F1M6Q3_RAT	collagen alpha-2(IV) chain	X	X
TR F1LNH3 F1LNH3_RAT	collagen alpha-2(VI) chain isoform X1	X	X

Journal Name		ARTICLE	
SP P62898 CYC_RAT	cytochrome c, somatic	X	X
TR D4A5L9 D4A5L9_RAT	cytochrome c, somatic	X	X
TR A0A0G2JTX5 A0A0G2JTX5_RAT	dipeptidyl peptidase 4	X	X
TR A0A0G2K238 A0A0G2K238_RAT	dipeptidyl peptidase 4	X	X
TR F1M7X5 F1M7X5_RAT	dipeptidyl peptidase 4	X	X
SP P62630 EF1A1_RAT	Elongation factor 1-alpha 1	X	X
TR M0R757 M0R757_RAT	elongation factor 1-alpha 1	X	X
SP P06399 FIBA_RAT	fibrinogen alpha chain	X	X
TR A1L114 A1L114_RAT	fibrinogen alpha chain	X	X
TR Q7TQ70 Q7TQ70_RAT	fibrinogen alpha chain	X	X
SP P14480 FIBB_RAT	Fibrinogen beta chain	X	X
SP P02680 FIBG_RAT	fibrinogen gamma chain isoform X1	X	X
TR A0A096P6L8 A0A096P6L8_RAT	fibronectin isoform X1	X	X
TR C0JPT7 C0JPT7_RAT	filamin-A isoform X1	X	X
SP P23764 GPX3_RAT	Glutathione peroxidase 3	X	X
TR A0A0G2K531 A0A0G2K531_RAT	Glutathione peroxidase 3	X	X
SP P04797 G3P_RAT	glyceraldehyde-3-phosphate dehydrogenase	X	X
SP P62804 H4_RAT	histone 4	X	X
TR A0A0G2K654 A0A0G2K654_RAT	histone H1.2	X	X
TR M0R7B4 M0R7B4_RAT	histone H1.2	X	X
SP P15865 H14_RAT	histone H1.4	X	X
TR A0A0G2K2V6 A0A0G2K2V6_RAT	keratin, type I cytoskeletal 10 isoform X1	X	X
SP Q6IFU7 K1C42_RAT	keratin, type I cytoskeletal 42	X	X
SP Q6IMF3 K2C1_RAT	keratin, type II cytoskeletal 1	X	X
TR A0A0G2JST3 A0A0G2JST3_RAT	keratin, type II cytoskeletal 1	X	X
TR A0A0G2JWX4 A0A0G2JWX4_RAT	keratin, type II cytoskeletal 2 epidermal	X	X
SP Q6IG03 K2C73_RAT	keratin, type II cytoskeletal 73	X	X
TR A0A0G2JXH6 A0A0G2JXH6_RAT	keratin, type II cytoskeletal 73	X	X
TR D4A409 D4A409_RAT	laminin subunit alpha-1	X	X
TR E3W9F8 E3W9F8_RAT	laminin subunit alpha-1	X	X
TR F1MAN8 F1MAN8_RAT	laminin subunit alpha-5	X	X
TR D3ZQN7 D3ZQN7_RAT	laminin subunit beta-1 isoform X1	X	X
SP P15800 LAMB2_RAT	laminin subunit beta-2	X	X
TR M0R6K0 M0R6K0_RAT	laminin subunit beta-2	X	X
TR F1MAA7 F1MAA7_RAT	laminin subunit gamma-1	X	X
SP P98158 LRP2_RAT	low-density lipoprotein receptor-related protein 2	X	X
SP P00697 LYSC1_RAT	lysozyme C-2	X	X
TR F1M8E9 F1M8E9_RAT	lysozyme C-2	X	X
TR Q6PDV1 Q6PDV1_RAT	lysozyme C-2	X	X
TR A0A0G2K6S9 A0A0G2K6S9_RAT	myosin-11 isoform X1	X	X
TR E9PTU4 E9PTU4_RAT	myosin-11 isoform X1	X	X
SP Q64319 SLC31_RAT	neutral and basic amino acid transport protein rBAT	X	X
TR F1LM84 F1LM84_RAT	nidogen-1	X	X
SP B5DFC9 NID2_RAT	nidogen-2 isoform X1	X	X
SP P04785 PDIA1_RAT	Prolyl 4-hydroxylase, beta polypeptide	X	X

Please do not adjust margins

ARTICLE		Journal Name		
TR A0A0G2JSH5 A0A0G2JSH5_RAT	serum albumin	X	X	
TR Q66HF6 Q66HF6_RAT	Tubulointerstitial nephritis antigen	X	X	
TR Q4V8N0 Q4V8N0_RAT	tubulointerstitial nephritis antigen-like	X	X	

Please do not adjust margins



[# Home](#)

[/ Author](#)

[Review](#)

Submission Confirmation

[Print](#)

Thank you for your submission

Submitted to
Biomaterials Science

Manuscript ID
BM-ART-10-2018-001301

Title
Time optimization in rat kidney decellularization process: ECM characterization by mass spectrometry.

Authors
Nogueira, Breno
Destefani, Afrânio
Sirtoli, Gabriela
Amorim, Fernanda
Taufner, Gabriel
Zanardo, Tadeu
Kitano, Eduardo
Iwai, Leo

Date Submitted
16-Oct-2018

[Author Dashboard](#)

6. CAPÍTULO 3

Artigo III

**THE DECELLULARIZATION PROCESS CAUSES SIGNIFICANT CHANGES IN THE
3D STRUCTURE OF THE SCAFFOLD REQUIRING CORRECTIONS IN THE
HISTOMORPHOMETRIC ANALYSIS.**

The decellularization process changes 3D structure of the scaffold requiring corrections in the histomorphometric analysis

A. C. Destefani^{a,b†}, G. M. Sirtoli^{b,c†}, F. G. Amorim^{a,d}, G. H. Taufner^{a,b}, T. E. C. Zanardo^{a,b}, E. S. Kitano^e, L. K. Iwai^e and B. V. Nogueira^{a,b*}

^aGraduate Program in Biotechnology/RENORBIO of Federal University of Espírito Santo (UFES), Brazil

^bTissue Engineering Core/ Laboratory of Cellular Ultrastructure, Department of Morphology, Federal University of Espírito Santo (UFES), Brazil

^cCentro Universitário Católico de Vitória (UCV), Espírito Santo, Brazil

^dPharmaceutical Sciences Graduate Program, Vila Velha University, Espírito Santo, Brazil

^eSpecial Laboratory of Applied Toxinology (LETA), Center of Toxins, Immune-Response and Cell Signaling (CeTICS), Instituto Butantan, São Paulo, Brazil

†Contributed equally

*Corresponding author Breno Valentim Nogueira

Laboratory of Cellular Ultrastructure Carlos Alberto Redins, Department of Morphology, CCS/UFES, Av. Marechal Campos, 1468, CEP: 29.043-900. Brazil.

E-mail: brenovalentim@gmail.com, Tel/Fax. +55 27-3335-7365; 27-3335-7367

The use of tissue bioengineering strategies has emerged as a promisor alternative for the shortage of organs for transplantation. The analysis correction of decellularized scaffold microarchitecture can provide a real characterization of the extracellular matrix components and determine the success of organ reconstruction. In this study, we decellularized whole rat kidneys by ionic detergent solutions (SDS, 1%) and developed a strategy to quantify the extracellular matrix components by histochemical analysis with normalization of the results based on the shrinkage of the organs. Electron microscopy, spectrophotometric quantification, and mass spectroscopy analyses were performed to compare the results. We demonstrated that histological analysis, an easy and inexpensive technique, presented excellent results when the normalization by reached Retraction Index is performed. Thus, the use of the Retraction Index corrects mistakes commonly made in the analysis of decellularized organs and provides a baseline for studies on the characterization of the renal scaffold by the decellularization process.

Introduction

Whole organ decellularization has emerged as a promisor alternative for the shortage of organs for transplantation. It is possible to remove the cells of organs using biological, physical or chemical reagents

preserving the extracellular matrix (ECM) components, which may be used as a scaffold for tissue recellularization and reconstruction of the entire organ. This approach has been improved by many researchers, with several complex organs, such as kidneys¹.

The success of the decellularization process depends on several parameters, for example, body weight, lipid content, cell density as well as the organ thickness. Besides the parameters related to the decellularization method, such as the intrinsic properties of the decellularization agent, the flow of perfusion, pressure, and other factors. After the decellularization, there is necessary to analyses if there are no more cells or cell debris and DNA residues, and if the ECM components are preserved to allow the new cells to attach. In this context, the primary and simplest methods used to observe the absence of cells and maintenance of ECM components are histological analyses.

Histology is a classical technique that is used to study the tissues, by sectioning specimens into thin sections. Even with the advent of real-time imaging technology, histological slicing and staining remain as necessary techniques to visualize cell and ECM morphology in tissues. Depending on the type of analysis required for an experiment, there are many available histological techniques, each with its advantages and disadvantages. Among the most common techniques are cryo-embedding, inclusion in paraffin and inclusion in plastic resin for sectioning. As the cryo-packed samples do not need to be fixed before incorporation, the sections can be prepared rapidly, and the epitopes are typically well preserved in the sample; however, cell morphology is generally lost due to the freezing process. Samples used for paraffin inclusion require fixation before the inclusion procedure and a more considerable amount of tissue processing steps compared to cryo-embedding. However, morphology is substantially preserved. Methacrylate resin presents several advantages compared to paraffin, such as the velocity of the procedure, less distortion of the tissue, possibility to obtain thinner tissue sections and lower cost, with the disadvantage of poor staining for some dyes².

Khorrarnirouz and colleagues tested the effect of three different protocols for decellularization of aortic valve conduits (AVCs), and evaluated collagen and elastin preservation by histologic staining, but without quantification of the dye of the tissue sections. Indeed, quantification of collagen was made by hydroxyproline quantification, and the decellularized AVCs showed increased collagen content in all the treated samples compared to the native samples³. They suggested that it was due to a naturally higher

content of collagen among the samples. Just like them, other researches show the higher collagen content in decellularized organs⁴⁻⁶. Furthermore, most of the studies also evaluate collagen and other ECM components by histological staining only for qualitative analyses, without quantification of the stain, needing additional quantification methods for this purpose⁶⁻⁸. In our study, rat kidneys were decellularized, and the ECM components were analyzed by histologic staining with traditional dyes, and quantification of these components was made considering the percentage of shrinkage of the organ after decellularization procedures. This correction was named by us as Retraction Index, and our results indicate the quantification of ECM proteins on stained histological sections is possible and provides a valuable tool for evaluation of the success of organs decellularization.

Experimental Procedures

Kidney decellularization

Thirty-Two Wistar male adult rats (250-300g) were used, provided by the Bioterio Central of the Health Sciences Center/UFES. The animals were kept in cages in a light/dark cycle environment (12h/12h), with controlled temperature and humidity, received *ad libitum* water and standard commercial feed. The use of the animals was carried out by standards established by national and international scientific entities (Committee of Ethics in Research with Animals - CEUA/UFES n° 033/2014 and 042/2016).

For the surgical procedure of kidney extraction, the animals were pre-segregated in individual cages identified on a fasting diet for 12 hours, and 15 minutes before sacrifice were heparinized with 10 units of Heparin sodium (Hepamax-s, Blausiegel). They were then anesthetized with intraperitoneal (i.p.) administration of Ketamine (Quetamina®, Vetnil) 90 mg/kg and Xylazine (Rompun®, Bayer) 10 mg/kg. After visual confirmation of complete anesthetic induction, laparotomy and sternotomy were performed to access the kidneys. Subsequently, for the Control group, a 4% paraformaldehyde fixative solution in 0.1 M phosphate buffer (PBS) was perfused for 30 min pH 7.2. The kidney was released from the surrounding fat, extracted, weighed and stored in fixative solution at 2°C-8°C for further histological analysis⁹.

For the decellularized group, after the perfusion with heparinized saline solution, the left/right kidney (randomly) was released from the surrounding fat, mobilized and the renal artery was cannulated with a silicone cannula (Micro-Renathane - 0,040 mm OD X 0,025 mm ID; Braintree) with a narrowed lumen by

heating and secured with a 4.0 silk thread suture. The kidney was extracted, weighed, packed in a decellularization apparatus and the cannula was connected to a peristaltic pump (Gilson®) which provided a constant control of perfusion pressure (100 ± 10 mmHg), as measured by inserted nanometer (BD®) in line at the infusion line, and flow (1.0 ± 0.1 mL/min). A solution of 0.1 M PBS pH 7.2 heparinized 1:1000 was perfused for 30 min, and the perfusate was depleted. SDS (sodium dodecyl sulfate-Sigma Aldrich®) solution was then perfused at 1% for 6 hours. At the end of this time, a solution of 0.1 M PBS pH 7.2 for 30 min was perfused, and the organ was frozen at -80°C for further analyzes.

For histologic analyzes, an additional perfusion step was performed with 4% paraformaldehyde fixative solution in 0.1 M PBS pH 7.2 also for 30 minutes. The kidney was weighed (wet) and maintained in fixative solution at 2°C - 8°C for 24h before inclusion in paraffin.

Microscopic Analysis - Inclusion in Paraffin (Protocol I)

The kidneys were previously dehydrated in alcoholic solutions of increasing concentration: Alcohol 70% for 12 hours; 80% alcohol for 1 hour; 90% alcohol for 1 hour; 100% alcohol for 3 hours with change of the solution each 1 hour; 100% alcohol solution and xylene (1/1) for 1 hour; xylene for 3 hours with change of solution each 1 hour. Subsequently, the process of inclusion in histological paraffin was initiated with baths of xylol and paraffin solution at 56°C (1/1) in an oven for 1 hour; paraffin bath at 56°C for 3 hours; with a change of solution each 1 hour, when it was left at room temperature to harden. Once blocked in paraffin, the kidneys were sectioned at five μm in a hand microtome (Leica® LM2125RT), and the sections were arranged in matte-edge glass slides. In the hydration process, three xylene baths were used for 5 min each; 100% alcohol solution and xylene (1/1) for 5 min; 3 alcohol baths 100% for 5 min each; running water for 10 minutes. The tissue sections were then stained with different dyes: Hematoxylin and Eosin (HE), Picro Sirius, Alcian Blue staining in pH 2.5 and 0.5 and Periodic Schiff Acid (PAS) staining (detailed in supplementary data). After the staining, 100% alcohol and xylol solution (1/1) was used for 5 min; 3 xylol baths for 5 min each and laminated with Distyrene Plasticizer Xylene (DPX).

Microscopic Analysis - Inclusion in Histoiresin (Protocol II)

The organs were fixed in 4% paraformaldehyde buffered with PBS for 24h. The previously fixed samples were conditioned in 15 mL conic tubes and dehydrated in 70%, 95%, and 100% ethanol, and then soaked for 12h at 4°C in a 1:1 solution of 100% alcohol and historesin 2-hydroxyethyl methacrylate (Jung®, Germany) to be immersed in pure historesin solution for 24 hours at 4°C. After processing, the material was then packed into plastic forms containing resin enriched with hardening solution for 24 hours at 37°C. The prepared resin blocks were sealed in wood using the JET mounting medium (Clássico®, Brazil). Histological sections were made with 5 µm thick in a manual microtome (Leica Biosystems®, Germany) and displayed on universal slides for histochemistry.

Hydroxyproline Quantification

After the decellularization, the organs were divided into small pieces, proceeding with dehydration in 30%, 50%, 70%, 90% alcohol and three baths in 100% ethanol, with 15 min times each bath and then taken to a critical point (CO₂). The samples were immediately weighed after drying. After that, a portion of about 10 mg was removed, fractionated into smaller portions, and transferred into a 15 mL capacity polypropylene conical tube (Falcon®, Nunc®). Then, 500 µL of 7N NaOH was added for sample hydrolyzes, capping the flask, but not wholly sealing it, and submitted to the autoclave at 120°C (p≈98,1kPa) for 40 minutes. After the hydrolysis, the hydrolysate was acidified with 500 µL of 3.5 M H₂SO₄, transferred to a 10 mL volumetric flask, and rinsed with ultrapure water. The fluid was filtered; 500 µL of the sample was aliquoted and transferred to a glass/Falcon® tube, adding 4.5 mL of chloramine-T solution, shaking and allowing the reaction at room temperature for 25 minutes. Afterward, 5.0 mL of Ehrlich reagent was added, the flask was capped, stirred and the reagents were incubated in a water bath at 60°C for 15 minutes. The spectrophotometer was read at 560 nm. A standard 10-point hydroxyproline curve was performed starting from a solution containing 2,600 µg/mL of the amino acid. Dilutions were performed in 2mL microtubes using ultrapure water where the final volume was 100 µL (1:1) having concentrations between 2.5 and 1,300 µg of hydroxyproline ¹⁰⁻¹⁸.

Sulphated GAG's Quantification

For the determination of chondroitin sulfate, a type of GAG, an 8-point standard curve was prepared to start from a solution containing 800 µg/mL of chondroitin sulfate. Dilutions were performed in 2mL microtubes using distilled water, where the final volume was 100 µL (1:1) containing concentrations between 3.1 and 400 µg of chondroitin sulfate. From each tube, 50 µL of the diluent was transferred to new microtubes. Samples and blank (8M guanidine-HCl), 50 µL of 8M guanidine-HCl solution were added to standard, sample and blank aliquots. The final volume after the addition of the guanidine-HCl should be 100 µL. To the tubes, 50 µL of SAT reagent (0.3% H₂SO₄/0.75% Triton X-100) was added. The microtubes stand for 15 minutes; then 750 µL of Alcian Blue reagent was added and remained overnight at 4°C. The tubes were centrifuged at 12,000g for 15 minutes, and then the supernatant was discarded. We added 500 µL of DMSO in each tube to resuspend the pellet and kept them in constant agitation for 15 minutes. Subsequently, we centrifuged again at 12,000g for 15 minutes and discarded the supernatant. We finally added 500 µL of guanidine hydrochloride buffer (GuHCl, 4 M guanidine hydrochloride, 50 mM sodium acetate and 25 mM EDTA, pH 5.8 with proteinase inhibitors) reagent and resuspended the pellet. Samples were aliquoted into 96-well plates and read at 605 nm in plate reader¹⁹.

Samples Preparation for the Proteomics Analysis

Extraction of proteins from the extracellular matrix

The following protocol was performed based on Barallobre-Barreiro *et al.*^{20,21}, with modification. Decellularized and native tissues were kept frozen until the use. 100 mg of each sample were cut one by one to avoid the complete thawing of the tissues and placed them into 1.5 mL tubes. Prior partial decellularization was performed for the native organs for the removal of plasma contaminants and minimize the cellular proteins contamination. For that, the native tissues were washed 5 times with PBS, following by a second wash with of NaCl buffer (0.5 M NaCl, 10 mM Tris-HCl and 25 mM EDTA, pH 7.5) at 10 times (v:w) the tissue weight. Samples were vortexed at room temperature for 1 h at minimum speed (600 rpm) and then centrifuged at 16,000 x g for 10 min. The supernatants were discarded, and 1% SDS (w/v) was added to the pellet at ten times (v:w) the tissue weight. The tubes were vortexed at room temperature for 4 h at minimum speed. After that, the tubes were centrifuged at 16,000 x g for 10 min, the supernatants were discarded, and the pellets were washed with double distilled water (ddH₂O). After that,

we performed ECM protein extraction with GuHCl buffer. From now on, we proceeded the experiments with both samples (decellularized and native tissues). Samples were incubated in a GuHCl buffer for 48h at room temperature and vortexed vigorously to enhance mechanical disruption of the ECM components. Then the supernatants were transferred to new tubes and centrifuged at $16,000 \times g$ for 10 min at 4°C and store at -20°C until use. Protein concentration was estimated by UV absorbance at 280 nm using an extinction coefficient of 1.1 of 0.1% mg/mL solution ²². An aliquot of 100 μg of protein for each sample was precipitated with 10 times the volume of ethanol and incubated overnight at -20°C .

In-solution Trypsin Digestion

Proteins of each sample were denatured using 6 M urea and 2 M thiourea (final concentrations), followed by reduction by adding 100 mM dithiothreitol (DTT, final concentration: 10 mM) and incubation at 37°C for 1 h. After that, the samples were alkylated with 0.5 M iodoacetamide (final concentration: 50 mM) and incubated in the dark for 1 h. The materials were precipitated with cold acetone at 6 times the volume of the sample and incubated overnight at -20°C . The solutions were centrifuged at $14,000 \times g$ for 25 min, and the supernatants were aspirated without disturbing the precipitated pellet. Protein pellets were dried using a vacuum concentrator for 30 min at room temperature. Pellets were resuspended with 20 μL of 0.1 M ammonium bicarbonate buffer, pH 8.2, containing trypsin (1:50 trypsin:protein) and digested overnight at 37°C . Digestions were stopped by addition of 10% trifluoroacetic acid (TFA, the final concentration of 1% TFA). Digested peptide samples were purified using a Pierce™ C18 Tips of 100 μL bed (ThermoFisher Scientific, Waltham, MA, USA) according to the manufacturer's recommendations for LC-MS/MS and eluted in 0.1% TFA/50% acetonitrile/50% ddH₂O. Samples were dried in a vacuum concentrator for 30 min at room temperature and subjected to LC-MS/MS analysis.

Mass Spectrometry Analysis

Mass spectrometry analysis was performed on an LTQ-Orbitrap Velos mass spectrometer (ThermoFisher Scientific, Waltham, MA, USA) coupled to an EASY-nLC II liquid chromatography (ThermoFisher Scientific, Waltham, MA, USA). A gradient segmented was performed with 50 min of 5 to 30% solvent B (0.1% formic acid in acetonitrile) followed by a 20 min of 30 to 95% of solvent B at a flow rate of 200

nL/min in-house prepared pre-column (ID 100 μm x OD 360 μm) packed with 5 cm of C18 10 μm Jupiter beads (Phenomenex Inc., Torrance, CA, USA). This pre-column was attached to an in-house fritted-tip analytical column (ID 75 μm x OD 360 μm) packed with 15 cm of C18 5 μm AQUA beads (Phenomenex Inc., Torrance, CA, USA). Data were acquired in a data-dependent acquisition mode where the top five precursor ions in each cycle were selected for fragmentation by collision-induced dissociation excluded for 90 seconds with a nanospray voltage set to 2.3kV and the source temperature set to 250 °C. Ion trap injection time was set to 100ms and FT-MS injection time was set to 100 ms with a resolution of 30,000 across an m/z of 300-1800.

Mass Spectrometry

Raw data were processed with Peaks Studio 8.5 software²³, and protein identification was performed with “Extracellular matrix protein + rat” package from UniProt database downloaded in April 2018 (1,148 sequences). Carbamidomethylation was set as fixed modification, while oxidation (M) were set as variable modification, with maximum mixed cleavages at 3. Parent mass and fragment mass error tolerance were set at 10 ppm and 0.5 Da, respectively. False discovery rate (FDR) of 1% and unique peptide ≥ 1 were used for filtering out inaccurate proteins for the PEAKS search. A $-10\lg P > 20$ (equivalent to a p-value of 0.01) indicates that the detected proteins are relatively high in confidence as it targets very few decoy matches above that threshold. The label-free quantifications were performed in the same software using PEAKQ analysis that considers the most three abundant unique peptides for protein label-free quantification. For that, we considered the retention time between 10 and 95 min, and for peptide features, we applied quality ≥ 8 , peptide ID count ≥ 1 , charge between 1-10 and at least 3 positive samples. For protein filters, we used FDR of 1%, fold change ≥ 1.5 , unique peptides ≥ 1 , PEAKQ as a significant method and we applied the total ion current (TIC) of the samples to calculate the normalization factors.

Histological Image Analysis

For each section and each staining, images of random regions encompassing renal corpuscles, glomeruli, and transverse tubules were obtained through an Olympus® AX70 light microscope coupled to the AxioCam Zeiss® ERc5s camera interfaced to the Axio Vision® LE version 4.8.2.0 software under a 40X

objective. The images were analyzed using Image J software version 1.51j8. The total area of each image analyzed was 58,325.146 μm^2 .

Tissue Retraction by the Decellularization Process

With appropriate and standardized adjustments for the images stained with HE (paraffin and resin) at the grey coloring threshold with the aid of Image J, measurements of renal corpuscles, glomeruli and transverse tubules (3 different regions of the same image obtained) were performed. The regions of interest were quantified at the area level, in μm^2 , which occupied all the histological regions. Thus, a proportion/fraction of the area can be reached, in percentage (%). The area values of the control group were compared to that of the decellularized group to determine if there was a significant increase, decrease or non-existence of alteration in the size of the renal histological structures by the decellularization process, a variable then denominated Retraction Index (RI) in percentage (%). Then, the distribution of collagen fibres, sulfated and non-sulphated GAGs and GLPs was analyzed in sections previously stained for this purpose. The area values of the Control group were compared to that of the Decellularized group to determine whether there was an increase, decrease or no change in the size of the renal histological structures by the Decellularization process. Afterward, the RI was applied in percentage (%) to the proportionality previously obtained. The data were again compared between the two groups to verify statistical significance or not.

Statistical analysis

Data were compiled and analyzed using GraphPad Prism® 7.00 software. Regarding normality (Shapiro-Wilk test) the data were analyzed by Student's *t*-test for unpaired samples. Significant values were considered when $p < 0.05$. Values expressed as Mean \pm Standard Error Mean (SEM).

Results

The kidney scaffolds obtained were analyzed to confirm the success of decellularization. During the procedure, it was possible to observe the gradual loss of cell content, while the organ became translucent. It was also noted that vasculature and three-dimensional architecture were visually preserved. DNA quantification confirmed the removal of nuclei content at the end of the decellularization (**Figure 01**). The quantification of collagen fibers, sulfated and non-sulphated GAGs, and GLPs were made by histomorphometric analyses (**Table 02**). It was observed that, on paraffin included tissues, the quantification of collagen were higher in the decellularized group compared to the control group. In contrast, the sulfated and non-sulphated GAGs and the GLPs presented decreased in the decellularized group compared to the control group. On plastic resin included tissues, collagen staining was higher in the decellularized group compared to the control group, while sulphated GAGs presented decreased and non-sulphated GAGs and GLPs were not different in the decellularized group compared to control group. For both paraffin and plastic resin decellularized samples it was also possible to visually observe a shrinkage of the tissue when compared to the native samples (**Figures 02 and 03**).

Considering that the quantification of the components of ECM such as collagen fibers, sulfated and non-sulfated GAGs, and GLPs depends on the area of the tissue analyzed, the shrinkage observed on the tissue after the decellularization may invalidate the quantification of such parameters. These quantifications are very useful to verify if the tissue scaffold obtained by the decellularization process retains structures essential for subsequent processes of cell repopulation. Therefore, it is necessary to develop a way to quantify these parameters correctly. For this purpose, Images obtained from H&E staining were analyzed, and the mean areas of glomerular capsules, glomerular tufts and transverse tubules both at paraffin and historesin samples were measured. When compared the mean areas of these regions from native and decellularized kidneys, there was a significant difference between the two groups in all the investigated regions, confirming that the decellularized organ suffers significant shrinkage during tissue preparation for histology in all regions analyzed (**Table 01**). The percentages of total organ shrinkage were then calculated from the average between the shrinkage percentages of each analyzed area (glomerular capsules, glomerular tufts, and transverse tubules) both for the paraffin (a reduction of 22.67% of mean area) and historesin samples (a reduction of 22.11% of mean area), There was no significant difference between the percentages of total organ shrinkage obtained from the two methods (**Table 01**).

Based on the calculated percentage of shrinkage of the decellularized tissues, the quantification of collagen fibers, sulfated and non-sulfated GAGs, and GLPs were corrected by area. After correction, the results were compared between groups (**Table 02**). On paraffin included tissues, the quantification of collagen on decellularized samples presented no difference compared to native tissue, indicating that the higher quantification previously observed was due to the shrinkage of the organ. However, when the values of quantification of sulfated GAG's were corrected by shrinkage percentage, it became lower on decellularized tissue than on native tissue, and non-sulfated GAG's and GLP's were now, even more, lower than before correcting the values. On historesin samples, collagen fibers and non-sulfated GAG's were not different between native and decellularized tissues, while GLP's were lower and sulfated GAG's were, even more, lower on decellularized tissues compared to native tissues.

To confirm the results obtained by histomorphometric analyses, collagen fibers and sulfated GAG's were quantified by spectrophotometric analyses (**Figure 04**). It was observed a significant decrease in the amount of sulfated GAG's on decellularized organs compared to native samples (91.24% decrease). This result corroborates the quantification of GAG's by histomorphometric analyses both in paraffin or historesin included tissues. When collagen fibers were analyzed by hydroxyproline quantification, there was no difference between the amount of this component on decellularized and native samples, confirming the results obtained with histomorphometric analyses corrected by the percentage of shrinkage, indicating that the correction was reliable.

Another attempt to confirm the results obtained on histomorphometric analyses corrected by percentage of shrinkage was the quantification of ECM proteins by mass spectrometry. We analyzed the data against a database of UniProt "Extracellular matrix protein + rat" (1,148 sequences). It was notable the differences between both groups concerning the protein identifications. Native organs identified 124 (SD± 11.12) proteins compared to 38 (SD± 10.57) proteins from Decellularized organs. Therefore, the Native group showed 3.26-time proteins matched against the database. Peaks Studio v8.5 software was applied to perform the label-free quantification to determine proteins that were differentially regulated between protein samples from native and decellularized organs with a p-value < 0.01 and a minimum fold change of 1.5 between groups.

Overall, 29 proteins were detected as significantly altered: 20 proteins were downregulated, and 9 proteins were upregulated with decellularization process (**Figure 05**). Collagen type IV alpha 3 (tr|F1LRJ1|F1LRJ1_RAT), Collagen type V alpha 2 (tr|F1LQ00|F1LQ00_RAT), Collagen alpha-1(I) (P02454|CO1A1_RAT), Collagen type IV alpha 2 (tr|F1M6Q3|F1M6Q3_RAT) were one of the ECM proteins that were highly expressed in the decellularized compared to native group. All the proteins quantified in this analysis are described in material supplementary with their respective intensity and expression ratio between the groups.

Discussion

The organ decellularization and scaffold production have been repeatedly demonstrated to be successful, and generation of tissues and organs engineered after the decellularization process seems to be promising in a range of tissue types²⁴⁻²⁸. These scaffolds provide a biologically active model appropriate for subsequent cellular repopulation with the goal of regenerating an organ and making it functional²⁹⁻³¹. An entire organ scaffold is considered viable for cell repopulation when maintaining its three-dimensional extracellular histoarchitecture. It is postulated that only the ECM of intact organs satisfactorily represents the complex microenvironments *in vivo* and, therefore, provides the generation of all the functioning of complex tissues³². Intact architecture is particularly relevant for the kidney because its blood filtration function requires a coordinated and accurate arrangement of numerous cell types with different underlying ECMs³³. In this sense, techniques that allow a precise evaluation of the ECM components maintenance is of paramount importance for the success of the kidney decellularization. Since a histological visualization of the matrix components is essential after decellularization, the histological techniques used can be powerful allies for basic research. Here we demonstrated that, by quantifying the staining allied to correction of its values by its percentage of shrinkage (Retraction Index), histomorphometric analyses allow qualitative and quantitative evaluation of the success of the decellularization. Most of the studies already published only used histomorphometric analyses for qualitative evaluation of the process^{6,31,34-37}. Histology is a classical technique that is used to study the morphology of cellular and subcellular structures, sectioned specimens into thin sections. Even with the advent of real-time imaging technology, histological slicing and staining remain the significant methods for visualizing cell morphology in tissues.

Depending on the type of analysis required for an assay, there are many available histological techniques, each with its advantages and disadvantages³⁸. Among the most common techniques are the inclusion in paraffin and the inclusion in plastic resin for sectioning³⁹⁻⁴¹. Although some dyes routinely used in paraffin included tissues have shown a weak contrast in plastic resin sections, Cerri and Sasso-Cerri adapted some alternative dyes with appropriate staining contrast and detection of different substances in glycol methacrylate tissue sections⁴¹. Sullivan-Brown and coworkers, in 2010, also demonstrated the advantages on the use of methacrylate resin instead of paraffin, with obtention of ultrathin (0.5–1 μM) or semithin (2–3 μm) sections⁴². Here we demonstrate that both techniques are useful for evaluating the efficacy of kidney decellularization and can be used together to ensure the best results since some dyes present the best impregnation with one or another inclusion method.

Despite the good results we obtained with histologic staining, the decellularization process promoted changes in histological structures (histological retraction) and, therefore, may end up influencing the quantification of collagen fibers, sulfated GAG's and non-sulphates and GLP's. These results were similar to those from Peloso and colleagues⁴³, which observed a reduction of around 45% of glomerular volume and glomerular afferent and efferent arterioles diameter on decellularized kidneys. Therefore, they only used the histological data for qualitatively comparisons and did additional experiments for quantification of ECM components. Considering that the quantification of these parameters is very useful in verifying if the scaffold retains structures essential for subsequent processes of cell repopulation, we used the percentage of shrinkage to correct the histomorphometric values of the decellularized renal scaffold. This strategy allowed us to reliably quantify collagen fibers, sulfated and non-sulphated GAGs, and GLPs. At the end of the organ decellularization, there should be no remaining cellular or nuclear residues since they could disrupt the attempt to repopulating the organ scaffold or promote undesirable immune responses. The DNA quantification is, therefore, another important approach to ensure the efficacy of the decellularization⁴⁴. However, normalization of the data may be necessary due to the differences between the samples before and after the process. Many papers have adopted different strategies for data normalization, such as wet tissue weight, dry tissue weight, whole tissue, volume, protein content, and others⁴⁵. Here, we quantify the DNA residue in the decellularized samples and compare it with the amount of DNA in the non-decellularized samples, using prior drying of the samples. Drying samples method was

developed to ensure the removal of the aqueous content that may interfere with the actual analysis result. At the end of the process, the quantification was normalized based on the whole organ weight. According to Bruyneel and Carr⁴⁵, whole organ weight, as well as the use of pretreatment tissue weight provides the most appropriate normalization.

Recent advances in mass spectrometry techniques have made it possible to study the proteomes of complex tissues, including extracellular matrix rich tissues⁴⁶. However, ECM proteins have been notoriously difficult to analyze because of their covalent crosslinking and numerous modifications^{47,48}. Because of the large size of many ECM-related proteins, it was necessary to analyze tryptic peptides from the decellularized tissue rather than intact proteins, for that, it was employed shotgun proteomics based on label-free quantification to evaluate the decellularization process affect the ECM matrix.

Decellularization process consists of enrichment of ECM proteins with significant removal of numerous cellular proteins. In our study, it is clear to note that the significant ECM components, such as collagen, were preserved in the decellularized tissue. Similar results, with different proteomics techniques, were described in several studies⁴⁹⁻⁵³. Hill *et al.* reported that the decellularization procedure removes over 98% of intracellular proteins evaluated and retains, to varying degrees, proteoglycans and glycoproteins of the ECM⁵³. However, the upregulation of ECM proteins observed after decellularization indicates that this technique is not the most appropriate for ECM components quantification. Once the procedure cannot drive the synthesis of new proteins, the upregulation observed is due to the method, which does not happen in the histological analyzes corrected by area. Nonetheless, mass-level quantification is still relatively expensive and almost inaccessible in developing countries, so that researchers still need to look for more available strategies for this purpose.

The main obstacle in working with histological analyzes for quantification of proteins before and after organ decellularization is the fact that the decellularized tissue undergoes shrinkage due to the absence of cells filling the tissue. Here, when collagen was quantified in the histological sections after staining, we observed an increase in the staining of collagen in the decellularized tissue. This increase cannot be real since there is no way to increase collagen expression with decellularization, but the shortening of the tissue can explain it, and consequently, the higher percentage of tissue were analyzed by histological section.

Correction of the quantification based on the percentage of tissue shortening (22.67% for paraffin samples

and 22.11% for historesin samples) allows normalization of the amount of tissue analyzed per histological section area, allowing a real quantification of the proteins present in these samples. When the amount of collagen was quantified by mass spectroscopy, the decellularized samples presented an increase in the expression of four types of collagen compared to native samples, similar to those results obtained by histological quantification without correction by shrinkage percentage. Again, these results cannot be real. These alterations may be explained by the technique used to prepare the samples for mass-level quantification. According to Barallobre-Barreiro²⁰, for the extraction of extracellular proteins from a tissue to be further analyzed by mass spectrometry, prior partial decellularization is necessary for the removal of plasma contaminants and minimization of cellular proteins contamination. However, the native tissue remains some cellular proteins that can be ionized preferably to the glycoproteins from the ECM due to the competitive ionization⁵⁴. Therefore, the enrichment of ECM content by the decellularization process and removal of the cellular proteins allowed the detection of ECM proteins in the mass spectrometry analysis. Thus, the application of mass spectrometry in order to compare the ECM contents between native and decellularized tissue maybe not the first choice to this analysis²⁰. We suggest that histological quantification with correction of the percentage of shrinkage (Retraction Index) seems to be, until now, the most efficient and reliable for the quantification of the components of ECM on decellularized organs.

Conclusions

Histological analysis is one of the most formidable ways of observing tissue. Through the staining of tissues, these reveal specific microscopic peculiarities. Regarding the studies in the field of Tissue Bioengineering, histology is very useful in the evaluation of decellularized scaffolds concerning the structure of the obtained matrix. However, it should be noted that, like any other technique, adjustments are necessary. Here we conclude that after using the Retraction Index, the quantitative results of histology are comparable to the other quantification techniques, even the most advanced ones.

Conflicts of interest

The authors declare that there is no conflict of interest regarding the publication of this article.

Acknowledgements

The authors were supported by grants from Fundação de Amparo à Pesquisa e Inovação do Espírito Santo (EDITAL FAPES Nº 006/2014-UNIVERSAL: process number 0606/2015; EDITAL FAPES/CNPq Nº 012/2014-DCR: process number 0832/2015; EDITAL PROFIX FAPES/CAPES 009/2014-63/2017 process number 79522882/17); Rede Nordeste de Biotecnologia (RENORBIO), Coordenação de Aperfeiçoamento de Pessoal de Nível Superior (CAPES); National Council for Scientific and Technological Development (CNPq, process number 150037/2018-0) and Fundação de Amparo à Pesquisa do Estado de São Paulo (FAPESP) [No. 2013/07467-1, 2016/04000-3 and 2017/17943-6 to L.K.I.]

References

1. Destefani, A. C., Sirtoli, G. M. & Nogueira, B. V. Advances in the Knowledge about Kidney Decellularization and Repopulation. *Front. Bioeng. Biotechnol.* **5**, 34 (2017).
2. Agodoa, L. C., Striker, G. E. & Chi, E. Glycol methacrylate embedding of renal biopsy specimens for light microscopy. *Am. J. Clin. Pathol.* **64**, 655–60 (1975).
3. Khorramirouz, R. *et al.* Effect of three decellularisation protocols on the mechanical behaviour and structural properties of sheep aortic valve conduits. *Adv. Med. Sci.* **59**, 299–307 (2014).
4. Poornejad, N. *et al.* Efficient decellularization of whole porcine kidneys improves reseeded cell behavior. *Biomed. Mater.* **11**, 025003 (2016).
5. Poornejad, N. *et al.* Freezing/Thawing without Cryoprotectant Damages Native but not Decellularized Porcine Renal Tissue. *Organogenesis* **11**, 30–45 (2015).
6. Poornejad, N. *et al.* The impact of decellularization agents on renal tissue extracellular matrix. *J. Biomater. Appl.* **31**, 521–533 (2016).
7. Orlando, G. *et al.* Production and Implantation of Renal Extracellular Matrix Scaffolds From Porcine Kidneys as a Platform for Renal Bioengineering Investigations. *Ann. Surg.* **256**, 363–370 (2012).
8. Momtahan, N. *et al.* Automation of Pressure Control Improves Whole Porcine Heart Decellularization. *Tissue Eng. Part C. Methods* **00**, 150714090832003 (2015).
9. Srinivasan, M., Sedmak, D. & Jewell, S. Effect of fixatives and tissue processing on the content and integrity of nucleic acids. *Am. J. Pathol.* **161**, 1961–71 (2002).
10. Chaudhuri, J. & Al-Rubeai, M. *Bioreactors for Tissue Engineering. Biotechnology letters* (Springer, 2005).
11. Gunwar, S. *et al.* Glomerular Basement Membrane: IDENTIFICATION OF A NOVEL DISULFIDE-CROSS-LINKED NETWORK OF 3, 4, AND 5 CHAINS OF TYPE IV COLLAGEN AND ITS IMPLICATIONS FOR THE PATHOGENESIS OF ALPORT SYNDROME. *J. Biol. Chem.* **273**, 8767–8775 (1998).
12. Hughes, R. C. *Membrane Glycoproteins: A review of structure and function.* (BUTTERWORTHS, 1976).
13. Vavken, P., Joshi, S. & Murray, M. M. TRITON-X is most effective among three decellularization agents for ACL tissue engineering. *J. Orthop. Res.* **27**, 1612–8 (2009).
14. Wu, Q. *et al.* Optimizing Perfusion-Decellularization Methods of Porcine Livers for Clinical-Scale Whole-Organ Bioengineering. *Biomed Res. Int.* **2015**, 1–9 (2015).

15. Samuel, C. S. in *Methods in molecular biology (Clifton, N.J.)* (eds. Becker, G. J. & Hewitson, T. D.) **466**, 223–235 (Humana Press, 2009).
16. Merna, N., Robertson, C., La, A. & George, S. C. Optical imaging predicts mechanical properties during decellularization of cardiac tissue. *Tissue Eng. Part C. Methods* **19**, 802–9 (2013).
17. Elder, B. D., Eleswarapu, S. V. & Athanasiou, K. A. Extraction techniques for the decellularization of tissue engineered articular cartilage constructs. *Biomaterials* **30**, 3749–3756 (2009).
18. Yang, B. *et al.* Development of a porcine bladder acellular matrix with well-preserved extracellular bioactive factors for tissue engineering. *Tissue Eng. Part C. Methods* **16**, 1201–11 (2010).
19. Karlsson, M. & Björnsson, S. Quantitation of proteoglycans in biological fluids using Alcian blue. *Methods Mol. Biol.* **171**, 159–73 (2001).
20. Barallobre-Barreiro, J., Didangelos, A., Yin, X., Doménech, N. & Mayr, M. A sequential extraction methodology for cardiac extracellular matrix prior to proteomics analysis. *Methods Mol. Biol.* **1005**, 215–223 (2013).
21. Barallobre-Barreiro, J., Baig, F., Fava, M., Yin, X. & Mayr, M. Glycoproteomics of the Extracellular Matrix: A Method for Intact Glycopeptide Analysis Using Mass Spectrometry. *J. Vis. Exp.* (2017). doi:10.3791/55674
22. Barallobre-Barreiro, J. *et al.* Extracellular matrix remodelling in response to venous hypertension: proteomics of human varicose veins. *Cardiovasc. Res.* **110**, 419–430 (2016).
23. Ma, B. *et al.* PEAKS: powerful software for peptide de novo sequencing by tandem mass spectrometry. *Rapid Commun. Mass Spectrom.* **17**, 2337–2342 (2003).
24. Peloso, A. *et al.* The Human Pancreas as a Source of Protolerogenic Extracellular Matrix Scaffold for a New-generation Bioartificial Endocrine Pancreas. *Ann. Surg.* **XX**, 1 (2015).
25. Soto-Gutierrez, A. *et al.* A whole-organ regenerative medicine approach for liver replacement. *Tissue Eng. Part C. Methods* **17**, 677–686 (2011).
26. Chang, J. Studies in flexor tendon reconstruction: Biomolecular modulation of tendon repair and tissue engineering. *J. Hand Surg. Am.* **37**, 552–561 (2012).
27. Kasimir, M. T. *et al.* Comparison of different decellularization procedures of porcine heart valves. *Int. J. Artif. Organs* **26**, 421–427 (2003).
28. Bonandrini, B. *et al.* Recellularization of Well-Preserved Acellular Kidney Scaffold Using Embryonic Stem Cells. *Tissue Eng. Part A* **20**, 1486–1498 (2014).
29. Luo, L., Eswaramoorthy, R., Mulhall, K. J. & Kelly, D. J. Decellularization of porcine articular cartilage explants and their subsequent repopulation with human chondroprogenitor cells. *J. Mech. Behav. Biomed. Mater.* **55**, 21–31 (2015).
30. Ng, S. L. J., Narayanan, K., Gao, S. & Wan, A. C. A. Lineage restricted progenitors for the repopulation of decellularized heart. *Biomaterials* **32**, 7571–7580 (2011).
31. McKee, R. & Wingert, R. Repopulating Decellularized Kidney Scaffolds: An Avenue for Ex Vivo Organ Generation. *Materials (Basel)*. **9**, 190 (2016).
32. Koh, C. J. & Atala, A. Tissue engineering, stem cells, and cloning: opportunities for regenerative medicine. *J. Am. Soc. Nephrol.* **15**, 1113–25 (2004).
33. Takasato, M. & Little, M. H. Making a Kidney Organoid Using the Directed Differentiation of Human Pluripotent Stem Cells. *Methods Mol. Biol.* **1597**, 195–206 (2017).
34. Sambhi, M. *et al.* Acellular Mouse Kidney ECM can be Used as a Three-Dimensional Substrate to Test the Differentiation Potential of Embryonic Stem Cell Derived Renal Progenitors. *Stem Cell Rev. Reports* (2017). doi:10.1007/s12015-016-9712-2
35. Heyner, S. *et al.* *Kidney Research*. **1397**, (Springer New York, 2016).
36. Song, J. J. *et al.* Regeneration and experimental orthotopic transplantation of a bioengineered kidney. *Nat. Med.* **19**, 646–51 (2013).
37. Park, J. B. *et al.* Phospholipase signalling networks in cancer. *Nat. Rev. Cancer* **12**, 782–92 (2012).

38. Alturkistani, H. A., Tashkandi, F. M. & Mohammedsaleh, Z. M. Histological Stains: A Literature Review and Case Study. *Glob. J. Health Sci.* **8**, 72–9 (2015).
39. Rubin, N. H. & Baur, P. S. A Sample-Grouping Technique for Paraffin Embedments. *Stain Technol.* **58**, 157–160 (1983).
40. Canene-Adams, K. Preparation of formalin-fixed paraffin-embedded tissue for immunohistochemistry. *Methods Enzymol.* **533**, 225–33 (2013).
41. Cerri, P. . S. & Sasso-Cerri, E. Staining methods applied to glycol methacrylate embedded tissue sections. *Micron* **34**, 365–72 (2003).
42. Sullivan-Brown, J., Bisher, M. E. & Burdine, R. D. Embedding, serial sectioning and staining of zebrafish embryos using JB-4 resin. *Nat. Protoc.* **6**, 46–55 (2011).
43. Peloso, A. *et al.* Renal Extracellular Matrix Scaffolds From Discarded Kidneys Maintain Glomerular Morphometry and Vascular Resilience and Retains Critical Growth Factors. *Transplantation* **99**, 1807–1816 (2015).
44. Crapo, P. M., Gilbert, T. W. & Badylak, S. F. An overview of tissue and whole organ decellularization processes. *Biomaterials* **32**, 3233–3243 (2011).
45. Bruyneel, A. A. N. & Carr, C. A. Ambiguity in the Presentation of Decellularized Tissue Composition: The Need for Standardized Approaches. *Artif. Organs* **41**, 778–784 (2017).
46. Naba, A. *et al.* Characterization of the Extracellular Matrix of Normal and Diseased Tissues Using Proteomics. *J. Proteome Res.* **16**, 3083–3091 (2017).
47. Holding, A. N. XL-MS: Protein cross-linking coupled with mass spectrometry. *Methods* **89**, 54–63 (2015).
48. Leitner, A. Cross-linking and other structural proteomics techniques: how chemistry is enabling mass spectrometry applications in structural biology. *Chem. Sci.* **7**, 4792–4803 (2016).
49. Bringans, S. D. *et al.* Comprehensive mass spectrometry based biomarker discovery and validation platform as applied to diabetic kidney disease. *EuPA Open Proteomics* **14**, 1–10 (2017).
50. Jung, J. W. *et al.* Mass spectrometric imaging of metabolites in kidney tissues from rats treated with furosemide. *Am. J. Physiol. Physiol.* **310**, F1317–F1327 (2016).
51. Lalowski, M. *et al.* Imaging mass spectrometry: a new tool for kidney disease investigations. *Nephrol. Dial. Transplant.* **28**, 1648–1656 (2013).
52. Liu, W.-Y. *et al.* Xenogeneic decellularized scaffold: a novel platform for ovary regeneration. *Tissue Eng. Part C Methods* **23**, ten.TEC.2016.0410 (2016).
53. Hill, R. C., Calle, E. A., Dzieciatkowska, M., Niklason, L. E. & Hansen, K. C. Quantification of Extracellular Matrix Proteins from a Rat Lung Scaffold to Provide a Molecular Readout for Tissue Engineering. *Mol. Cell. Proteomics* **14**, 961–973 (2015).
54. Mechref, Y. in *Current Protocols in Protein Science* 12.11.1–12.11.11 (John Wiley & Sons, Inc., 2012). doi:10.1002/0471140864.ps1211s68
55. Junqueira, L. C., Bignolas, G. & Brentani, R. R. Picrosirius staining plus polarization microscopy, a specific method for collagen detection in tissue sections. *Histochem. J.* **11**, 447–55 (1979).
56. Grimm, P. C. *et al.* Computerized image analysis of Sirius Red-stained renal allograft biopsies as a surrogate marker to predict long-term allograft function. *J. Am. Soc. Nephrol.* **14**, 1662–8 (2003).
57. Sund, S. Computerized image analysis vs semiquantitative scoring in evaluation of kidney allograft fibrosis and prognosis. *Nephrol. Dial. Transplant.* **19**, 2838–2845 (2004).
58. da Silva, C. M. L., Spinelli, E. & Rodrigues, S. V. Fast and sensitive collagen quantification by alkaline hydrolysis/hydroxyproline assay. *Food Chem.* **173**, 619–623 (2015).

Table 1: Mean area measurement of the Renal corpuscles, Glomeruli and Transverse tubules by histological analysis.

Renal Section	Mean Area Fraction (μm^2)					
	<i>Paraffin</i>			<i>Histoiresin</i>		
	<i>Control (native)</i>	<i>Decellularized</i>	Variation	<i>Control (native)</i>	<i>Decellularized</i>	Variation
Renal corpuscles	5502±53	4813±91*	(-) 12.52%	14723± 248	11184±536*	(-) 24.04%
Glomeruli	4419±153	3421±58*	(-) 22.58%	9644±246	8327±301*	(-) 13.66%
Transverse tubules	1162±51	780±15*	(-) 32.90%	2061±120	1471±13*	(-) 28.63%
Mean Retraction Index			(-) 22.67%			(-) 22.11%

All reported results are Mean ± Standard Error Mean (SEM). NS=no significant difference ($p>0.05$); *significantly different ($p\text{-value}<0.05$) from native tissue. Student's *t*-test.

Table 2: Mean area measurement of the Collagen, Sulphated/Non-sulphated GAG's and GLP's by histological analysis.

		<i>Control (native)</i>	<i>Decellularized</i>	<i>Adjusted Decellularized</i>
Collagen Fibers (μm^2)	<i>Paraffin</i>	12.51±0.30	15.50±0.45*	11.99±0.34
	<i>Histoiresin</i>	6.09±0.14	7.97±0.04*	6.20±0.03
Non-sulphated GAG's (μm^2)	<i>Paraffin</i>	9.37±0.24	5.12±0.13*	3.96±0.10*
	<i>Histoiresin</i>	8.66±0.23	8.39±1.19	6.53±0.92
Sulphated GAG's (μm^2)	<i>Paraffin</i>	6.28±0.62	4.83±0.27*	3.73±0.21*
	<i>Histoiresin</i>	8.39±0.19	4.08±0.07*	3.18±0.05*
GLP's (μm^2)	<i>Paraffin</i>	6.89±0.34	2.04±0.17*	1.58±0.13*
	<i>Histoiresin</i>	17.28±0.45	17.70±0.48	13.79±0.37*

GAG's: glycosaminoglycans; GLP's: glycoproteins.

All reported results are Mean ± Standard Error Mean (SEM). NS=no significant difference ($p>0.05$); *significantly different ($p\text{-value}<0.05$) from native tissue. Student's *t*-test.

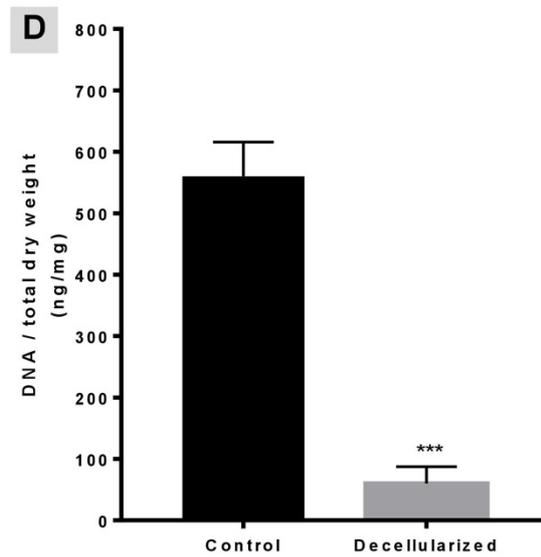
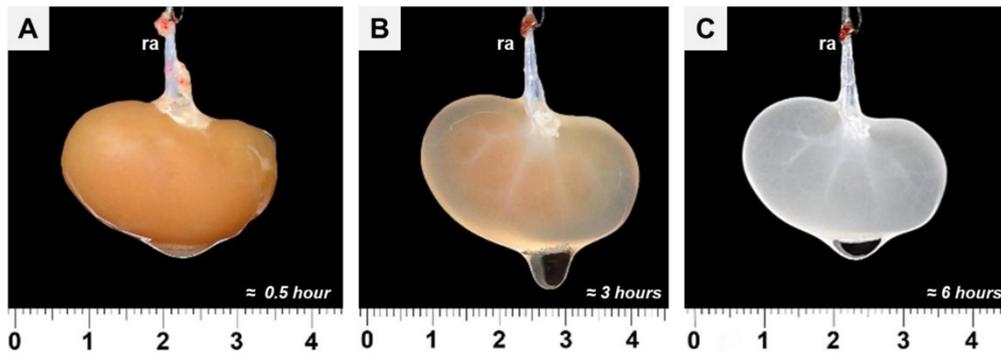


Fig. 1 A-C) Timeline, in hours (h), of the sequence decellularization kidneys process and gross appearance of harvested kidney scaffolds. In "A" observe the beginning of the process after kidney harvest from animals. In "B" after 3 hours of decellularization following standard protocol by our group. "C" after 6 hours of infusion SDS solution at 1%. Note the gradual loss of one's color organ during the progression of detergent infusion. **D)** DNA Residual the control (native) showed 560.00±32.15 ng/mg while decellularized group represent 60.00±15.72 ng/mg of DNA by total dry weight ($p < 0.0001$). Student's *t*-test. Scale bar = 1 cm. Time in hours (h).

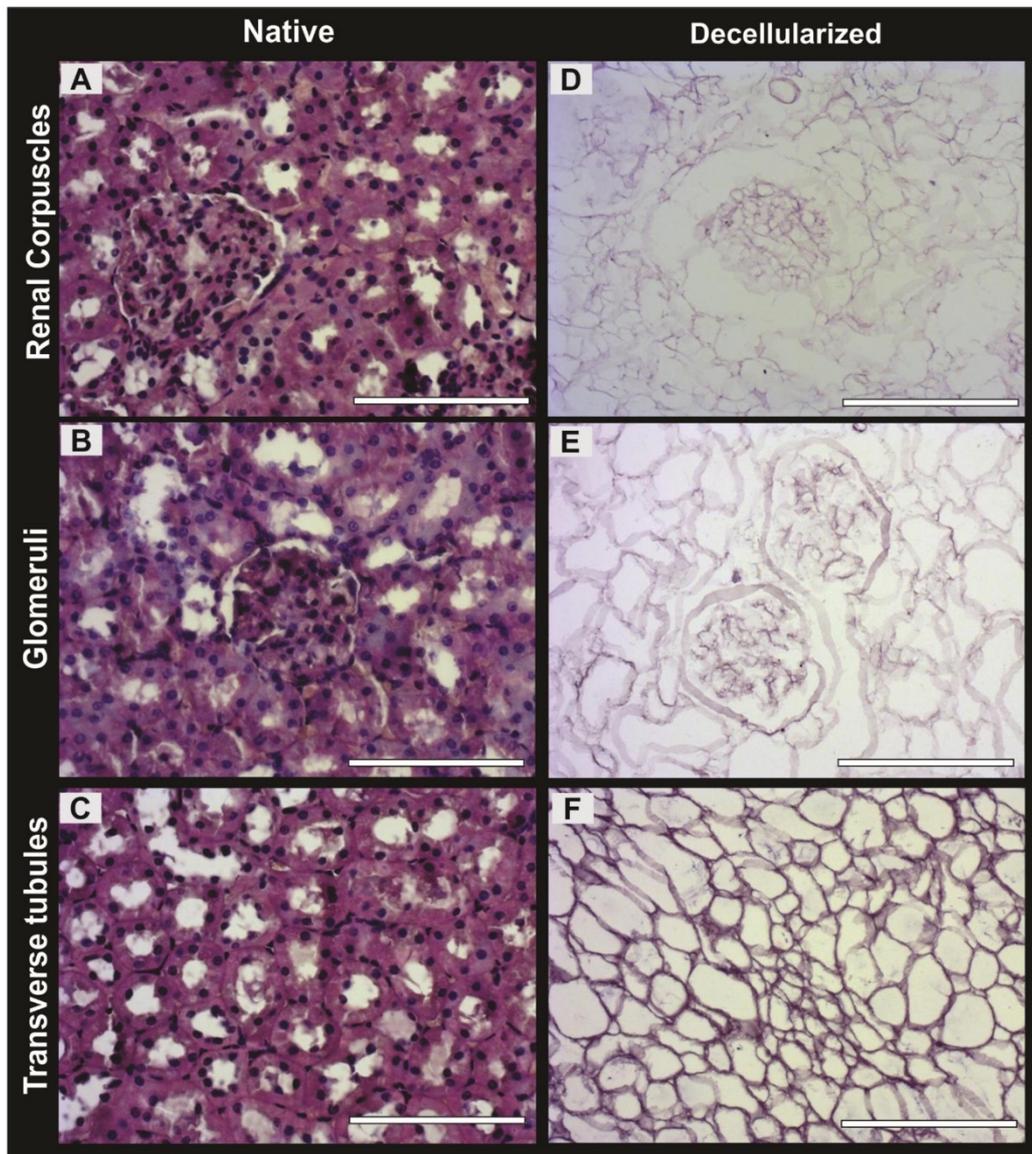


Fig. 2: Renal histomorphometry

Native kidneys in the control group (A-C) were analyzed in three different regions: renal corpuscles (A, D), glomeruli (B, E) and transverse tubules (C, F) to verify tissue integrity and presence of primordial renal structures. Decellularized (D-F) kidneys were morphologically over-estimated if essential renal structures were retained for subsequent repopulation. Note the absence of cells and undetectable levels of cellular debris. HE staining, scale bar corresponds to 100 μm .

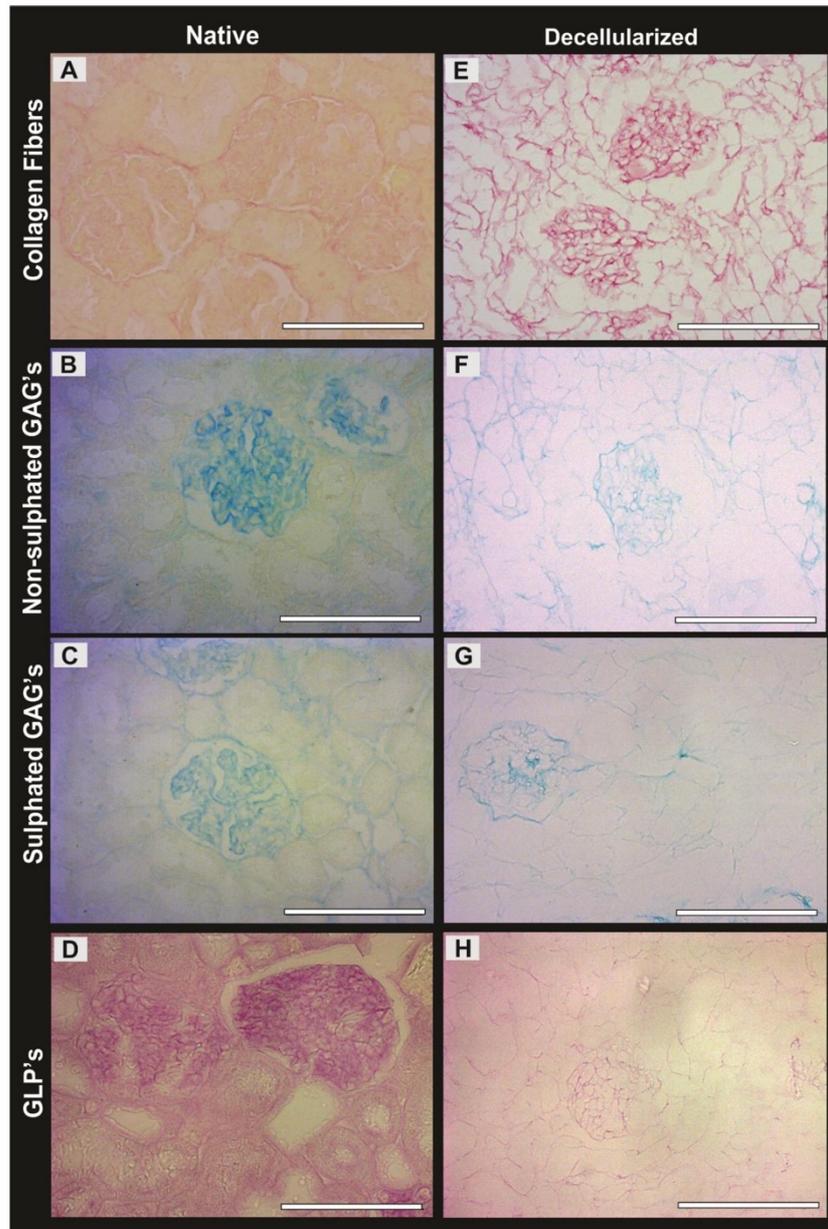


Fig. 3: Histological analysis of collagen fibers, sulfated and non-sulfated GAG's and glycoproteins.

Native kidneys relative to the control group (A-D) and decellularized (E-H) kidneys were stained by different techniques, according to figure. It is possible to see the need to perform corrections in the area values given the retraction visualization of the ECM components. Scale bar corresponds to 100 μm .

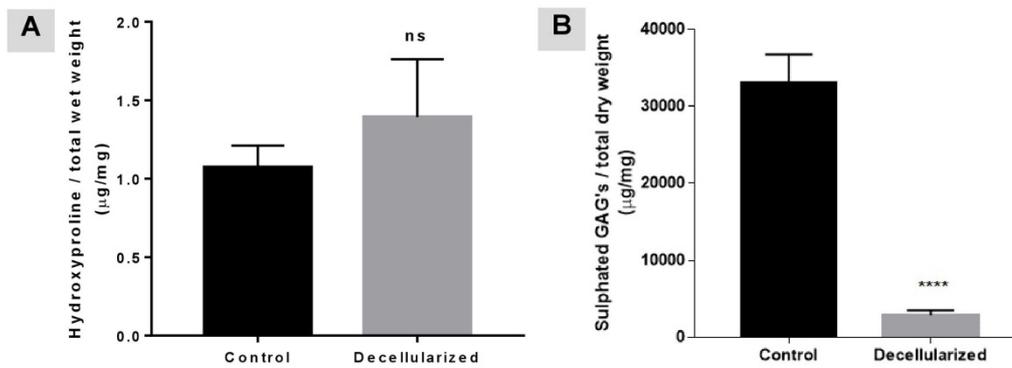


Fig. 4: Hydroxyproline and Sulphated GAG's quantification.

Collagen fibers were analyzed by hydroxyproline quantification (A), there was no difference between the amount of this component on decellularized ($1.39 \pm 0.36 \mu\text{g}/\text{mg}$) and native ($1.07 \pm 0.13 \mu\text{g}/\text{mg}$) samples. In (B) the Sulphated GAG's quantification showed the remarkable difference ($p < 0.0001$) when compare native ($33033 \pm 3712 \mu\text{g}/\text{mg}$) with decellularized ($2894 \pm 637 \mu\text{g}/\text{mg}$) group. Data were analyzed by Student's *t*-test.

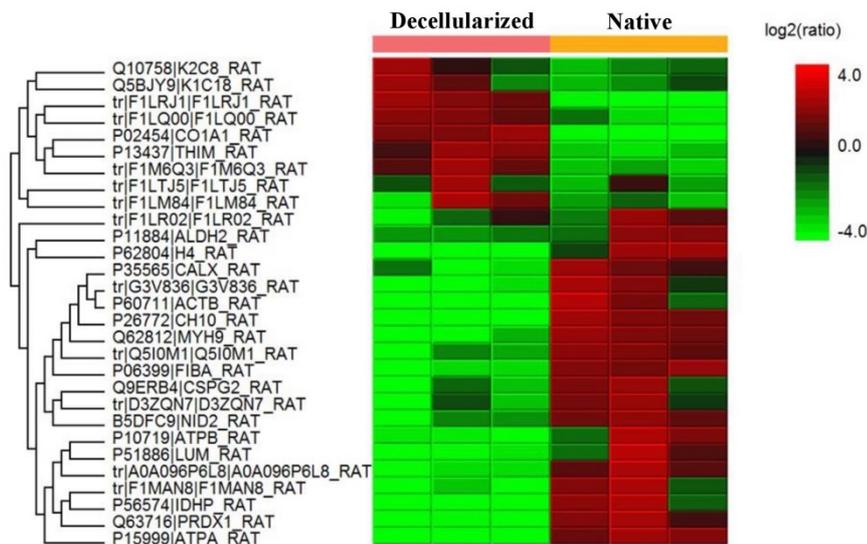


Fig. 05: Heatmap of significantly up- and downregulated proteins identified after decellularization procedure and analyzed by PEAKS label-free quantification software ($p < 0.01$, min fold change > 1.5 , quality ≥ 8 , and at least one unique peptide). Data refer to 3 biological replications/replicates.

SUPPLEMENTARY DATA

Table 1: Threshold Color Parameters in Image J

Parameters	Histological Staining			
	Picro Sirius	Alcian Blue pH 2.5	Alcian Blue pH 0.5	PAS
<i>Threshold method</i>	<i>Default</i>	<i>Default</i>	<i>Default</i>	<i>Default</i>
<i>Threshold color</i>	<i>Black</i>	<i>Black</i>	<i>Black</i>	<i>Black</i>
<i>Colour space</i>	YUV	YUV	YUV	YUV
<i>Y</i>	163/255	0/255	0/255	162/255
<i>U</i>	0/255	0/186	0/186	0/255
<i>V</i>	0/255	113/255	113/255	0/255
<i>Dark background</i>	<i>Yes</i>	<i>Yes</i>	<i>Yes</i>	<i>Yes</i>

Table 2: Histological Staining Methods

<p>Cytoplasm and Nuclei by Hematoxylin and Eosin (HE) staining After the hydration process the slides containing the renal sections were immersed in Harris Hematoxylin for 5 min; differentiation in alcohol-acid solution (1 passage); running water for 10 min; Eosin for 2 min; 3 alcohol baths 100% for 5 min each and by the process of assembling the sections according to laboratory routine. This coloration stains the acidophilic cytoplasm in red, basophilic cytoplasm in purple and nuclei in blue.</p> <p>Collagen Fibers by Picro Sirius staining After the hydration process the slides containing the renal sections were immersed in Picro Sirius solution for 1 hour; differentiation in alcohol-acid solution and by the process of assembling the sections according to laboratory routine. The coloration of Picrosirius (also known as 'Sirius Red') is specific for types of collagen I and III under polarized light⁵⁵⁻⁵⁷. This staining blends the collagen fibres in red, and the background is pale yellow.</p> <p>Non-sulphated Glycosaminoglycans (GAG's) by Alcian Blue staining in pH 2.5 After the hydration process the slides containing the renal sections were immersed in 3% aqueous acetic acid solution for 3 min; Alcian blue 1% for 2 hours; 3% aqueous acetic acid solution for 3 min; running water and by the process of assembling the sections according to the routine of the laboratory. Non-sulfated GAG's (e.g., hyaluronic acid) are stained in turquoise blue.</p> <p>Sulphated Glycosaminoglycans (GAG's) by Alcian Blue staining in pH 0.5 After the hydration process the slides containing the renal sections were immersed in 0.2 N aqueous HCl solution for 3 min; Alcian blue 1% for 30 min; 0.2 N aqueous HCl solution for 3 min; running water and by the process of assembling the sections according to the routine of the laboratory. Sulphated GAG's (e.g., heparan-, chondroitin- sulphated) are colored in turquoise blue.</p> <p>Glycoproteins (GLPs) by Periodic Schiff Acid (PAS) staining After the hydration process the slides containing the renal sections were immersed in 1% aqueous periodic acid solution for 15 min at 2°C-8°C in the dark; running water for 5 min and then distilled water; Schiff reagent for 1 hour at 2°C-8°C in the dark; running water for 5 min and by the process of</p>
--

assembling the sections according to laboratory routine. The collagen fibres blush in green and the nuclei in blue/black.

Table 3: Hydroxyproline Quantification

In the spectrophotometric determination of hydroxyproline concentration, the sample was alkaline hydrolyzed, achieved with incubation with $\text{NaOH} \geq 2\text{N}$ in an autoclave at 120°C ($p \approx 98, 1\text{kPa}$) for 40 minutes. The free amino acid is determined colorimetrically after oxidation to pyrrole and reaction with 4-dimethylaminobenzaldehyde (Ehrlich reagent), resulting in a red-purple coloring compound. Chloramine-T is currently the preferred oxidizing agent in the formation of the pyrrole⁵⁸. Briefly, after the decellularization, the organs were divided into small pieces, proceeding with dehydration in 30%, 50%, 70%, 90% alcohol and three baths in 100% ethanol, with 15 min times each bath and then taken to a critical point (CO_2). The samples were immediately weighed after drying. After that, a portion of known weight (about 10 mg) was removed, fractionated into smaller portions, and transferred into a 15 mL capacity polypropylene conical tube (Falcon®, Nunc®). 500 μL of 7N NaOH was added, capping the flask, but not fully sealing it. After the hydrolysis, the hydrolysate was acidified with 500 μL of 3.5 M H_2SO_4 , transferred to a 10 mL volumetric flask, and rinsed with ultrapure water. The fluid was filtered; 500 μL of the sample was aliquoted and transferred to a glass/Falcon® tube, adding 4.5 mL of chloramine-T solution, shaking and allowing the reaction at room temperature for 25 minutes. Afterward, 5.0 mL of Ehrlich reagent was added, the flask was capped, stirred and the reagents were incubated in a water bath at 60°C for 15 minutes. The spectrophotometer was read at 560 nm. A standard 10-point hydroxyproline curve was performed starting from a solution containing 2,600 $\mu\text{g}/\text{mL}$ of the amino acid. Dilutions were performed in 2mL microtubes using ultrapure water where the final volume was 100 μL (1:1) having concentrations between 2.5 and 1,300 μg of hydroxyproline¹⁰⁻¹⁸.

Table 4: Sulphated GAG's Quantification

For the determination of chondroitin sulfate, a type of GAG, an 8-point standard curve was prepared to start from a solution containing 800 $\mu\text{g}/\text{mL}$ of chondroitin sulfate. Dilutions were performed in 2mL microtubes using distilled water, where the final volume was 100 μL (1:1) containing concentrations between 3.1 and 400 μg of chondroitin sulfate. From each tube, 50 μL of the diluent was transferred to new microtubes. Samples and blank (8M guanidine-HCl), 50 μL of 8M guanidine-HCl solution were added to standard, sample and blank aliquots. The final volume after the addition of the guanidine-HCl should be 100 μL . To the tubes, 50 μL of SAT reagent (0.3% $\text{H}_2\text{SO}_4/0.75\%$ Triton X-100) was added. The microtubes stand for 15 minutes; then 750 μL of Alcian Blue reagent was added and remained overnight at 4°C . The tubes were centrifuged at 12,000g for 15 minutes, and the supernatant was discarded. We added 500 μL of DMSO in each tube to resuspend the pellet and kept them in constant agitation for 15 minutes. Subsequently, we centrifuged again at 12,000g for 15 minutes and discarded the supernatant. We finally added 500 μL of Gu-Prop- H_2O reagent and resuspended the pellet. Samples were aliquoted into 96-well plates and read at 605 nm in plate reader¹⁹.

Table 5: Native Sequences



Native_blast2go_go
_table_20180802_11:

Table 6: Decellularized Sequences



Dec_blast2go_gotable_20180730_1825

SubmissionsLogout English ▼

Close

Thank you for selecting this.

We're currently running a test to see if a Chinese translation of this form would be easier for you. Would you be interested to have this in the future?

Interested

Not interested

No preference

Nature Methods

ARTICLE

The decellularization process changes 3D structure of the scaffold requiring corrections in the histomorphometric analysis

Thanks for submitting

Here is your unique Manuscript ID: NMETH-A36683.

Please use this in any correspondence with us regarding your submission.

We're currently converting all your files into PDFs. Once we've done that, we'll email a link to the files for your review.

This usually happens quickly. If you haven't heard from us within 2 hours, please contact us either by email, at platformsupport@springernature.com, or using our web form.

[Return to submission homepage](#)

The personal information you provide is extremely important to us. In this instance we collect and use personal data to process the manuscript you're submitting. We may also use this personal data internally and share it with our affiliates for purposes of peer-review, publication, internal reporting and third party abstracting and indexing services. If appropriate, we may contact you about submitting this manuscript to a Springer Nature journal other than this journal. Please refer to our full [Privacy Policy](#) (opens in a new window).

7. CONCLUSÕES

Aqui nós demonstramos a obtenção de arcabouços renais descelularizados através da perfusão de SDS (1%) sob pressão de 100 mmHg e fluxo de 1,0 mL/min. Com base em protocolos encontrados na literatura, o protocolo utilizado proporcionou a obtenção do arcabouço renal com preservação de estruturas de MEC específicas, retenção de moléculas extracelulares fundamentais e remoção celular com mínimo resíduo de DNA.

O processo removeu com sucesso proteínas celulares e DNA, preservando componentes da MEC, tais como, colágeno, laminina e GAG's. As estruturas extracelulares permaneceram intactas, incluindo uma rede vascular completa e a membrana basal de filtração glomerular.

Sumariamente, a natureza e os parâmetros dos protocolos de descelularização evoluirão à medida que mais determinantes do comportamento celular forem reconhecidos e medidos. Além disso, esses protocolos são, em última instância, destinados a produzir um dispositivo biocompatível que possibilite o desenvolvimento de órgãos *in vitro* para transplante. Provavelmente esses serão influenciados por espécies doadoras, técnica de esterilização, espécies receptoras, estado imunitário do paciente, natureza específica do tratamento clínico, intumescimento pós-processamento ou pré-implante, regulamentos federais, otimização de processos industriais e pressões do mercado.

8. REFERÊNCIAS

- ALLMAN, A. J. et al. Xenogeneic extracellular matrix grafts elicit a TH2-restricted immune response. **Transplantation**, v. 71, n. 11, p. 1631–1640, 15 jun. 2001.
- ATALA, A. Recent applications of regenerative medicine to urologic structures and related tissues. **Current opinion in urology**, v. 16, n. 4, p. 305–9, jul. 2006.
- BADYLAK, S. F. The extracellular matrix as a scaffold for tissue reconstruction. **Seminars in Cell and Developmental Biology**, v. 13, p. 377–383, 2002.
- BAPTISTA, P. M. et al. **Whole organ decellularization - A tool for bioscaffold fabrication and organ bioengineering**. Proceedings of the 31st Annual International Conference of the IEEE Engineering in Medicine and Biology Society: Engineering the Future of Biomedicine, EMBC 2009. **Anais...**jan. 2009Disponível em: <<http://www.ncbi.nlm.nih.gov/pubmed/19964173>>
- BAPTISTA, P. M. et al. The use of whole organ decellularization for the generation of a vascularized liver organoid. **Hepatology**, v. 53, n. 2, p. 604–617, fev. 2011.
- BASU, J. et al. Functional evaluation of primary renal cell/biomaterial neo-kidney augment prototypes for renal tissue engineering. **Cell Transplantation**, v. 20, n. 11–12, p. 1771–1790, 1 nov. 2011.
- BHRANY, A. D. et al. Development of an esophagus acellular matrix tissue scaffold. **Tissue Eng**, v. 12, n. 2, p. 319–330, fev. 2006.
- BONANDRINI, B. et al. Recellularization of Well-Preserved Acellular Kidney Scaffold Using Embryonic Stem Cells. **Tissue Engineering Part A**, v. 20, n. 9–10, p. 1486–1498, 2 maio 2014.
- BROOKS, D. N. et al. Processed nerve allografts for peripheral nerve reconstruction: A multicenter study of utilization and outcomes in sensory, mixed, and motor nerve reconstructions. **Microsurgery**, v. 32, n. 1, p. 1–14, jan. 2012.
- BROWN, J. W. et al. Performance of the CryoValve* SG human decellularized pulmonary valve in 342 patients relative to the conventional CryoValve at a mean follow-up of four years. **Journal of Thoracic and Cardiovascular Surgery**, v. 139, n. 2, p. 339–348, fev. 2010.
- BUINEWICZ, B.; ROSEN, B. Acellular Cadaveric Dermis (AlloDerm): A New Alternative for Abdominal Hernia Repair. **Annals of Plastic Surgery**, v. 52, n. 2, p. 188–194, fev. 2004.
- BURBKART, R. et al. Decellularized kidney matrix for perfused bone engineering. **Tissue engineering. Part C, Methods**, v. 20, n. 7, p. 553–61, jul. 2014.
- CARALT, M. et al. Optimization and Critical Evaluation of Decellularization Strategies to Develop Renal Extracellular Matrix Scaffolds as Biological Templates for Organ

Engineering and Transplantation. **American Journal of Transplantation**, v. 15, n. 1, p. 64–75, jan. 2015.

CHAE, S. Y. et al. Development of renal extracellular matrix (ECM) scaffold for kidney regeneration. **Tissue Engineering and Regenerative Medicine**, v. 11, n. S1, p. 1–7, 26 fev. 2014.

CHAN, B. P.; LEONG, K. W. Scaffolding in tissue engineering: general approaches and tissue-specific considerations. **European Spine Journal**, v. 17, n. S4, p. 467–479, dez. 2008.

CHEUNG, D. Y.; DUAN, B.; BUTCHER, J. T. Current progress in tissue engineering of heart valves: multiscale problems, multiscale solutions. **Expert opinion on biological therapy**, v. 15, n. 8, p. 1155–1172, 1 jun. 2015.

CHIU, Y.-C. et al. Sustained delivery of recombinant human bone morphogenetic protein-2 from perlecan domain I - functionalized electrospun poly (ϵ -caprolactone) scaffolds for bone regeneration. **Journal of experimental orthopaedics**, v. 3, n. 1, p. 25, 6 dez. 2016.

CHOI, S. H. et al. Development of a porcine renal extracellular matrix scaffold as a platform for kidney regeneration. **Journal of Biomedical Materials Research Part A**, v. 103, n. 4, p. 1391–1403, abr. 2015.

CHUNG, H.-J. et al. Surgical Outcomes of Anterior Cervical Fusion Using Demineralized Bone Matrix as Stand-Alone Graft Material : Single Arm , Pilot Study. **Korean Journal of Spine**, v. 13, n. 3, p. 114–119, set. 2016.

CONRAD, C. et al. Bio-engineered endocrine pancreas based on decellularized pancreatic matrix and mesenchymal stem cell/islet cell coculture. **Journal of the American College of Surgeons**, v. 211, n. 3, p. S62, set. 2010.

CORESH, J. et al. Prevalence of chronic kidney disease in the United States. **JAMA : the journal of the American Medical Association**, v. 298, n. 17, p. 2038–47, 7 nov. 2007.

CORTIELLA, J. et al. Influence of Acellular Natural Lung Matrix on Murine Embryonic Stem Cell Differentiation and Tissue Formation. **Tissue Engineering Part A**, v. 16, n. 8, p. 2565–2580, ago. 2010.

CRAPO, P. M.; GILBERT, T. W.; BADYLAK, S. F. An overview of tissue and whole organ decellularization processes. **Biomaterials**, v. 32, n. 12, p. 3233–3243, abr. 2011.

DE KOCK, J. et al. Simple and quick method for whole-liver decellularization: a novel in vitro three-dimensional bioengineering tool? **Archives of toxicology**, v. 85, n. 6, p. 607–12, 22 jun. 2011.

DEHGHANI, F.; ANNABI, N. **Engineering porous scaffolds using gas-based techniques** **Current Opinion in Biotechnology**, 2011. Disponível em: <<http://www.sciencedirect.com/science/article/pii/S095816691100067X>>. Acesso em: 12 jun. 2017

DESTEFANI, A. C.; SIRTOLI, G. M.; NOGUEIRA, B. V. Advances in the Knowledge about Kidney Decellularization and Repopulation. **Frontiers in Bioengineering and Biotechnology**, v. 5, p. 34, 1 jun. 2017.

EL-KASSABY, A. W. et al. Urethral stricture repair with an off-the-shelf collagen matrix. **The Journal of urology**, v. 169, n. 1, p. 170–3; discussion 173, jan. 2003.

GAO, R. et al. Hepatocyte Culture in Autologous Decellularized Spleen Matrix. **Organogenesis**, n. February 2015, p. 37–41, 2015.

GILBERT, T. W.; SELLARO, T. L.; BADYLAK, S. F. Decellularization of tissues and organs. **Biomaterials**, v. 27, n. 19, p. 3675–3683, jul. 2006.

GOH, K.; HOLMES, D. Collagenous Extracellular Matrix Biomaterials for Tissue Engineering: Lessons from the Common Sea Urchin Tissue. **International Journal of Molecular Sciences**, v. 18, n. 5, p. 901, 25 abr. 2017.

GRIFFIN, M. et al. Biomechanical Characterization of Human Soft Tissues Using Indentation and Tensile Testing. **Journal of Visualized Experiments**, n. 118, 13 dez. 2016.

GUAN, Y. et al. Porcine kidneys as a source of ECM scaffold for kidney regeneration. **Materials Science and Engineering: C**, v. 56, p. 451–456, nov. 2015a.

GUAN, Y. et al. The effective bioengineering method of implantation decellularized renal extracellular matrix scaffolds. **Oncotarget**, v. 6, n. 34, p. 36126–38, 2 nov. 2015b.

GUYETTE, J. P. et al. Bioengineering Human Myocardium on Native Extracellular Matrix. **Circulation research**, 26 out. 2015.

HARTMAN, O. et al. Biofunctionalization of electrospun PCL-based scaffolds with perlecan domain IV peptide to create a 3-D pharmacokinetic cancer model. **Biomaterials**, v. 31, n. 21, p. 5700–5718, jul. 2010.

HUBBELL, J. A. **Materials as morphogenetic guides in tissue engineering** *Current Opinion in Biotechnology*, out. 2003. Disponível em: <<http://www.ncbi.nlm.nih.gov/pubmed/14580588>>. Acesso em: 12 jun. 2017

HUDSON, T. W. et al. Optimized Acellular Nerve Graft Is Immunologically Tolerated and Supports Regeneration. **Tissue Engineering**, v. 10, n. 11–12, p. 1641–1651, nov. 2004.

IOP, L.; GEROSA, G. **Guided Tissue Regeneration in Heart Valve Replacement: From Preclinical Research to First-in-Human Trials** *BioMed Research International*, 2015. Disponível em: <<http://www.ncbi.nlm.nih.gov/pubmed/26495295>>. Acesso em: 13 jun. 2017

ISAACS, J.; SAFA, B. A Preliminary Assessment of the Utility of Large-Caliber Processed Nerve Allografts for the Repair of Upper Extremity Nerve Injuries. **HAND**, v. 12, n. 1, p. 55–59, jan. 2017.

JORAKU, A. et al. In vitro generation of three-dimensional renal structures. **Methods**, v.

47, n. 2, p. 129–133, fev. 2009.

KANG, T. Y. et al. Construction of large-volume tissue mimics with 3D functional vascular networks. **PLoS ONE**, v. 11, n. 5, p. e0156529, 26 maio 2016.

KHAN, A. A. et al. Repopulation of decellularized whole organ scaffold using stem cells: an emerging technology for the development of neo-organ. **Journal of Artificial Organs**, v. 17, n. 4, p. 291–300, 17 dez. 2014.

LAI, C.-F. et al. Withdrawal from long-term hemodialysis in patients with end-stage renal disease in Taiwan. **Journal of the Formosan Medical Association = Taiwan yi zhi**, v. 112, n. 10, p. 589–99, out. 2013.

LANZA, R. P. et al. Generation of histocompatible tissues using nuclear transplantation. **Nature Biotechnology**, v. 20, n. 7, p. 689–696, 3 jul. 2002.

LEE, S. J. et al. Development of a composite vascular scaffolding system that withstands physiological vascular conditions. **Biomaterials**, v. 29, n. 19, p. 2891–2898, jul. 2008.

LITTLE, M. H. Regrow or Repair: Potential Regenerative Therapies for the Kidney. **Journal of the American Society of Nephrology**, v. 17, n. 9, p. 2390–2401, 9 ago. 2006.

MATSUNUMA, H. et al. Constructing a tissue-engineered ureter using a decellularized matrix with cultured uroepithelial cells and bone marrow-derived mononuclear cells. **Tissue engineering**, v. 12, n. 3, p. 509–518, mar. 2006.

NAKAYAMA, K. H. et al. Renal tissue engineering with decellularized rhesus monkey kidneys: age-related differences. **Tissue engineering. Part A**, v. 17, n. 23–24, p. 2891–901, dez. 2011.

NARITA, Y. et al. Decellularized ureter for tissue-engineered small-caliber vascular graft. **Journal of Artificial Organs**, v. 11, p. 91–99, 2008.

NEAL, R. A. et al. Laminin Nanofiber Meshes That Mimic Morphological Properties and Bioactivity of Basement Membranes. **Tissue Engineering Part C: Methods**, v. 15, n. 1, p. 11–21, mar. 2009.

OTT, H. C. et al. Perfusion-decellularized matrix: using nature's platform to engineer a bioartificial heart. **Nature Medicine**, v. 14, n. 2, p. 213–221, 13 fev. 2008.

OTT, H. C. et al. Regeneration and orthotopic transplantation of a bioartificial lung. **Nature medicine**, v. 16, n. 8, p. 927–33, ago. 2010.

OTT, H. C. Perfusion Decellularization of Discarded Human Kidneys: A Valuable Platform for Organ Regeneration. **Transplantation**, 22 jul. 2015.

PARK, K. M.; WOO, H. M. Porcine bioengineered scaffolds as new frontiers in regenerative medicine. **Transplantation proceedings**, v. 44, n. 4, p. 1146–50, maio 2012a.

PARK, K. M.; WOO, H. M. **Systemic decellularization for multi-organ scaffolds in rats.**

Transplantation Proceedings. **Anais...maio** 2012bDisponível em: <<http://www.ncbi.nlm.nih.gov/pubmed/22564650>>. Acesso em: 16 jul. 2014

PELOSO, A. et al. Considerations on the development of a model of kidney bioengineering and regeneration in rats. **Expert review of medical devices**, v. 10, n. 5, p. 597–601, set. 2013.

PETERSEN, T. H. et al. Tissue-engineered lungs for in vivo implantation. **Science (New York, N.Y.)**, v. 329, n. 5991, p. 538–41, 30 jul. 2010.

PHILP, D. et al. Complex Extracellular Matrices Promote Tissue-Specific Stem Cell Differentiation. **Stem Cells**, v. 23, n. 2, p. 288–296, fev. 2005.

PLACE, E. S. et al. Synthetic polymer scaffolds for tissue engineering. **Chemical Society Reviews**, v. 38, n. 4, p. 1139, 24 mar. 2009.

PLENICEANU, O.; HARARI-STEINBERG, O.; DEKEL, B. Concise review: Kidney stem/progenitor cells: differentiate, sort out, or reprogram? **Stem cells (Dayton, Ohio)**, v. 28, n. 9, p. 1649–60, set. 2010.

POORNEJAD, N. et al. Efficient decellularization of whole porcine kidneys improves reseeded cell behavior. **Biomedical materials (Bristol, England)**, v. 11, n. 2, p. 025003, 10 mar. 2016.

PU, L. L. Q. Small intestinal submucosa (Surgisis) as a bioactive prosthetic material for repair of abdominal wall fascial defect. **Plastic and Reconstructive Surgery**, v. 115, n. 7, p. 2127–2131, jun. 2005.

SEDDON, A. M.; CURNOW, P.; BOOTH, P. J. **Membrane proteins, lipids and detergents: Not just a soap opera***Biochimica et Biophysica Acta - Biomembranes*, 3 nov. 2004. Disponível em: <<http://www.ncbi.nlm.nih.gov/pubmed/15519311>>. Acesso em: 13 jun. 2017

SHUPE, T. et al. Method for the decellularization of intact rat liver. **Organogenesis**, v. 6, n. 2, p. 134–136, 2010.

SONG, J. et al. Extracellular matrix of secondary lymphoid organs impacts on B-cell fate and survival. **Proceedings of the National Academy of Sciences of the United States of America**, v. 110, p. E2915-24, 2013a.

SONG, J. J. et al. Regeneration and experimental orthotopic transplantation of a bioengineered kidney. **Nature medicine**, v. 19, n. 5, p. 646–51, maio 2013b.

SUN, M. et al. Influences of decellularization processes on immunogenicity of chemically acellular nerve allografts. **Zhonghua wai ke za zhi [Chinese journal of surgery]**, v. 44, n. 4, p. 275–278, 15 fev. 2006.

SUN, X.; ALTALHI, W.; NUNES, S. S. Vascularization strategies of engineered tissues and their application in cardiac regeneration. **Advanced Drug Delivery Reviews**, 2015.

SWETHA, G. et al. Glomerular parietal epithelial cells of adult murine kidney undergo EMT to generate cells with traits of renal progenitors. **Journal of cellular and molecular medicine**, v. 15, n. 2, p. 396–413, fev. 2011.

TAKAHASHI, K. et al. Induction of Pluripotent Stem Cells from Adult Human Fibroblasts by Defined Factors. **Cell**, v. 131, n. 5, p. 861–872, 30 nov. 2007.

USRDS. **CKD in the United States: An Overview of the USRDS Annual Data Report, Volume 1** **American Journal of Kidney Diseases**. [s.l: s.n.]. Disponível em: <<http://www.sciencedirect.com/science/article/pii/S027263861500709X>>. Acesso em: 16 mar. 2016.

USRDS. **Chapter 7: Transplantation** **American Journal of Kidney Diseases**. [s.l: s.n.]. Disponível em: <http://www.usrds.org/2015/view/v2_07.aspx>.

UYGUN, B. E. et al. Organ reengineering through development of a transplantable recellularized liver graft using decellularized liver matrix. **Nature Medicine**, v. 16, n. 7, p. 814–820, 13 jul. 2010.

UZARSKI, J. S. et al. Dual-Purpose Bioreactors to Monitor Noninvasive Physical and Biochemical Markers of Kidney and Liver Scaffold Recellularization. **Tissue Engineering Part C: Methods**, v. 21, n. 10, p. 1032–1043, 1 maio 2015a.

UZARSKI, J. S. et al. Epithelial Cell Repopulation and Preparation of Rodent Extracellular Matrix Scaffolds for Renal Tissue Development. **Journal of Visualized Experiments**, n. 102, 10 ago. 2015b.

WAINWRIGHT, J. M. et al. Preparation of cardiac extracellular matrix from an intact porcine heart. **Tissue engineering. Part C, Methods**, v. 16, n. 3, p. 525–532, jun. 2010.

WANG, J. C. et al. A comparison of commercially available demineralized bone matrix for spinal fusion. **European Spine Journal**, v. 16, n. 8, p. 1233–1240, ago. 2007.

WANG, Y. et al. Method for perfusion decellularization of porcine whole liver and kidney for use as a scaffold for clinical-scale bioengineering engrafts. **Xenotransplantation**, v. 22, n. 1, p. 48–61, 7 out. 2015.

WILLENBERG, B. J. et al. Repurposed biological scaffolds: kidney to pancreas. **Organogenesis**, v. 11, n. 2, p. 47–57, 2015.

XUE, J.-D. et al. Seeding cell approach for tissue-engineered urethral reconstruction in animal study: A systematic review and meta-analysis. **Experimental Biology and Medicine**, v. 241, n. 13, p. 1416–1428, 1 jul. 2016.

YOKOO, T.; MATSUMOTO, K.; YOKOTE, S. Potential use of stem cells for kidney regeneration. **International journal of nephrology**, v. 2011, p. 591731, jan. 2011.

YU, Y. L. et al. Decellularized kidney scaffold-mediated renal regeneration. **Biomaterials**, v. 35, n. 25, p. 6822–6828, ago. 2014.

ZVAROVA, B. et al. Residual Detergent Detection Method for Nondestructive Cytocompatibility Evaluation of Decellularized Whole Lung Scaffolds. **Tissue Engineering Part C: Methods**, v. 22, n. 5, p. 418–428, maio 2016.

9. ANEXOS

9.1. Anexo1: Protocolo CEUA nº 033/2014 de 03/10/14.

	<p>UNIVERSIDADE FEDERAL DO ESPÍRITO SANTO CENTRO DE CIÊNCIAS DA SAÚDE COMISSÃO DE ÉTICA NO USO DE ANIMAIS - CEUA</p>	
<h1>CERTIFICATE</h1>		
<p>We certify that the Protocol 033/2014 related to research project entitled "Rats organs decellularization and repopulation with mesenchymal stem cells.*, under responsibility of Breno Valentim Nogueira, is in accordance with the ethical principles of animal experimentation adopted by this Ethics Committee on Animal Use (CEUA-UFES), being approved at the regular assembly in October 03, 2014.</p>		
<p>*Title as supplied by author.</p>		
<p>Vitória (ES), October 03, 2014.</p>		
<p> Presidente do Comitê de Ética no Uso de Animais CEUA/UFES</p>		

9.2. Anexo 2: Protocolo CEUA nº 042/2016 de 07/10/16.

	<p>UNIVERSIDADE FEDERAL DO ESPÍRITO SANTO CENTRO DE CIÊNCIAS DA SAÚDE COMISSÃO DE ÉTICA NO USO DE ANIMAIS - CEUA</p>	
<h2 style="text-align: center;">CERTIFICATE</h2>		
<p>We certify that the Protocol 42/2016 related to research project entitled "<u>Decellularization and recellularization of rodent organs for Development of Functional Bioartificial Organs</u>", under responsibility of Breno Valentim Nogueira, is in accordance with the ethical principles of animal experimentation adopted by this Ethics Committee on Animal Use (CEUA-UFES), being approved at the regular assembly in October 07, 2016.</p>		
<p> Prof. Roger Lyrio dos Santos Presidente do Comitê de Ética no Uso de Animais CEUA/CCS/UFES</p>		<p>Vitória (ES), October 07, 2016.</p>

9.3. Anexo 3: Produções Correlatas

9.3.1. Patente referente à Sensor Óptico aplicado à Descelularização de Órgãos.

< Uso exclusivo do INPI >



02/05/2017 02517000033
14:51 REES
BR 10 2017 009187 2

Espaço reservado para o protocolo Espaço reservado para a etiqueta Espaço reservado para o código QR



INPI INSTITUTO NACIONAL DA PROPRIEDADE INDUSTRIAL
Sistema de Gestão da Qualidade
Diretoria de Patentes

DIRPA	Tipo de Documento: Formulário	DIRPA	Página: 1/3
Título do Documento: Depósito de Pedido de Patente		Código: FQ001	Versão: 2
		Procedimento: DIRPA-PQ006	

Ao Instituto Nacional da Propriedade Industrial:
O requerente solicita a concessão de um privilégio na natureza e nas condições abaixo indicadas:

1. **Depositante (71):**
 - 1.1 Nome: UNIVERSIDADE FEDERAL DO ESPÍRITO SANTO
 - 1.2 Qualificação: IES
 - 1.3 CNPJ/CPF: 32479123000143
 - 1.4 Endereço Completo: AV FERNANDO FERRARI N° 514-CAMPUS UNIVERSITARIO GOIABEIRAS
 - 1.5 CEP: 29075-910
 - 1.6 Telefone: (27)40097885 1.7 Fax:
 - 1.8 E-mail: josecarlos.init@gmail.com

continua em folha anexa

2. **Natureza:** Invenção Modelo de Utilidade Certificado de Adição

3. **Título da Invenção ou Modelo de Utilidade (54):**
SENSOR ÓPTICO APLICADO À DESCELULARIZAÇÃO DE ÓRGÃOS

continua em folha anexa

4. **Pedido de Divisão: do pedido N°** **Data de Depósito:**

5. **Prioridade:** Interna (66) Unionista (30)

O depositante reivindica a(s) seguinte(s):

País ou Organização do depósito	Número do depósito (se disponível)	Data de depósito



02/05/2017 02517000033
14:51 REES
52400.067208/2017-56

continua em folha anexa




UNIVERSIDADE FEDERAL DO ESPÍRITO SANTO
Pró-Reitoria de Pesquisa e Pós-Graduação
Instituto de Inovação Tecnológica

DECLARAÇÃO

Declaro, para os devidos fins, que Afrânio Côgo Destefani, brasileiro, Aluno de Pós-Graduação, CPF. 091.227.427-19, consta como inventor no pedido de privilégio de invenção denominado **"SENSOR ÓPTICO APLICADO À DESCELULARIZAÇÃO DE ÓRGÃOS"**, sob o número INPI – BR 10 20170091872, depositado junto ao INPI na data de 02/05/2017, tendo a Universidade Federal do Espírito Santo – UFES como titular.

Vitória/ES, 01 de junho de 2017.



Antonio Alberto Ribeiro Fernandes
Diretor do INIT/UFES

Jose Carlos Fundao Farias
Pró-Reitoria de Pesquisa e Pós-Graduação - INIT
Assistente em Administração
SIAPE Nº 1003217

Av. Fernando Ferrari, 514 - Campus Universitário - Goiabeiras - Vitória - ES
CEP 29075-910 - e-mail: nites@prppg.ufes.br - Tel: (27) 4009-7885



UNIVERSIDADE FEDERAL DO ESPÍRITO SANTO
Pró-Reitoria de Pesquisa e Pós-Graduação
Instituto de Inovação Tecnológica

DECLARAÇÃO

Declaro, para os devidos fins, que Marco Cesar Cunegundes Guimarães, Breno Valentin Nogueira, Tadeu Ériton Calimam Zanardo, Afrânio Côgo Destefani, Flávia Medina da Silva e Isadora Cavalcanti Barba, constam como inventores no pedido de privilégio de invenção denominado **"PROCESSO DE INDUÇÃO DE CÉLULAS-TRONCO PELA UTILIZAÇÃO DE PEPTÍDEOS"**, sob o número INPI – BR 10 2015 016701 6, depositado junto ao INPI na data de 13/07/2015, tendo a Universidade Federal do Espírito Santo – UFES, como titular.

Vitória/ES, 30 de setembro de 2015.

Antonio Alberto Ribeiro Fernandes
Diretor do INIT/UFES

PROF. ANTONIO ALBERTO RIBEIRO FERNANDES
DIRETOR DO INSTITUTO DE INOVAÇÃO TECNOLÓGICA
PRPG-UFES

9.3.3. Co-autoria no artigo “*Chronic administration of antioxidant resin from Virola oleifera attenuates atherogenesis in LDLr^{-/-} mice*”



Journal of Ethnopharmacology

Volume 206, 12 July 2017, Pages 65-72



Chronic administration of antioxidant resin from *Virola oleifera* attenuates atherogenesis in LDLr^{-/-} mice

Paola Nogueira Coutinho ^a ✉, Beatriz Peters Pereira ^a ✉, Ana Claudia Hertel Pereira ^a ✉, Marcella Leite Porto ^b ✉, Arícia Leone Evangelista Monteiro de Assis ^c ✉, Afrânio Côgo Destefani ^c ✉, Silvana Santos Meyrelles ^d ✉, Elisardo Corral Vasquez ^{a, d} ✉, Breno Valentim Nogueira ^c ✉, Tadeu Uggere de Andrade ^a ✉, Denise Coutinho Endringer ^{a, b} ✉, Marcio Fronza ^a ✉, Thiago Melo Costa Pereira ^{a, b} ✉

Disponível em: <https://doi.org/10.1016/j.jep.2017.05.015>